Evaluation of Space Station Meteoroid/Debris Shielding Materials

Prepared under Subcontract to

Lockheed Engineering and Management Services Co., Inc.

for the

Advanced Research Projects Office

at the

Johnson Space Center

by

Eagle Engineering, Inc.

Houston, Texas

NASA Contract No. NAS9-15800

Lockheed P.O. No. 02-001-12718

Eagle Contract No. TO-86-74

Final Report

Eagle Report No. 87-163

September 30, 1987

ORIGINAL CONTAINS COLOR ILLUSTRATIONS

(NASA-CR-185627) EVALUATION OF SPACE STATION METEOROID/DEBRIS SHIELDING MATERIALS Final Report (Diskette Supplement) (Eagle Engineering) 202 p

N93-72022

Unclas

Z9/18 0159250

Functional Color Pages 14

Evaluation of Space Station Meteoroid/Debris Shielding Materials

Prepared under Subcontract to

Lockheed Engineering and Management Services Co., Inc.

for the

Advanced Research Projects Office

at the

Johnson Space Center

by

Eagle Engineering, Inc.

Houston, Texas

NASA Contract No. NAS9-15800

Lockheed P.O. No. 02-001-12718

Eagle Contract No. TO-86-74

Final Report

Eagle Report No. 87-163

September 30, 1987

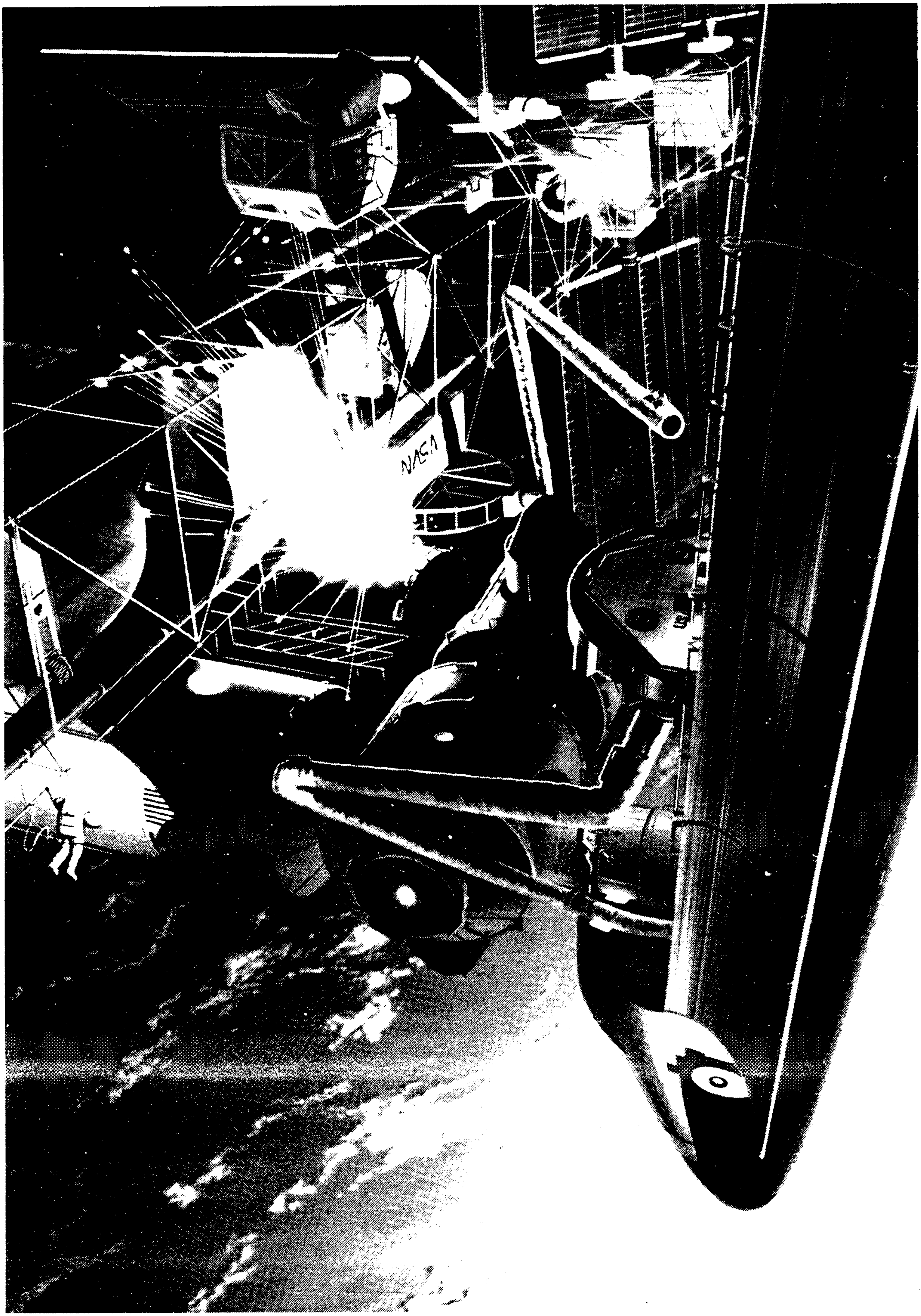
NASA

Foreword

This is the final report for a study of shielding materials for the Advanced Research Projects Office of the Solar System Exploration Division at the Johnson Space Center. Eagle Engineering, Inc. conducted the study between June 3, 1986 and September 30, 1987 through a Lockheed Engineering and Management Services Company subcontract (Lockheed P.O. No. 02-001-12718, Eagle contract No. TO-86-74). The purpose of the study was to evaluate the effectiveness of metallic, ceramic, and composite materials as meteoroid and orbital debris shields or "bumpers" for Space Station module protection. A second purpose was to develop analytical tools and procedures to help predict the response of materials to hypervelocity impact.

This report documents analytical and experimental evaluations of candidate shielding materials for Space Station applications. Analytical techniques used to indicate promising materials for testing are described. The test approach is defined and test results are documented. Shielding performance of several materials was rated superior to an aluminum bumper baseline; particularly two: a dual bumper concept utilizing a metallic mesh first bumper and a solid second bumper, and a tungsten microsphere/silicone rubber material. Other bumper materials show promise, including laminates of aluminum with graphite/epoxy and ceramics. Recommendations for the next phase of the study include additional screening tests at JSC and impact testing with a larger projectile at another research facility.

Ms. Jeanne L. Crews and Mr. Burton G. Cour-Palais were the NASA technical monitors for this study. Excellent hypervelocity impact data was provided by Lockheed personnel assigned to the JSC Hypervelocity Impact Research Laboratory (HIRL): Mr. Kenneth Oser, Mr. Earl Brownfield, and Mr. Thomas Thompson. Mr. Glen Jolly was the Lockheed technical administrator. Dr. Ching Yew of the University of Texas provided valuable advice and data.

Mr. Eric Christiansen was the Eagle Project Manager. Major technical contributions were provided by Dr. Charles H. Simonds and Dr. Larry J. Friesen. Mr. David Carson and Mr. Norman Smith have also made contributions. Artwork was produced by Mr. R. Patrick Rawlings and Mr. Mark Dowman of Eagle Engineering's Advanced Concepts Art Department.

About the Cover

The cover depicts an impact on a Space Station module shield by a relatively large orbital debris fragment, assumed in this case to be a spherical 1 cm diameter aluminum fragment (1.4 g), traveling at approximately 9 km/sec.

The projectile is shown striking the upper part of a module shield at a 45° angle to the Station velocity vector. An oblique impact is likely since the orbital debris flux is highly directional with most coming in on a 30°-70° angle to either side of the Station's orbital direction and parallel to the Earth.

A 1 cm particle is generally considered to be a worst-case particle, having a probability of impact on a set of two modules of 1 in 50 over a 30 year time period (assuming half of each module is shielded by other structures). Particles of this size are more likely to be man-made debris. A meteoroid particle having the same energy as a 1 cm orbital debris particle has only a 1 in 600 chance of striking the same dual module system.

The impact spawns a number of particles from the impacted surface (called ejecta) that have a cumulative mass 10 to 100 times the mass of the projectile. Some of these secondary particles will be traveling at hypervelocity and, given the correct geometry for the impact event, could subsequently strike additional Space Station elements as portrayed in the cover illustration. Therefore, design of all elements on Space Station exposed to primary impacts from meteoroids and debris should also consider the flux of secondary particles. In a previous study, the secondary flux factor was estimated to be on the order of 10 percent of the primary flux. The amount and size of secondary mass released in the impact is dependant on the type of material impacted, with certain non-metallic materials ejecting significantly less damaging material than aluminum as concluded in this report.

In addition to the secondary impacts, the cover also illustrates the bright flash visible from a hypervelocity impact. A calculation showed that a 1 cm aluminum projectile at 9 km/sec will release over 5 million lumens, or the same light intensity as over 3,000 hundred-watt light bulbs. Ejecta particles, due to their hypervelocity speed, will also likely emit visible radiation upon impact with adjacent structures.

Table of Contents

Table of Contents

Table of Contents

List of Figures

List of Figures

List of Tables

1.0 Executive Summary

A series of light gas gun shots were performed with 45 mg (3.2 mm) aluminum projectiles at 6 to 7 km/sec to evaluate the protective potential of different materials for Space Station meteoroid and orbital debris shields. A meteoroid/debris shield or "bumper" is a sacrificial first wall in a typical dual-wall system. Its function is to intercept oncoming projectiles and spread the impact intensity over a large area of the second wall or pressure hull of the Space Station common modules and other pressurized elements, thereby providing greater protection at less weight than a single-wall structure.

The purpose of the testing was to demonstrate that alternative shield materials held promise for offering equivalent protection with lower mass than present aluminum bumper concepts or, with the same mass, increasing the protection for Space Station crew and equipment from orbital debris/meteoroid impacts.

From consideration of no-penetration criterion requirements, module geometry (including self-shielding), and the orbital debris environment, the modules should be designed to protect against a 1.1 gm (0.92 cm) debris particle at a minimum. Protection beyond that offered by the baseline aluminum shield/multilayer insulation/aluminum backwall configuration may be necessary to prevent critical damage from this size orbital debris particle over a 10 year design life of the module. Detached spall (fragments released from the inside surface of a pressure hull) represents a significant potential hazard to crew and interior equipment and probably should be considered as much a critical failure as penetration. Preventing both spall and penetration makes it even more likely that upgraded shielding will be required for Space Station habitable volumes.

One possibility for increasing impact protection is to build that capability into the module shielding system from the start. This will require either (1) new shielding materials or concepts that provide added protection at less weight, or (2) thicker and more massive module walls, or (3) increasing the standoff distance between shield and pressure hull by using deployable shield mechanisms. Another possibility is to augment protection by deploying additional shielding some time (years) after the pressurized modules have been on orbit. Such augmentation can allow module design to proceed without great change as long as augmentation techniques are experimentally verified early and scars are added to the module exterior to accept additional shielding.

Prior to impact testing for this study, mathematical models were developed, based on one-dimensional shock wave theory, to assist in selecting suitable materials for the test program. The analytical models and other considerations detailed in this report were used to select a list of metallic, graphite composite, ceramic, and polymer test materials that satisfy known requirements for Space Station bumpers. In particular, it appeared from these analyses that ceramics (in designs borrowed from conventional armoring techniques), and laminates of ceramics and low-density fiber-reinforced composites offered advantages over aluminum (6061-T6), the currently baselined shield material for Space Station module protection.

The analyses also indicated that a low-density, fiber-reinforced composite such as graphite/-epoxy should be considered for the structure that provides the standoff and support to the bumper. This would reduce the lethality of the fragments projected against the second wall produced in direct hypervelocity impacts on the support elements.

Due to funding limitations, only selected materials were procured for the just completed phase of the test program. Materials for fourteen unclassified and additional classified bumper concepts were acquired for hypervelocity testing at JSC in scaled-down versions of representative Space Station dual-wall configurations. Screening tests involved testing equal areal density bumpers, except when a proper size bumper was unavailable, in which case the combined bumper/backwall areal density was kept constant. Projectile conditions (size, velocity, impact angle) and bumper/backwall spacing distance were also maintained essentially constant during the tests to ensure comparable results.

Despite the limited number of candidate materials tested, several materials out-performed baseline Al 6061-T6 by significantly reducing damage to the backwall. A dual-bumper concept incorporating a wire mesh and a backup plate separated by a short distance (approximately a quarter of the mesh/backwall standoff) showed particular promise. A tungsten micro-sphere/silicone material combination also performed well. The results of classified material testing is discussed in a separate (classified) addendum to this report.

It is recommended that the next phase of the shielding material program be in two parts: (1) continuation of efforts to find improved alternative shield and backwall concepts using analytical techniques and experimental testing at the JSC Hypervelocity Impact

Research Laboratory, and (2) testing the best candidates, scaled-up to actual Space Station configurations, at a larger ballistic facility in some other location. Because the development schedule for Space Station accomplishes major trades and essentially locks into a design path by the first Preliminary Design Review (PDR) currently scheduled for January 1989, expeditious planning for impact testing of Space Station scaled shield test articles is essential to prepare sufficiently mature justification for inclusion of new materials in shielding trade studies prior to PDR.

2.0 Introduction

The primary purpose of this study was to find alternative materials for Space Station module orbital debris and meteoroid shields which would provide greater protection at lower weight than the present aluminum bumper concepts. To accomplish this objective, study participants had to: (1) identify candidate materials for module shields, (2) formulate a suitably reliable hypervelocity impact test method, and (3) conduct impact tests on the candidate materials and evaluate the protective potential of each by assessing the extent of damage to the second wall.

Orbital debris and meteoroids are significant hazards to the Space Station and must be taken into account in its design. The structures of pressurized elements typically incorporate a shield to protect the inner hull from high velocity particles. These particles may be either meteoroids or man-made space debris, which travel at average speeds of 20 km/sec and 10 km/sec, respectively. The meteor bumper or shield is the first wall of a dual-wall protection system. Its purpose is to fragment, melt, or vaporize the incoming particle and spread its impact over a wider area of the second wall or backwall than would otherwise be the case, thereby reducing total damage to the spacecraft and decreasing the likelihood that the particle will actually penetrate the spacecraft. The terms used in this report to describe the dual-wall bumper protected system are represented in Figure 2-1 and a more complete description of the shock dynamics associated with hyper-velocity impact on thin targets is given in Section 3.1.

The space environment imposes certain requirements and design constraints on shielding systems. The Space Station module shields must be designed with proper consideration for the meteoroid and debris model, integral/deployable shielding issues, atomic oxygen attack, radiation protection, thermal protection, and repairability, as discussed in Sections 3.2-3.11.

The reasoning behind selecting candidate materials for testing is presented in Section 4. In Section 4.1, materials and concepts used in armored vehicles, particularly the relatively new use of ceramic materials, were examined for applicability to space protection require-ments. Bumper material properties such as density, shock compressibility, and thermodynamic properties are important in successful bumper operation as explained in Section 4.2.

Because the number of potential bumper materials is large and material procurement and hypervelocity testing is expensive, it is reasonable to develop computer models to assist in assessing potential materials for testing. Section 4.3 describes analytical tools developed for providing insight into the physics of hypervelocity impact events. Three computer models were developed to evaluate the effectiveness of different bumper materials. A figure-of-merit based on empirical correlations for hypervelocity impact and other material properties is explained in Section 4.3.1 and Appendix B. The results of a program that calculates the impact shock pressure in a technique that is often applied graphically are used in Section 4.2.2, with a detailed program description in Appendix C. An analytical model which calculates peak shock pressure, the energy partition between projectile and target, the state of the projectile material, and an optimal bumper thickness as a function of projectile velocity is described in Section 4.3.2 and Appendix A. The one-dimensional model uses Hugoniot-Rankine relationships and simplified equations-of-state to perform these calculations. The state of the projectile material and the optimal bumper thickness are used in a comparative sense to evaluate material alternatives.

The models and other considerations discussed in Sections 3 and 4 are applied to select a list of candidate materials for the hypervelocity testing program as given in Section 4.4.

A bumper testing plan presented in Section 5 bases experimental evaluation on testing equal areal density bumpers with constant projectile conditions. Section 6 gives results of the impact testing and material comparisons. Section 7 contains conclusions and recommendations.

Appendix D contains a complete listing of all shots of interest to this study (ordered by shot number) and data associated with them. Appendix E includes cost estimates for some material candidates proposed for later screening tests. Lotus 1-2-3 spreadsheet programs described in this report have been copied onto the computer diskette attached at the back (Appendix F).

Figure 2-1a. Impacts by hypervelocity projectiles will result in a debris plume of solid fragments, liquid, or vapor particles.

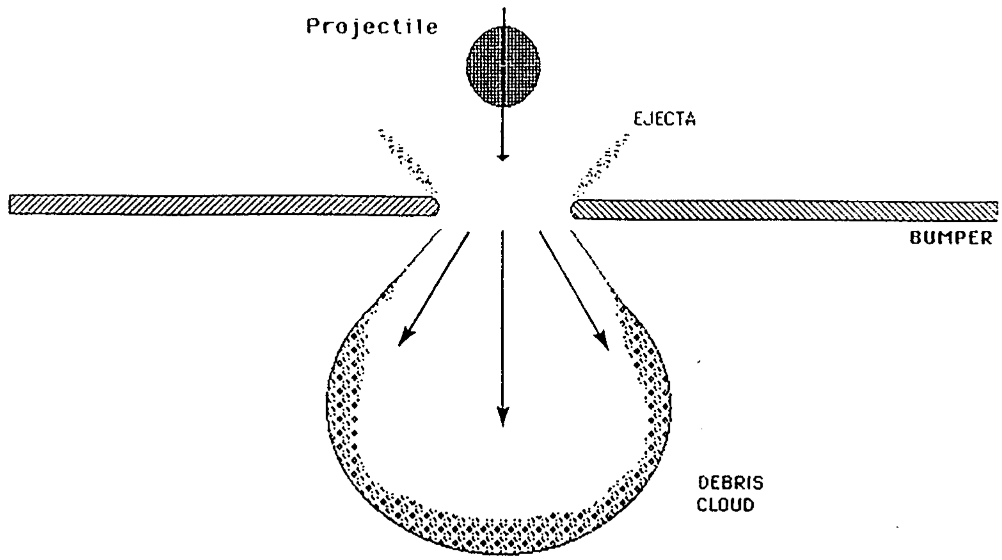

Figure 2-1b. The second wall must then survive the fragments and blast loading. It could rupture from the blast loading, or fail due to spall or perforation from individual fragments.

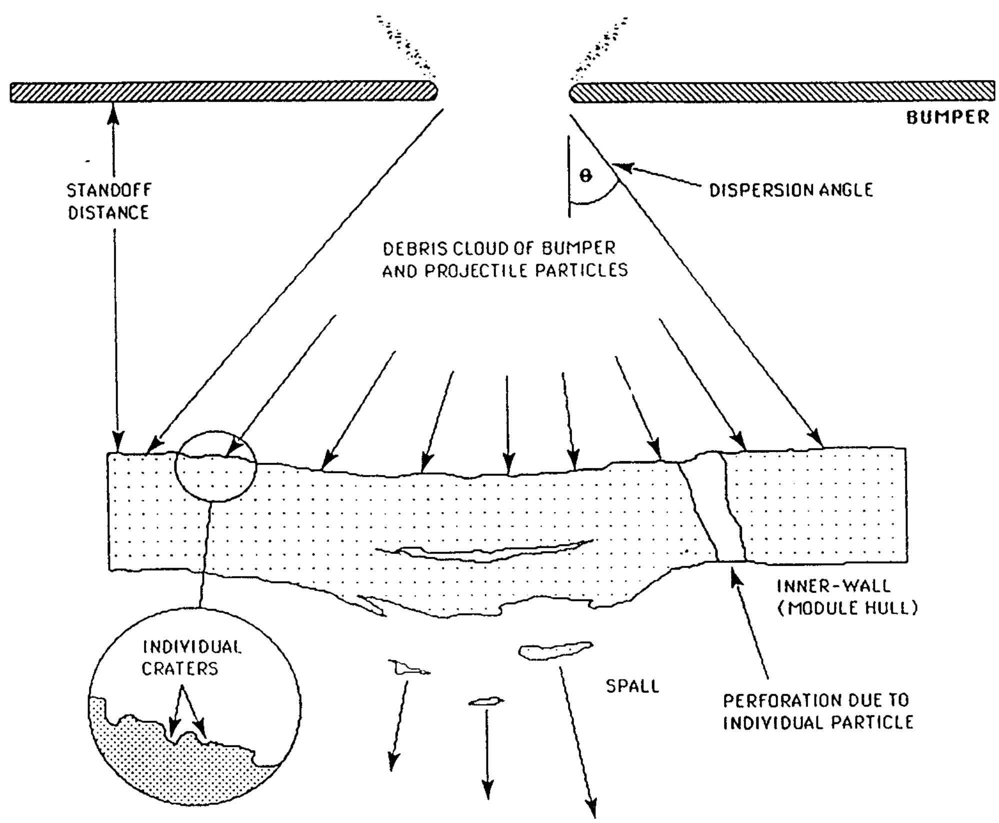

3.0 Meteoroid/Debris Shielding Requirements

The effects of environmental factors and system requirements on meteoroid/orbital debris shielding design is discussed in the following sections.

3.1 Bumper Concept

Manned modules and other sensitive Space Station elements will be shielded from direct meteoroid and orbital debris impacts by interposing a relatively thin plate of material, or bumper, some distance in front of the protected structure to intercept the incoming projectiles. Impacts with the bumper melts, fragments, or vaporizes the projectile, throwing material off the front (ejecta) and back (debris cloud) of the bumper. In previous experimental work, the ratio of ejecta to debris cloud mass was typically 3:7 for thin aluminum and graphite composite targets (42). The debris projected rearward is a relatively diffuse cloud of projectile and bumper particles that spreads the impact energy over an area of the inner wall or pressure hull, thus enabling significant weight reductions over single-wall structures with equivalent impact resistance. Experimental investigations have demonstrated weight savings of as much as 80 percent over single-wall configurations (25, 31).

Intense shock waves generated by the impact propagate at supersonic speeds forward into the bumper and backward into the oncoming projectile, compressing these materials beyond their original density and increasing temperatures and pressures by many orders of magnitude. When these compressional shock waves encounter free surfaces, they are reflected as tensile or rarefaction waves that relieve the pressure back toward zero and reduce temperatures. The initial compressive shock wave adds entropy to the material in an amount almost proportional to the peak shock pressure and the material's shock compressibility. The release from the shock-compressed state is nearly isentropic, thus, entropy is transferred to the material by transit of the shock waves. This entropy increase appears as internal energy or heat (12, p.108; 25, p.11). If the added heat is less than the material's heat of fusion, the shocked material releases into a solid but massively disrupted state. The shocked material becomes liquid if the added internal energy exceeds its heat of fusion and a gas if the material's vaporization energy is exceeded. Table 3-1 lists the shock pressures and required velocity for aluminum projectiles to melt and vaporize several different materials. For aluminum-on-aluminum impacts, shock heating causes incipient melting of the projectile at approximately 5 km/sec and completely melts it above 7 km/sec.

The phase of the debris plume--gas, liquid, or solid--is the dominant parameter that defines the effectiveness of the bumper in protecting underlying structures (3, 25, 33). Other important variables include the standoff distance between the bumper and inner wall, dispersion angle of the debris plume, and the size, velocity, and density of the solid fragments (if any) in the debris plume. Section 4.3 presents analytical model that quantifies some of these variables and an empirical model based on these variables to select a candidate list of materials for experimental evaluation as bumpers. Since testing of candidate materials for inner walls is not expected until a later stage of the program, no attempt is made to quantify the effect of inner-wall material properties on penetration protection.

Material properties such as projectile and bumper density, melting and vaporization temperatures and energies, and shock compressibility or Hugoniot parameters determine the peak shock pressure and state of the debris plume. The bumper thickness is also important. An optimally sized bumper will cause the rarefaction wave from the bumper to overtake the compressive shock wave in the projectile at the instant it has swept through the entire projectile, i.e., at the back of the projectile. This results in the greatest projectile heating and greatest likelihood of projectile melting or vaporization. In addition, the rarefaction from the bumper imparts particle velocities with the greatest dispersive effect on the projectile. If, complete shock compression and rarefaction of the projectile has been accomplished with the thinnest bumper, the mass of bumper and projectile material in the debris plume which subsequently impacts the inner wall will be minimized.

An impact on too thin a bumper causes the rarefaction wave from the bumper to overtake the compressive shock wave in the projectile and sharply attenuate it before it completely traverses the projectile. This means that a portion of the projectile is only lightly shocked and will likely strike the pressure hull as an intact solid fragment, with far greater destructive potential than the rest of the debris plume.

A much more common occurrence is an impact on too thick a bumper. Bumpers are sized for the largest orbital debris or meteoroid particle that is expected (with a certain probability) to impact a structure over the duration of the mission. The critical meteoroid and orbital debris particle size for design purposes is determined for the Space Station habitat module in Section 3.2.1. Because orbital debris and meteoroid fluxes decrease with increasing size, almost all particles impacting the bumper during the mission will be smaller than the bumper was designed to protect against. In such cases the projectile is completely shocked (although it will not be dispersed as well because the rarefaction comes from the back and sides of the projectile), but the bumper will not be because the rarefaction from the projectile overtakes the compressive shock wave in the bumper. Since the rarefaction wave traverses shock compressed material (density significantly higher that unshocked state), its acoustic velocity is higher than the compressive shock wave. When the rarefaction overtakes the compressive shock wave, it attenuates it; thus, the debris cloud striking the pressure hull will likely contain solid fragments of the bumper. The penetrability of these fragments depends on their size, velocity, and density. The larger any of these factors are, the more penetrating the fragments will be. Low density bumper materials are preferred in this case because they produce the least penetrating fragments.

Impact shock pressure and the resulting phase of the debris plume also depends on projectile velocity (see equations in Appendix A and C). Generally, shock pressure increases with projectile velocity. The phase of the particles in the debris cloud tends to be solid at low velocity, then liquid or vapor as velocity increases.

Thus, the damage potential of the debris plume varies with projectile velocity which governs the state or phase of the projectile, as depicted in Figure 3-1. This shows the critical particle size that will penetrate a representative Space Station dual-wall design as a function of projectile velocity. The baseline module shield configuration consists of a 0.063" Al 6061-T6 bumper separated by a 4.5" standoff from a 0.125" Al 2219-T87 pressure hull (69). Multilayer insulation (MLI) consisting of 20 to 30 layers of double aluminized mylar interleaved with Dacron net spacers is mounted between the bumper and inner wall for thermal control. For this particular dual-wall configuration, projectile velocity in the 2-4 km/sec range is the most penetrating to the backwall as indicated by the minimum in the critical projectile diameter curve at these velocities in Figure 3-1. An extension of this type of curve into higher velocity ranges is given in Figure 3-2. Typically several minimums in the curve occur at transitions in the phase of the projectile.

Hypervelocity impacts of aluminum projectiles into aluminum (and its alloys) have been well studied. For the all-aluminum dual wall design represented in Figure 3-1, projectile velocity and the projectile/bumper debris plume state can be correlated with the "critical" projectile size that will completely penetrate the second wall. At low velocity (less than 2-3 km/sec for Al on Al impacts), the projectile remains essentially intact, and as a result, the critical particle size to completely penetrate the second wall decreases with increasing velocity because the kinetic energy of the debris plume (essentially single projectile and multiple bumper fragments) increases. At higher velocities (greater than 3 km/sec for Al on Al impacts), both the projectile and affected bumper material will fragment into finer particles that are less damaging to the second wall. Thus, the critical particle size increases above approximately 3 km/sec until about 5 km/sec, when both the aluminum projectile and bumper begin to melt. Because molten material damages the second wall to a lesser extent than solid fragments, the critical projectile diameter will continue to increase until the projectile material has completely melted (at approximately 7 km/sec for Al on Al impacts). Between 7 and 10 km/sec, the material in the debris cloud remains molten, but gains kinetic energy and momentum, and thus more penetrating. This means the penetration threshold particle size will decrease after melting is complete (7 km/sec), or at the end of the dotted line in Figure 3-1. Vaporization begins above 10 km/sec and is not complete until approximately 24 km/sec (for Al on Al impacts). In this velocity range, the critical particle size will increase because the greater amounts of vapor in the debris cloud are less damaging than liquid alone to the underlying structure. Above 24 km/sec, critical particle size will decrease with increasing projectile velocity while the state of the debris cloud remains vapor (until the transition to a plasma begins).

Table 3-1. Impact Pressures and Projectile Velocities Which Result in Melting and Vaporization (Ref. 40)

Target Material	Melting				Vaporization				Source
	Incipient		Complete		Incipient		Complete		
	Pressure Mb	Al Impact Velocity km/sec	Pressure Mb	Al Impact Velocity km/sec	Pressure Mb	Al Impact Velocity km/sec	Pressure Mb	Al Impact Velocity km/sec	
Magnesium	0.48	5.40							A
Aluminum	0.70	5.60	1.00	7.0					A
	0.67	5.50	0.88	6.6	1.67	10.2	4.70		B
	0.61	5.10	0.85	6.5					C
Titanium	1.30	7.60							A
Iron (Steel)	1.80	7.90	2.10	8.80					A
Cadmium	0.33	2.50	0.46	3.20					A
	0.40	3.0	0.59	3.9	0.88	5.2	1.80	8.1	B
	0.33	2.5	0.43	3.15	0.70	4.4	5.30		C
Copper	1.40	6.60	1.84	8.00					A
	1.40	6.60	1.84	8.00	3.40	12.6	34.00		C
Nickel	2.3	9.00							A
Lead	0.25	2.00	0.35	2.60					A
	0.27	2.1	0.34	2.5	0.84	4.8	2.30	9.1	B

Figure 3-1. Ballistic Limit For Dual-Wall Structure (Ref. 47)

(Penetration occurs above the line, no penetration below)

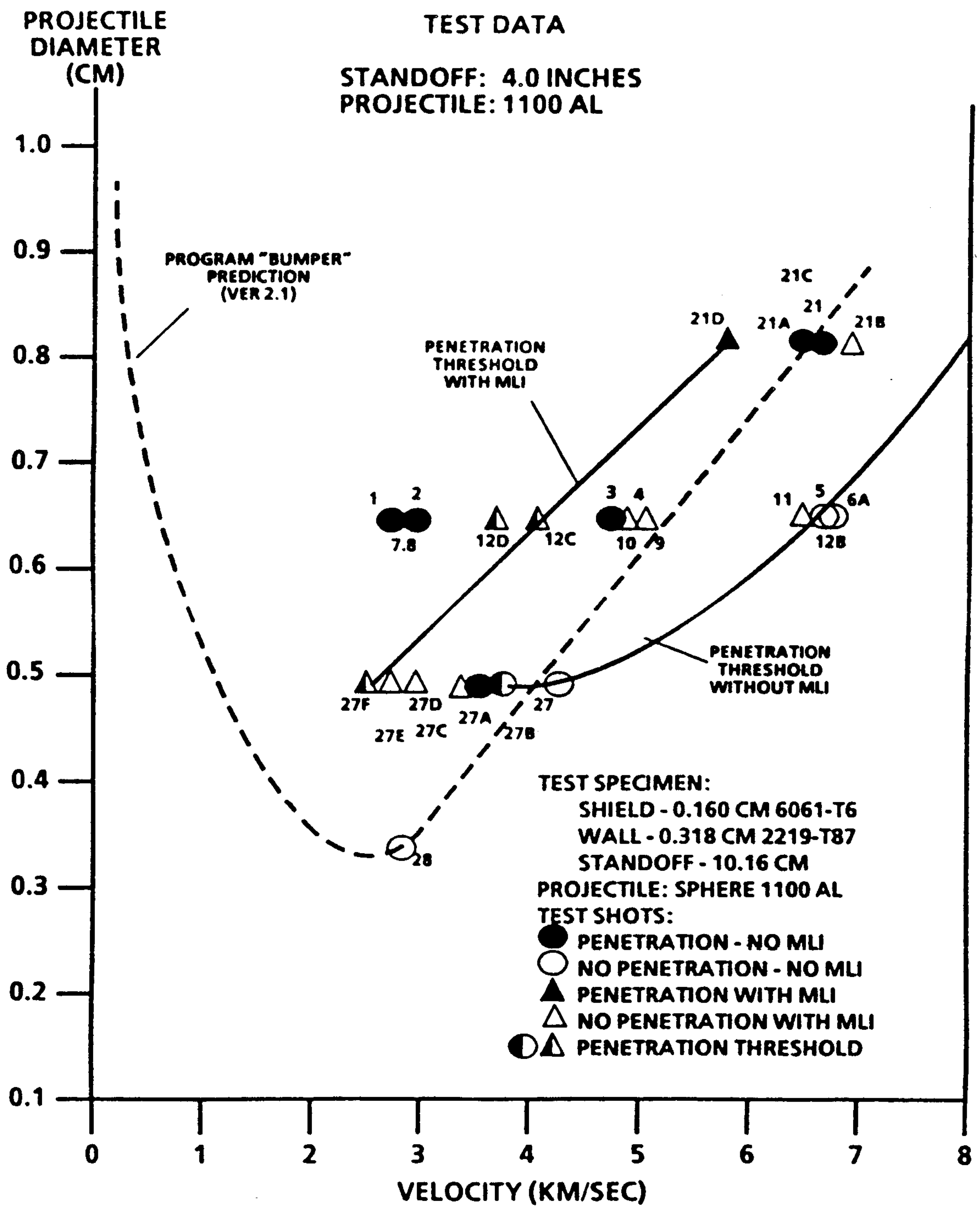

Figure 3-2. Penetration Mechanisms as Function of Projectile Velocity for Impacts on Dual-Wall Structures

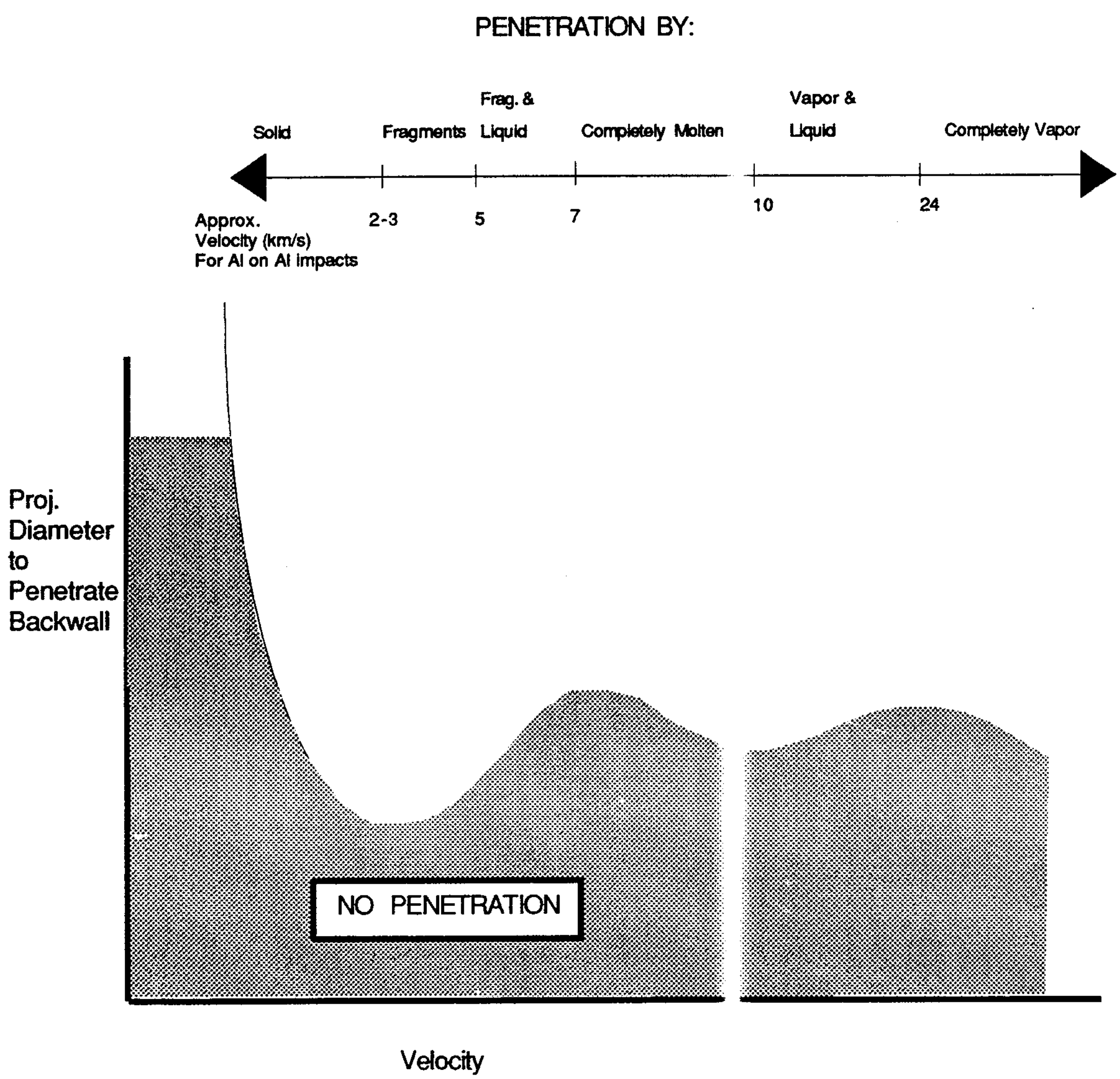

3.2 Space Station Habitation and Laboratory Module Shielding Requirements

Factors important in low weight and cost effective shielding design for Space Station pressurized modules include survival in the orbital debris and meteoroid environment, allowable spacing or "standoff" distance between the bumper and backwall, thermal control, atomic oxygen protection, radiation degradation resistance, bumper support structures, and repairability issues. Each are described in more detail in the following sections. The U.S. habitat/station operation (HSO) module and manufacturing and technology laboratory (MTL) module will be referred to as common modules in this report.

3.3 Orbital Debris and Meteoroid Environment

As given in the Space Station Project Requirements Document (67, p.3-4), all pressurized volumes (including the habitation, laboratory, and logistics modules, nodes, and airlocks) shall be considered critical Space Station core equipment (SSCE) covered by the "design goal" of having a minimum probability of not experiencing a failure that would endanger crew or Space Station survivability due to meteoroid or debris impact of 0.9955 for its 30-year life (1 chance in 222). A critical failure is defined as a penetration of the pressure vessel. Project requirements also state that due to uncertainties in both the meteoroid/debris environments and the behavior of materials in this environment, the initial design requirement will use a 10-year exposure time period with a minimum probability value of 0.9955. However, because the environmental and materials databases are anticipated to grow during the design and development phase of the Space Station, each SSCE's protection must be capable of being incrementally improved to provide the required protection. In addition, the design requirements will probably become more severe as the various databases mature.

The following sections will assume the 0.9955 probability of no penetration over 10 years applies to each <u>individual</u> pressurized element. If it applied to the entire pressurized volume of 9 elements (2 modules, 4 nodes, 2 airlocks, 1 logistics module), each module would require enough protection to drop the probability of no penetration to 0.9995 (or 1 chance in 2000).

3.3.1 Critical Particle Size for Bumper Design

The bumper for the Space Station common module is sized based on the maximum size particle that the dual-wall system must stop to meet the required no penetration criterion. NASA's recommended orbital debris model (48) and meteoroid model (49), along with the design criterion of 0.9955 probability of no penetration over a ten-year lifetime in orbit (50), were used to calculate the critical particle size of meteoroid and orbital debris that impact the Space Station common module. A total surface area of 192.2 m^2 was assumed, based on the common module design given in Figure 3-3. A more recent design gave a 204 m^2 bumper surface area (68). This difference will not greatly affect our conclusions. As given in Table 3-2, the common module bumper should be designed to stop an orbital debris particle of 1.2 cm diameter (2.54 g given a density of 2.8 g/cc) if module self-shielding is not taken into account. The calculational procedure was described in a previous report (42, pp. 183-184).

The orbital debris flux is highly directional, concentrated mainly in the plane parallel to the Earth's surface and particularly in a region extending 30°-70° right and left of the direction of flight as given in Figure 3-4. Because of the directionality of orbital debris, the modules will shield each other from some of the debris flux. Figure 3-5 shows the critical debris particle size for the common module as a function of the percentage of module surface area that is exposed to the debris flux. Given a rough approximation of the self-shielding factor of 0.5 from considerations of the module configuration geometry (i.e., half the module surface area is exposed to debris flux), the orbital debris particle size for design purposes would be 0.92 cm (1.13 g). The critical particle size that the bumper should be designed to stop increases approximately 50 percent to 1.4 cm (4.0 g) if the design lifetime of the common module increases from ten to thirty years and the no penetration criterion remains at 0.9955.

The 0.92 cm particle diameter represents a lower bound estimate (based on 50 percent self-shielding) for the maximum orbital debris diameter a Space Station common module should be designed to protect against based on the 10-year, 0.9955 no penetration criterion. This design particle prediction contains no information on impact velocity or direction. However, it appears from examination of actual experimental results given in Figure 3-1 that a 0.92 cm particle would completely penetrate a dual-wall structure representative of the "baseline" Space Station configuration (including multilayer insulation) at nearly <u>all</u> particle velocities. In addition, the tests on the baseline configuration were made at normal impact angles. It is known that oblique impacts (a more realistic case in actual space impacts) up to approximately 60° from normal are often more damaging to the pressure hull than normal impacts (64, p.525 and 12, p.495). Thus, the penetration curves in Figure 3-1 may even be the best possible by showing only normal impacts. Clearly then, additional debris and meteoroid impact protection for the common modules is required. Protection augmentation alternatives include increasing the pressure hull thickness (high mass penalty), increasing the shield standoff distance, or developing new shield concepts.

In design calculations, the critical particle is typically assumed to be an aluminum sphere. In experimental work, the test particle is commonly spherical. However, it has been shown in experimental testing that a tumbling cylindrically shaped projectile is more penetrating to dual-wall structures than an equal mass sphere (64, p.525). Currently, not much information exists on the length to diameter ratio of orbital debris (48) although limited data on aluminum and graphite/epoxy secondary particle L/D ratios has been published (42). As the orbital debris modeling effort develops and publishes data on debris particle shape and mass, it will be important to factor this information into Space Station module development and experimental hypervelocity impact tests to validate the shielding design.

3.3.2 Bumper Thickness and Mass

The optimum bumper thickness to projectile diameter ratio (t_s/d) for aluminum-on-aluminum impacts at approximately the average orbital debris velocity was determined in Apollo studies to range from 0.1 to 0.25 (3, 33, 43, 73). More recent investigations for ESA interplanetary vehicle protection concluded that the optimal bumper should have an areal density to projectile areal density of 0.25 (25, 32), which also corresponds to t_s/d for aluminum-on-aluminum impacts. Thus, based on the 0.92 cm design particle for a 50 percent shielded common module, an aluminum bumper should be approximately 0.09 cm to 0.23 cm (.035"-0.09") thick depending on the optimal ratio selected. This means the shield for each common module will weigh 470 to 1210 kg (1040 - 2660 lb) if it is made of Al 6061-T6. Bumper structural support columns or rings will add weight to this estimate. However, the added weight is not expected to be significant. An early Space Station module design estimated the weight of the support elements as less than 10 percent of the bumper weight (63). The amount of support will depend on the rigidity of the bumper, with thinner, less rigid bumpers probably requiring more support.

For a proposed common module design, Martin Marietta estimated the 0.08" Al 6061-T6 bumper mass as 1128.8 kg and the standoff support structure mass as 278.9 kg (68, p.3-36). Boeing proposed a thinner 0.04" Al 6061-T6 bumper weighing 919 kg including the support structure (70, p.29).

3.3.3 Module Orientation

The structural design of the inhabited pressurized modules will be driven mainly by the orbital debris environment. For a 0.92 cm particle and a half self-shielded common module, the probability of impact from orbital debris is approximately 1 chance in 240 (0.9959 probability of no debris impact), but from meteoroids only 1 chance in 2640 (Table 3-2). From the standpoint of maximizing protection from orbital debris, the modules should be configured to take advantage of the highly directional nature of debris and maximize self-shielding. Therefore, with no other consideration than impact protection, the current Space Station module would be reconfigured so that: (1) all modules (including logistics modules) are in the same plane parallel to the Earth, and (2) for cylindrical objects, the long axis is perpendicular to the direction of the station's velocity vector. Because the debris flux is essentially parallel to the Earth (more than a few degrees in the vertical direction will cause the debris object to enter the Earth's atmosphere fairly rapidly), the modules can shield each other only if they are also in the plane parallel to the Earth. To understand why cylindrical objects should be turned perpendicular to the velocity vector, consider the situation illustrated in Figure 3-6. For the current configuration of 2 U.S. common modules and 4 resource nodes, the module perimeter exposed to debris impacts is twice the length of the configuration added to the width, or $2 * L + W$. However, for the alternative configuration which has been turned 90°, the exposed perimeter is reduced to $2 * W + L$. This reduction in exposed perimeter translates directly into a reduction of exposed area (approximately exposed perimeter $* \pi *$ module radius) and a decrease in orbital debris impact probability.

3.3.4 Module Commonality Requirements

The self-shielding factor for each Space Station module varies with the relative configuration of the other modules. Because sections of each module will be shielded by other modules from the directional debris flux, they need only be protected against the nearly omni-directional meteoroid flux. Thus, it may be advantageous to reduce weight by varying the shield structure with the amount of debris flux around the module. However, if the commonality concept is extended to sizing the dual-wall structure for the entire module (saving DDT&E costs and reducing spares/maintenance parts), the thickest bumper (i.e., heaviest) would have to be used for the entire module. In other words, commonality will force some of the module's bumper to be over-sized, which implies a weight penalty. This commonality/weight tradeoff also applies to every module and resource node since self-shielding will vary for each. Variable shielding configurations should be considered for the pressurized modules.

3.3.5 Orbital Debris Velocity Distribution

Although the average relative orbital debris velocity in 500 km altitude, 30° inclination orbit is about 9.3 km/sec, the velocity range is 0-16 km/sec, as given in Figure 3-7 (48). Only about 5 percent of the orbital debris in this orbit will impact at less than 4 km/sec, but over 20 percent will impact at less than 6.5 km/sec. Thus, a significant fraction of orbital debris at Space Station altitude will impact in the velocity region where peak shock pressures are less than enough to completely melt the projectile and bumper fragments. The lethality of these solid fragments can be lessened by substitution of different bumper materials either to increase peak shock pressures (such as ceramics), decrease the density and size of the fragments (such as graphite/epoxy or other fiber-reinforced composite), or a laminate or combination of the two.

3.3.6 Penetration Criterion

The penetration criterion described in Section 3.3 did not clearly specify whether the module shield/hull structure should be designed to prevent a complete perforation (or clear hole) in the pressure hull, or should also prevent spall into the interior. The spall from the inside of an aluminum hull can include a number of solid fragments with a clear damage potential to internal equipment racks or crew (12, p.472). One sure (but heavy) way to prevent spall is to increase the thickness of the pressure hull. For a certain set of impacts into a single aluminum wall, an empirical correlation developed to estimate the thickness to prevent complete perforation indicated the wall had to be twice the crater depth while the wall thickness to prevent the onset of spall was three times the crater depth (73). However, there are potentially more mass effective alternatives than to increase the pressure hull thickness by up to 50 percent. Spall can also be suppressed by the addition of a polyethylene liner on the inside of the module as illustrated in Figure 3-8. A similar concept, boron impregnated polyethylene, is used on the interior of military tanks and other armored vehicles as a combination anti-spall and anti-radiation liner (see Figure 4-3). A necessity, though, is a clear definition of the no penetration criterion in terms of perforation prevention or perforation/spall prevention because of it effect on design of the module meteoroid/debris protection system.

3.4 Effects of Hypervelocity Impact

Figure 3-9 illustrates a hypervelocity impact on a Space Station module by a relatively large orbital debris fragment, assumed in this case to be a 1 cm diameter aluminum particle striking at 9 km/sec. The main external effects of this and smaller debris impacts will be a bright impact flash and the release of a large amount of secondary particles.

The flash from hypervelocity impacts has been studied (71, 72). From equation 6 in Ref. 71, the light intensity, I (ergs/s), is proportional to projectile mass, m (g), and velocity, v (km/s), to the 4.1 power:

$$I = c1 * m * v^{4.1}$$

The coefficient, c1, was derived from graphs in Ref. 72 as 10^7. Using this equation, a 1 cm aluminum projectile at 9 km/sec impact will release over 5 million lumens, or the light intensity of over 3,000 hundred-watt light bulbs.

The amount of material ejected from impacts on aluminum structures has also been studied (42, 74, 75). More work needs to be done to better quantify the mass and size distribution of secondary particles, but these previous studies have demonstrated that hypervelocity impacts on thin plates remove 10 to 100 times their own mass from the target material, with approximately 30 percent of this mass ejected from the front surface of the target (for aluminum targets). The front surface ejecta then becomes secondary particles which could potentially collide immediately with other adjacent Space Station structures or might eventually contribute to orbital debris.

If the secondary particles have the correct geometry to immediately strike additional Space Station elements, as portrayed in Figure 3-9, they have the potential, because of their high velocity, to cause damage in their own right. All elements on Space Station exposed to primary impacts from meteoroids and debris should also consider the flux of secondary particles in their design. A previous study estimated the secondary flux will contribute approximately 10 percent to the primary flux (42). The amount and size of secondary mass released in the impact is dependant on the type of material impacted, with non-metallic materials tested in this study ejecting significantly less damaging material than aluminum.

3.5 Integral vs. Deployable Shields

The standoff distance for an integral (non-deployed) bumper is constrained to between 4 and 6 inches by the payload bay envelope of the Shuttle and the desire to maximize internal volume for crew and equipment. Increased standoff distances could substantially decrease the thickness and weight of the inner wall. Investigations for Apollo and Skylab determined that non-optimum pressure wall thicknesses varied as the inverse of the square root of standoff distance and that spacing was effective up to 100 times the design projectile diameter (3, 17, 33). Thus, for a 1 cm diameter design particle, increasing the standoff from 10 cm (4") to 100 cm would reduce the non-optimum pressure wall thickness and weight by 66 percent. There is a slight advantage to increasing standoff distance from 4" to 6" as indicated by the results of experimental impact testing given in Figure 3-10.

Standoff distances greater than 6" would require deployable or erectable shields; EVA becomes necessary for an erectable option, structural support complexity increases for a deployable option, and both involve higher DDT&E costs. Shield structural support mass for an erectable or deployable option may actually decrease since it would not have to react launch loads.

It appears that the current European Columbus module design utilizes a deployable aluminum bumper with a 20 cm standoff from a composite pressure hull (52, p.191). An early bumper deployment study (4, p.47) concluded that inflatable or expandable structures comprised of flexible materials offered many deployment advantages including low weight, small pre-deployment volume, and simple erection procedures. Because of the large mass savings from greater standoff distances, options for deployable or erectable bumpers should be studied.

3.5.1 Augmented Protection

Augmented protection for the modules is a compromise between integral and deployable/-erectable shields that may combine the advantages of both options. The principle of augmented protection is to proceed along the current design path of an integral shield except to add appropriate exterior scaring to accommodate additional shielding at a later date. Additional shielding could then be added after the modules were on-orbit if: (1) it was determined that adequate original integral shielding to meet the 10-year 0.9955 no penetration criterion was not possible due to weight constraints, or (2) that updates of the orbital debris environment definition required a severe increase in debris protection capability, or (3) additional shielding was necessary to meet the 30-year 0.9955 no penetration "design goal".

The scars could be as simple as several tapped-hole fittings positioned along the outside of the module bumper. These scars would allow additional shielding to be erected in EVA by first mounting 100 cm long graphite/epoxy tubes (with a screwed end-fitting on one end) into the holes, then attaching the shield to this light weight frame. The augmentable shield could be either rigid or flexible; rigid bumpers would not require as much framework (and scars) to keep in place, while flexible bumpers would be easier to package, launch, and install.

Since the orbital debris environment currently drives the module wall design, it is reasonable to assume that augmentable shields need only be designed to protect from orbital debris. This implies that additional shields need not completely encircle the modules to protect from omnidirection meteoroids; but that they only need protect the front and flanks of the modules from the highly directional orbital debris (front is in the direction of flight). Because the Shuttle docks at the nodes in front of the modules, the augmentable shields may only be positioned along the sides of the modules that face the solar arrays. Because these two sides of the group of pressurized elements contain most of the area exposed to orbital debris impact, just augmenting the protection in these areas is probably enough to significantly reduce the probability of penetration, although this should be studied in more detail. If this proves so, scars will be required only on one side of the common modules.

The original integral shielding design will without question meet the 0.9955 no penetration criterion for a certain time period. Deploying or erecting the additional shielding can wait until the penetration probability approaches the limit of the requirements. Scars can not wait, however, but must be designed and installed prior to launch. This requires early development and verification work.

3.6 Bumper Support Structure

In a proposed common module design by Martin Marietta, the shield support structure mass was 25 percent of the bumper mass (278.9 kg and 1128.8 kg, respectively) for each module (68). The support material in their design was graphite phenolic. In a Boeing design, thermal isolation pads are used between the support pieces and bumper suggesting the material for shield supports is probably metallic (70, p.40). The application of graphite composites for the bumper supports should be considered because of weight advantages over aluminum, inherent thermal isolation capability, and lower hypervelocity impact fragmentation risk.

Support structures for either integral or deployable bumpers should be constructed of low density materials to minimize the destructiveness of the large, solid fragments that would be produced from a direct impact on these relatively massive structures by meteoroids or debris particles (25, p.51). An excellent bumper support structure candidate is graphite/-epoxy, which is almost half the density of aluminum. Not only would a direct impact produce far less damaging particles than aluminum (dust vs. fragments - Ref. 42), but graphite/epoxy would also be extremely strong, rigid, light weight, have a low coefficient of thermal expansion, and depending on fiber, could either conduct heat or thermally isolate the bumper from the pressure hull. Low modulus carbon fiber composites have relatively low thermal conductivities (4 Btu-ft/hr-ft^2-°F) while high modulus carbon fiber composites have thermal conductivities about one third of aluminum's (32 vs. 99 Btu-ft/hr-ft^2-°F for Al 6061-T6). Thermal isolation, which would decouple the module from the external thermal environment, is preferred.

3.7 Atomic Oxygen Protection

Atomic oxygen interactions with organic and some metallic materials in low Earth orbit have resulted in material recession, degradation of optical and thermal coatings, and conversion of conductive coatings to nonconductive oxides. In general, materials containing only carbon, hydrogen, oxygen, and nitrogen have high reaction rates. Silicones and fluorinated polymers such as Teflon are basically stable. Metals, except for silver and osmium, resist atomic oxygen erosion (53-55).

The ceramic materials evaluated as bumpers in this study would not require protection from atomic oxygen. However, certain other materials tested, such as graphite/epoxy and Kevlar, would require protection against atomic oxygen erosion and degradation. Several atomic oxygen protection coatings have been proposed for the Space Station graphite/epoxy truss tubes including thin bonded aluminum foil (0.002"--which contributes less than 5 percent to the total weight of the tubes), vapor deposited aluminum, sputtered coatings, and silicone or teflon coatings (56-58). Coatings such as these could be applied to organic based bumper systems without incurring significant weight penalties. If coating technology developed for graphite/epoxy tubes can be applied to a composite bumper system, the impact of DDT&E costs for a bumper atomic oxygen coating would probably be minimal. However, flight hardware production costs would probably be greater.

3.8 Radiation Degradation and Protection

Some materials, such as Kevlar, Teflon, and many other organic compounds, are susceptible to ultraviolet radiation degradation. Metallic coatings to protect against atomic oxygen attack would be effective in UV protection of these materials.

The pressure hull of each module provides adequate protection from radiation (70, p.31). Therefore, alternative materials for meteoroid/debris shielding does not conflict with the radiation protection requirement for crew.

3.9 Thermal Control

The Space Station modules will have a passive thermal control system using multilayer insulation (MLI) and exterior coatings or finishes to decouple the module from the external thermal environment and to reduce the heat rejection load on the central thermal control system (52, 59). No integral radiator/bumper design is currently anticipated. Earlier, it was thought that some portion of the U.S. Laboratory and Habitation module's exterior will probably support a low-temperature, body-mounted radiator (52 p.215, 59 p.3-24) for active thermal control during the assembly phase of the station, and that a likely objective of thermal control efforts would be to develop an integral radiator/bumper design (64 p.568). This is no longer required. However, passive external coatings, other than an anodized surface treatment for aluminum shields, will be exposed to erosion or cracking/-flaking by small micrometeoroids and debris and may need testing to verify their longevity.

3.10 Repairability

In a ten-year lifetime, each common module's bumper (192.2 m^2) will suffer approximately 30 penetrations if the bumper is made of 0.09" thick aluminum bumper, or nearly 600 penetrations if made from 0.035" thick aluminum (see Table 3-3a and Table 3-3b). Based on experimental data for impacts on thin aluminum targets (12, p.117), it is estimated that the largest hole in the bumper will be 1.9 cm and 1.0 cm diameter for the 0.09" and 0.035" thick aluminum bumpers, respectively, after ten years.

Because most of the multilayer insulation (MLI) is positioned against the outside of the pressure hull, the debris cloud resulting from an impact on the bumper will spread over a large area of the MLI. Holes of the maximum size calculated may result in significant damage to the MLI between the bumper and inner wall. Cumulative damage to both MLI and bumper surface coatings may eventually affect module thermal control or increase the heat load on the central thermal control system to an unacceptable extent (59). Also, as the number of holes in the bumper increases, the probability of an impact centered on an existing hole in the bumper, which would impinge directly on the pressure hull, increases.

Thus, repairs to the bumper may become necessary at some point. However, no criterion that specifies what constitutes unacceptable bumper coating or module MLI damage exists to our knowledge. If repairs are necessary, they will be difficult on-orbit because they must be made by an EVA astronaut who would probably have to replace sections of aluminum bumper and MLI. Current efforts are directed at developing integrated bumper/MLI designs and EVA procedures for on-orbit repair (68). Current bumper designs incorporate on-orbit removable panels with quarter-turn quick release attachments to the standoff elements for easier change-out. Alternatively, the bumper could be repaired after returning the module to Earth for other refurbishment.

Certain composites under consideration for bumper evaluation may have some advantages in repairability. Thermoplastic/graphite fiber composites are being evaluated by the military because they are tougher than epoxy composites and are easier to repair. A Torlon/graphite fiber fighter wing is being built for the Air Force to test a concept for simplifying battle damage repair. It has been reported that heating the thermoplastic resin after an impact causes it to reflow around the reinforcing fibers, bringing strength back to nearly 100 percent (60). Presumably, a patch of thermoplastic backed by MLI and faced with a reflective aluminized coating could be inserted into a hole in a thermoplastic/fiber composite bumper by an EVA astronaut. Then using a microwave or thermal heating device, the astronaut would complete the repair process by heating the plug to reform the bumper.

Other composites under consideration may reduce the size of the hole. The ESA Giotto vehicle used a Kevlar/epoxy-foam sandwich inner wall because perforations in the front wall were partially closed by fibers that "fluffed" back into the hole after impact (25, 36). Other fiber reinforced composites may have similar properties. For instance, thin graphite/epoxy plates perforated by aluminum projectiles at 7 km/sec (30) had hole diameters approximately 25 percent less than predicted for equal areal density aluminum plates using the formula for hole diameter by Gehring (12, p.117).

Potential hypervelocity impact research needs are: (1) to develop a damage criterion that defines the required conditions for on-orbit removal of damaged bumper panels (2) to find alternative bumper materials or repair techniques that would minimize on-orbit EVA repair activities.

3.11 Current Module Wall Design

Both major WP-01 contractors have proposed shielding configurations similar to that shown in Figure 3-11a (68, 70). An aluminum (6061-T6) shield at a 4.5" standoff from a 0.125" thick aluminum (2219-T87) pressure hull. Multilayer insulation between the bumper and backwall provides thermal protection. The basic difference has been in shield thickness: with Boeing at 0.04", Martin Marietta at 0.08", and Marshall favoring (and testing) a 0.063" shield (69).

A distinguishing feature of the pressure hull is the attached waffling illustrated in Figure 3-11b. Waffling provides panel stiffness for shell stability during launch and landing. The waffle blades are 0.875 - 1.26" high and 0.09" - 0.12" thick in the Boeing and Martin Marietta designs, respectively.

The multilayer insulation is described by Martin (68, p.3-4) as 20 layers of double aluminized mylar interleaved with Dacron net spacers and sandwiched between Kevlar cloth, and by Boeing (47, p.42) as 30 layers of 0.0005" Kapton. Martin Marietta, Boeing, and Marshall have all reported that testing indicated MLI significantly increased the penetration resistance of dual-wall aluminum configurations. In the 4-7 km/sec projectile velocity range, the test data indicated that 30-layer MLI resulted in a mean improvement in the particle size causing backwall penetration of approximately 0.2 cm (Figure 3-1).

Figure 3-3. Common Module Dimensions and Surface Area (Ref. 51, 52)

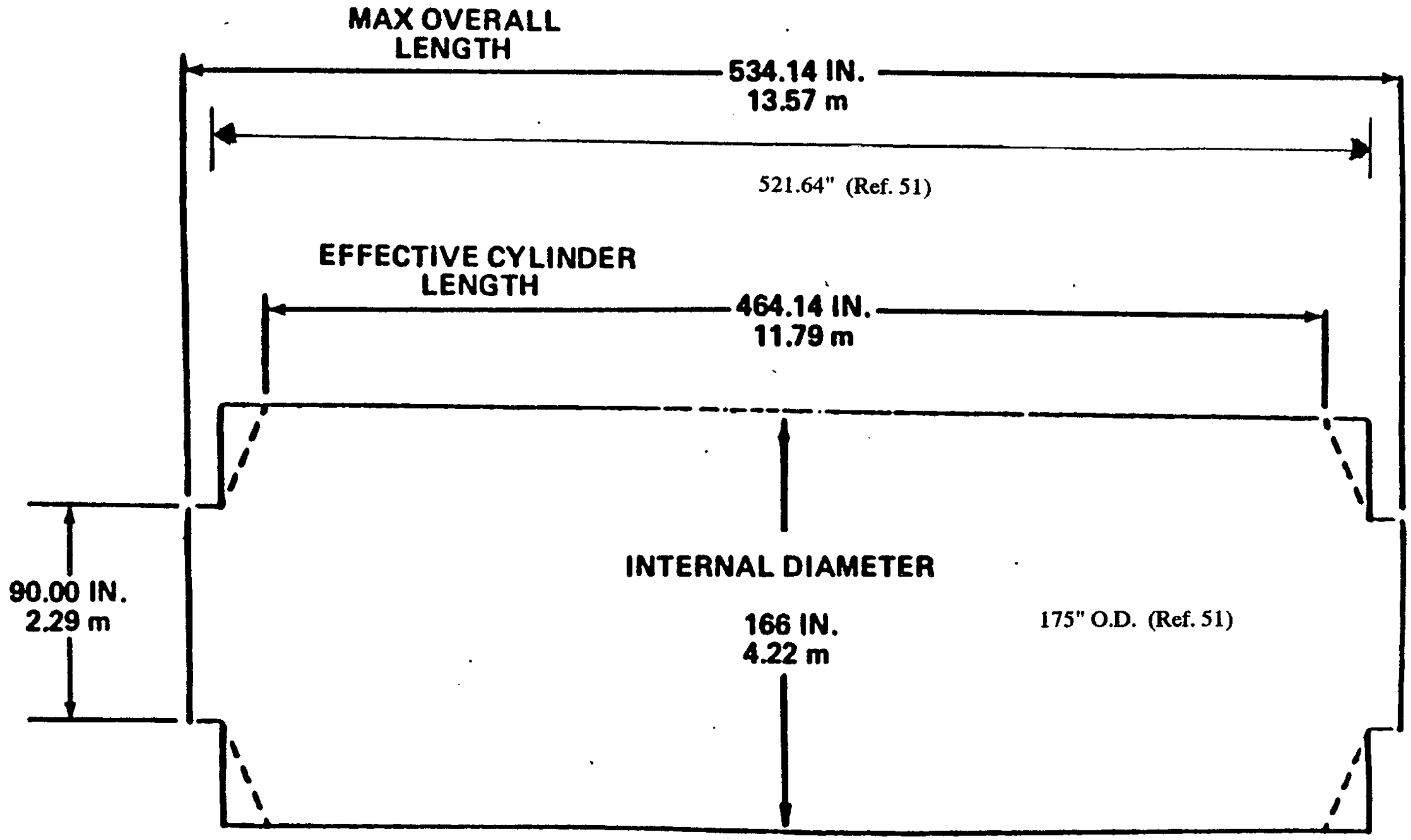

MODULE DIMENSIONS

(Ref. 52, p.219)

$$
\begin{aligned}
S_{end} &= \pi (R_1 + R_2) [(R_1 - R_2)^2 + h^2]^{0.5} \\
&= \pi (87.5 + 45)[(87.5 - 45)^2 + 28.75^2]^{0.5} \\
&= 21358.744 \text{ in}^2 = 148.32461 \text{ ft}^2 \\
&= 13.7798 \text{ m}^2
\end{aligned}
$$

$$
\begin{aligned}
S_{cyl} &= \pi D h' = \pi \times 175 \times 464.14 \\
&= 255{,}174.29 \text{ in}^2 = 1772.04 \text{ ft}^2 \\
&= 164.6283 \text{ m}^2
\end{aligned}
$$

$$\text{Total S.A.} = S_{cyl} + 2\,S_{end} = 192.188 \text{ m}^2 = 2068.69 \text{ ft}^2$$

Table 3-2. Space Station U.S. Common Module Meteoroid and Orbital Debris Design Particle Size

PARAMETER	VALUE
Meteoroid density (g/cc)	0.5
Orbital Debris dens. (g/cc)	2.8
Meteoroid Ave. Vel. (km/s)	20
Orb. Debris Ave. Vel (km/s)	10

Earth's radius (km)	6378.145
Station orb. altitude (km)	500
Alt. in Earth radii	1.078392
Earth defocusing factor	0.968596
Earth shielding factor	0.713070

Impact probability calculations for Space Station U.S. Hab & Lab modules with 10 and 30 year lifetimes

Item	Surf. Area (m^2)	Life-time (yr)	combined met&deb no impact prob-ability	crit mass (g)	crit. deb. dia. (cm)	debris flux @&> crit.mass #/m^2-yr	debris no impact prob. critical mass&>	critical deb.& met. energy (joule)	crit. met. mass (g)	crit. met. dia. (cm)	meteoroid flux at and > than crit.mass #/m^2-yr	meteoroid noimpact probability crit.mass &greater
US Lab Module	192.2	30	0.9955	9.06	1.835	7.510E-07	.99568	452937	2.26	2.053	4.526E-08	.9998
or												
Hab/Ops Module	192.2	10	0.9955	2.52	1.198	2.198E-06	.99578	126125	6.31	1.341	2.153E-07	.9997
Half-shielded Module	96.1	10	0.9955	1.13	0.918	4.299E-06	.99588	56744	2.84	1.027	5.705E-07	.9996

Figure 3-4. Spatial Distribution of Orbital Debris Flux (Ref. 48)

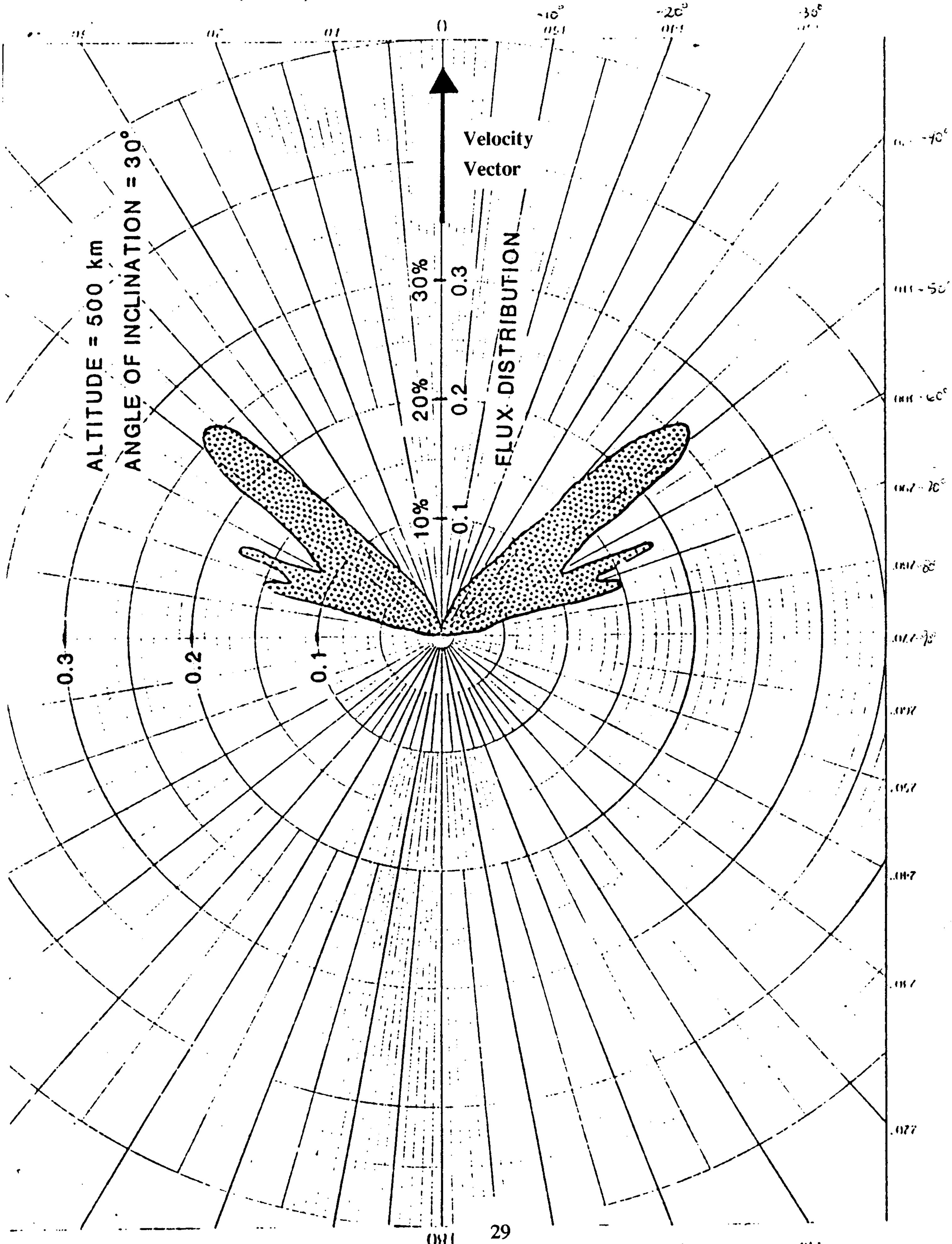

Figure 3-5. Critical Orbital Debris Size for the Space Station Common Module as a Function of Surface Area Exposed to the Debris Flux (i.e.: equal to 1 - self-shielding factor)

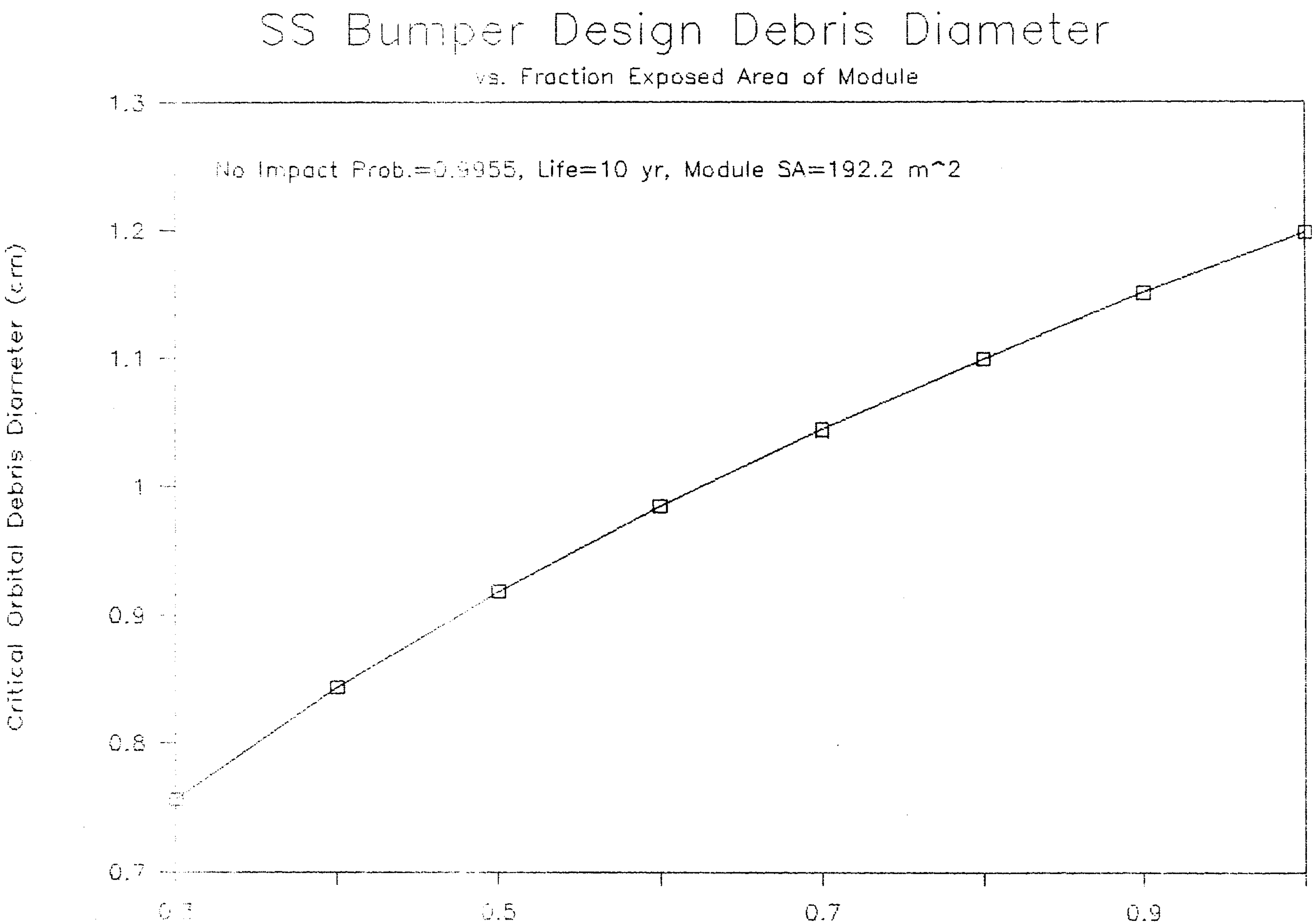

ORIGINAL PAGE IS OF POOR QUALITY

Figure 3-6. Module Orientation (Top View)

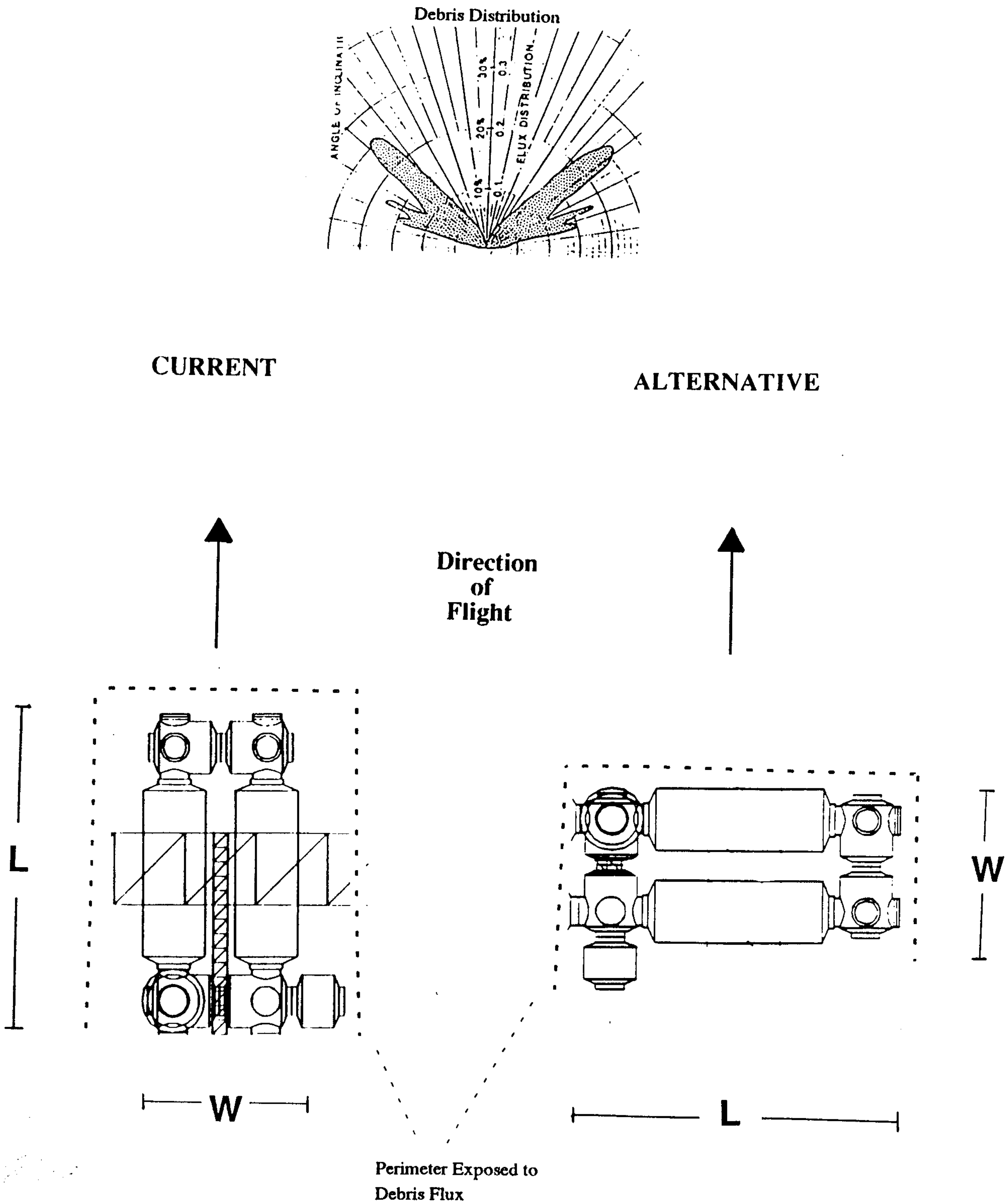

Figure 3-7. Orbital Debris Velocity Distribution (Ref. 48)

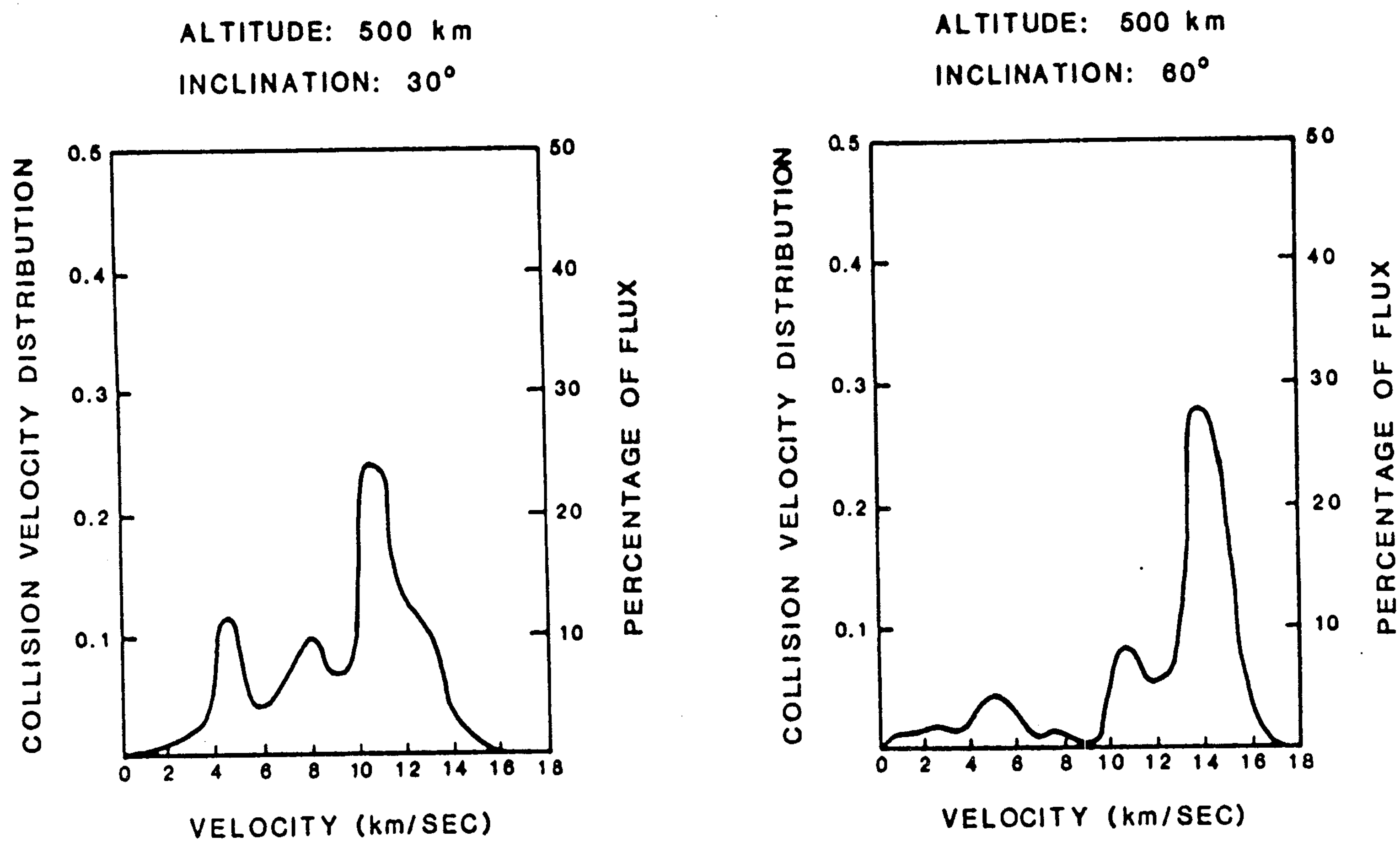

Figure 3-8. Effects of Laminates on Spall and Penetration (Ref. 12)

Effects of laminates on spall and penetration—flat targets. (a) 12-mm Al; (b) Al–polyethylene; (c) Al–Cu; (d) Cu–Al. Projectile: 3-mm Al spheres. Velocity: 7.4 km/sec. All targets equal weight per unit area—3.4 g/cm^2.

Figure 3-9. Depiction of Hypervelocity Impact Effects

Figure 3-10. Impact Testing with 6" Spacing (Ref. 47)

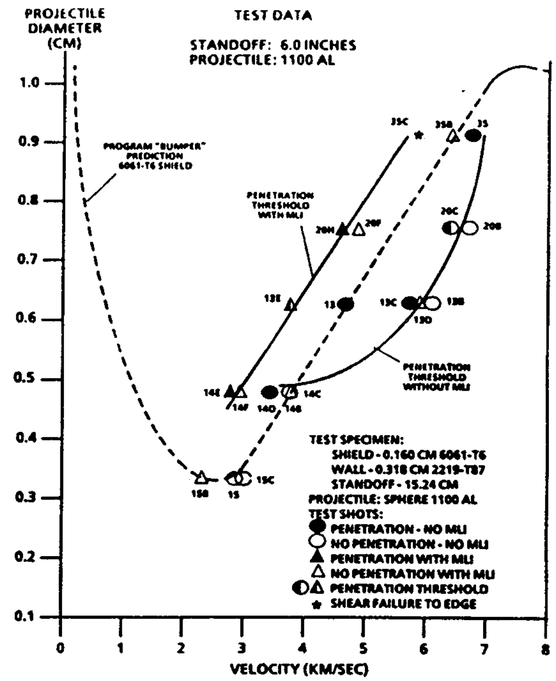

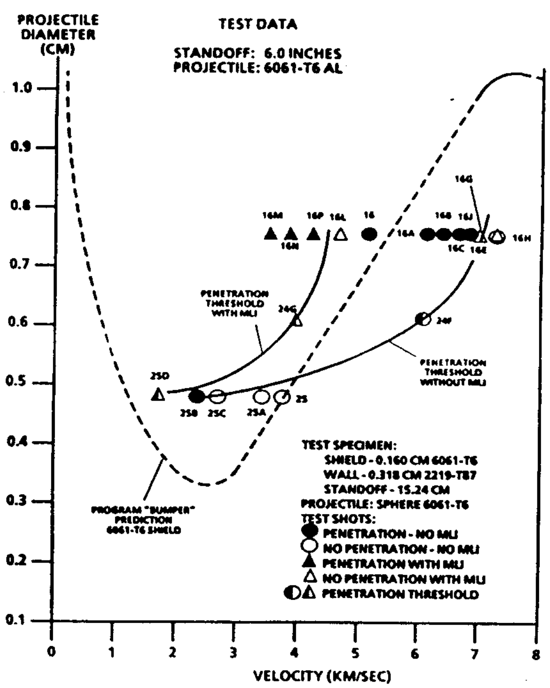

Table 3-3a. Expected Perforations and Maximum Hole Size from Meteoroid and Orbital Debris Impacts into a 0.09" Thick Aluminum 6061-T6 Plate

Al 6061-T6 Thickness	0.23 (cm)	0.09 (in)	
Density (g/cc)	2.713		
Hardness, Brinell	110		
Young's Modulus (dynes/cm^2)	6.83E+11		
Surface Area (m^2)	192.2		
Design Lifetime (yr)	10		
		Meteoroid	Debris
Particle Density (g/cc)		0.5	2.8
Particle Velocity (km/s)		20	9.3
Particle Critical Diameter (cm) to avoid perforation (from Cour-Palais, Ref. 43)		0.0663	0.0477
Particle Mass (g)		7.63E-05	1.59E-04
Particle Energy (J)		15.26	6.87
Particle Flux (#/m^2-yr) with critical diameter and greater		9.17E-03	7.43E-03
Number of Penetrations (total surface area over orbital lifetime)		18	14
Total Number of Penetrations		32	
Percent Flux		55.26	44.74

Average Critical Energy (J) 11.51
above which results in perforation of the aluminum bumper from Meteoroid & Orbital Debris Impacts

Max. Particle Size (cm)	0.146	0.137
Max Hole Size (cm) (Ref.6,p.117)	1.90	0.93

Table 3-3b. Expected Perforations and Maximum Hole Size from Meteoroid and Orbital Debris Impacts into a 0.035" Thick Aluminum 6061-T6 Plate

Al 6061-T6 Thickness	0.09 (cm)	0.035 (in)	
Density (g/cc)	2.713		
Hardness, Brinell	110		
Young's Modulus (dynes/cm^2)	6.83E+11		
Surface Area (m^2)	192.2		
Design Lifetime (yr)	10		

	Meteoroid	Debris
Particle Density (g/cc)	0.5	2.8
Particle Velocity (km/s)	20	9.3
Particle Critical Diameter (cm) to avoid perforation (from Cour-Palais, Ref. 43)	0.0271	0.0195
Particle Mass (g)	5.22E-06	1.09E-05
Particle Energy (J)	1.04	0.47
Particle Flux (#/m^2-yr) with critical diameter and greater	2.38E-01	7.07E-02
Number of Penetrations (total surface area over orbital lifetime)	457	136
Total Number of Penetrations	593	
Percent Flux	77.07	22.93

Average Critical Energy (J) 0.91
above which results in perforation of the aluminum bumper from Meteoroid & Orbital Debris Impacts

	Meteoroid	Debris
Max. Particle Size (cm)	0.146	0.137
Max Hole Size (cm) (Ref.6,p.117)	1.08	0.55

Figure 3-11a. Shield, Spacing, and Pressure Hull Configuration (Ref. 70)

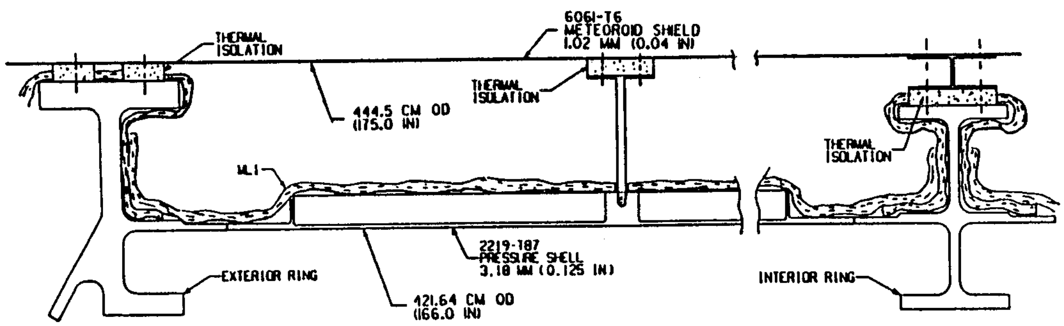

Figure 3-11b. Common Module Pressure Hull Waffling Pattern (Ref. 70)

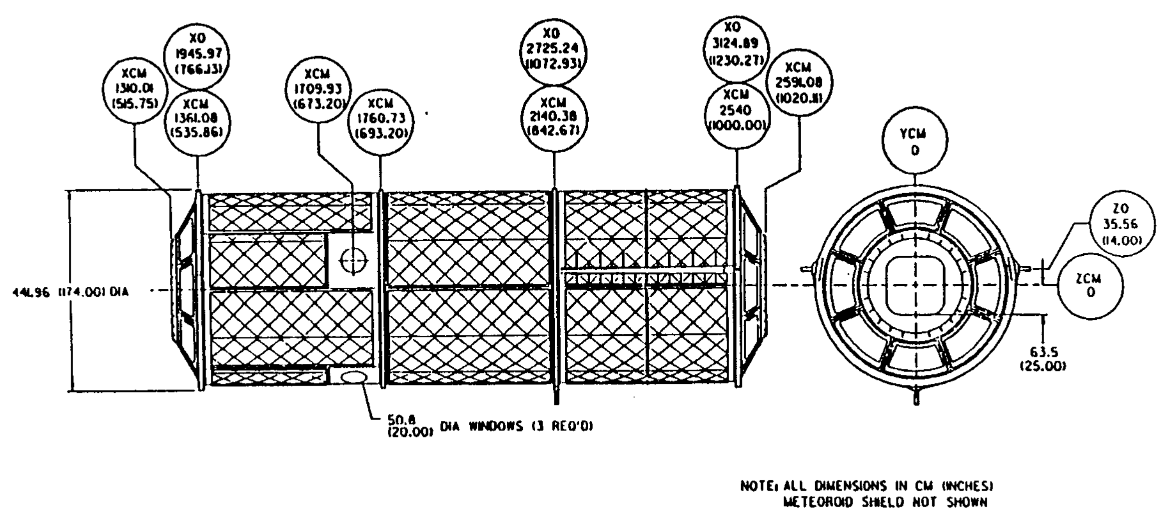

4.0 Shielding Methods and Materials

A spacecraft or other object can be protected from hypervelocity impact by either active or passive techniques. The target can actively protect itself by maneuvering away from the threat or by destroying it. As a backup, or--as in the case of large, flexible space structures--the most likely alternative, the target can be hardened or shielded to protect underlying structures from damage. For centuries, passive protective techniques have been employed to protect men and equipment. With the advent of shaped charges that produce hypervelocity jets of molten metal, conventional armor protection has evolved to produce designs having possible applications to space structure protection. The following section describes some current armor designs using materials that could be applied to meteoroid/debris bumpers.

4.1 Conventional Armor Protection

Shaped charge jets and explosively formed projectiles have reportedly attained velocities in excess of 10 km/sec (6, p.9-73; 45). To protect combat vehicles from these and lower velocity threats without incurring severe weight penalties, ceramic armor was developed and found to be lighter than steel armor for equivalent ballistic protection. Recent high priority Army demonstration projects include the Composite Turret and Composite Infantry Fighting Vehicle (CIFV) programs (78, p.38) which have established the advantages of using composite structural armor in place of aluminum in medium combat vehicles.

Ceramic armor disrupts the projectile by reducing its kinetic energy through erosion and by absorbing the impact energy through fracturing and shock compression. Protection is improved by increasing the amount of ceramic fractured, thereby increasing the energy absorbed during the impact. A backup plate holds the ceramic in place and allows the stress waves to spread away from the impact point. Figure 4-1 illustrates different stages of impact into a ceramic target.

Ceramic armor consists of a ceramic frontface with metallic or glass fabric reinforced plastic backing. An example of current armor design is a combination of alumina (Al_2O_3) backed by an equal thickness of aluminum (41, p.801). Monolithic ceramics such as boron carbide (B_4C), silicon carbide (SiC), and titanium boride (TiB_2) are armor candidates because they are less dense than alumina.

Although it is desirable to fracture the ceramic, present trends to improve ceramic armor performance are in toughening the ceramic matrix by adding reinforcements in the form of continuous fiber, whiskers, or platelets. Reinforcement fibers and whiskers include graphite, SiC, Al_2O_3, and silicon nitride (Si_3N_4), as well as metals. As given in Figure 4-2, the reinforcements significantly increase the toughness of the ceramic (46). The toughened ceramic increases the fracture energy and absorbs more of the projectile energy than monolithic ceramic does. Other toughening mechanisms include adding a dispersed phase in the reinforced ceramic (platelets or single crystal flakes of SiC or other ceramics), pre-loading the surface in compression, and adding a surface energy-absorbing layer to the composite.

A concept of modern ceramic armor as a laminate or composite is given in Figure 4-3. The ceramic is contained within special armor boxes between two metallic plates. Apparently, the box holds the ceramic tiles in place and may also put them in compression, increasing their effectiveness. The ceramic tiles overlap and are surrounded by a ballistic rubber that toughens the ceramic system by absorbing some of the impact induced shock deflections and mechanical strain. A metallized polyethylene liner protects against spall as well as providing radiation protection. Metal particles of lead or boron are used in these liners to enhance the neutron-stopping effect of polyethylene, for protection from nuclear weapon effects.

Figure 4-1. Phases of Impact into Ceramic/Metal Target (Ref. 6, p.6-90)

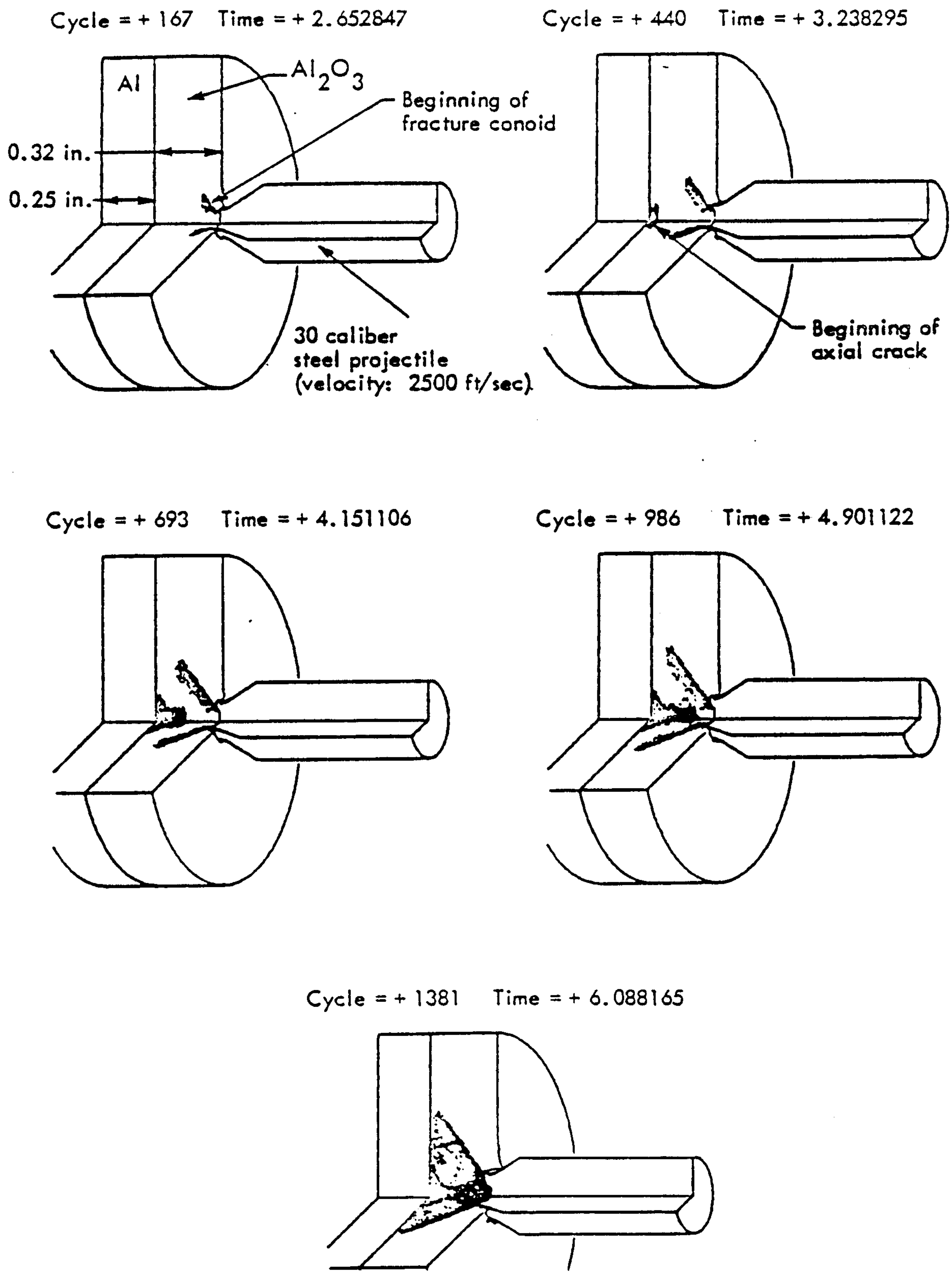

Figure 4-2. Toughness of Ceramics Increase with Reinforcement (Ref. 46)

TENSILE STRESS STRAIN CURVE

AVCO 5CS-6/MAS, NIPPON CARBON NICALON/LAS III REINFORCED COMPOSITES LAS III W/O REINFORCEMENT (0/90 LAY-UP)

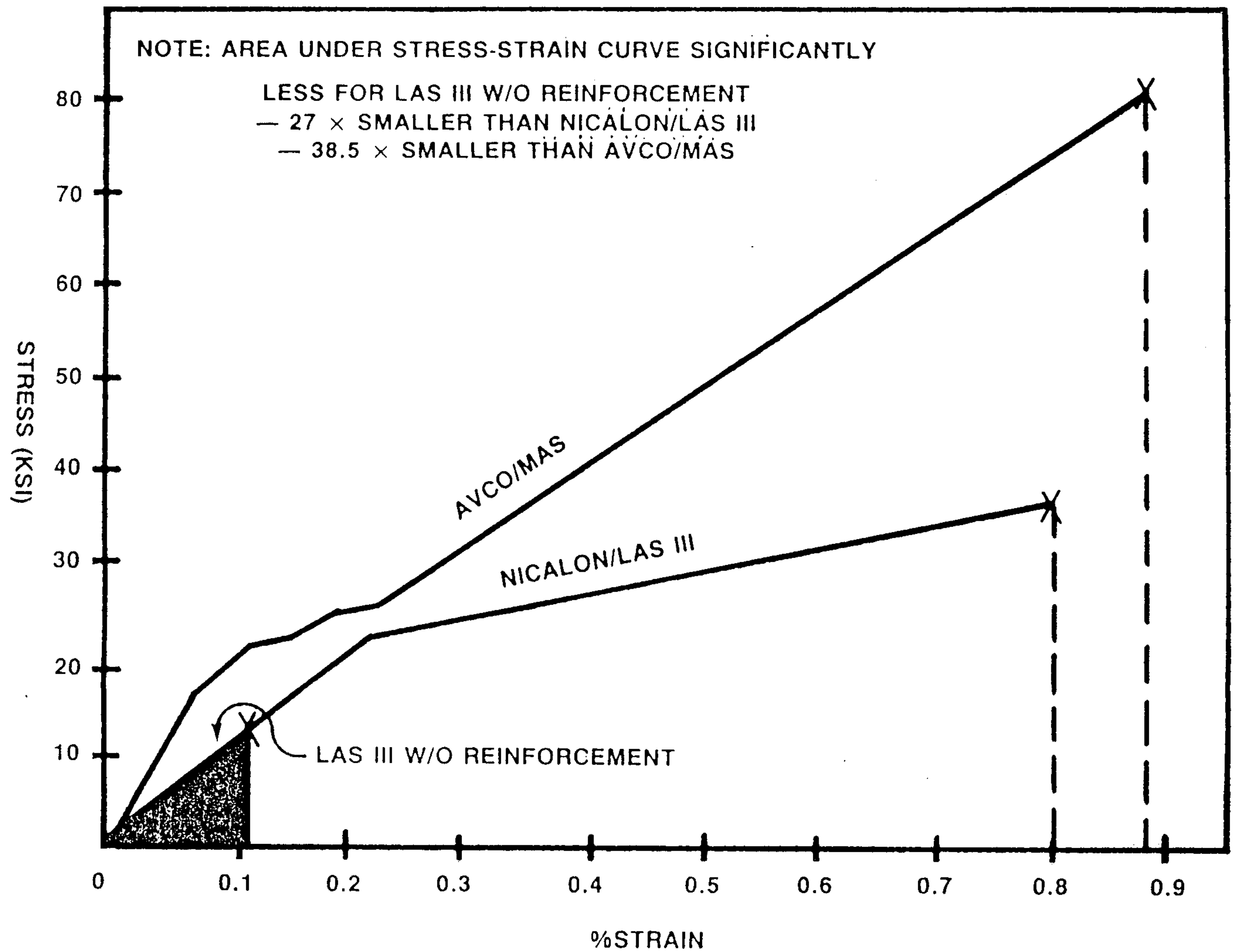

Figure 4-3. Modern Concepts of Ceramic Composite Armor (Ref. 45)

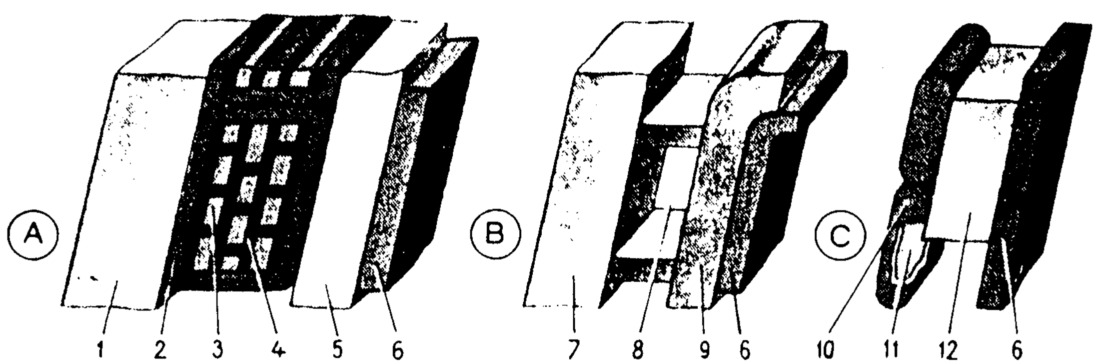

A = composite armour: 1) main armour, 2) special armour "boxes", 3) ceramic tiles, 4) support material, 5) secondary anti-spalling armour, 6) anti-radiation liner. B = spaced armour: 7) external plate, 8) spacing, 9) internal plate, C = reactive armour: 10) reactive elements, 11) explosive, 12) main armour.

4.2 Material Property Effects on Bumper Effectiveness

This section describes the effects of physical and material properties on bumper performance. As described in this section, several materials have characteristics and properties that make them good bumper candidates, including fiber-reinforced composites, ceramic/aluminum composites, and laminates. Supporting calculations are presented in Section 4.3. Specific material candidates are given in Section 4.4.

4.2.1 Density

Several experimental studies have been conducted to investigate the effects of bumper material properties on overall shield operation (5,8,13,31,34,40). Swift and Hopkins (5) impacted equal areal density bumper made from a variety of materials with aluminum projectiles at 7 km/sec and determined the ballistic limit thickness of a backup plate. They found that performance decreased for bumpers with densities less than approximately 2 g/cc. As discussed in Section 3.1, to defeat orbital debris and meteoroids, the impact with the bumper must generate shock waves strong enough to melt or vaporize the projectile. Apparently, the projectile in Swift's experiments was not completely shocked for impacts on the low density bumpers tested and fragments of solid projectile impacted the second wall. Further discussion of Swift's work can be found in Appendix B.

4.2.2 Hugoniot Equations-of-State

The peak shock pressure developed at impact can be used as a discriminator to compare the effectiveness of various bumper materials in disrupting a projectile. Impact pressures for aluminum projectiles at typical hypervelocity impact conditions (7 km/sec) were determined using a one-dimensional reverse Rankine-Hugoniot technique described in Appendix C. As given in Table 4-1 and Figure 4-4, high density metals and ceramics resulted in the highest impact pressures and would be expected to fragment, melt, or vaporize an impacting projectile to a greater extent than other materials at nearly any velocity. (As given in Table 3-1, incipient and complete melting for Aluminum impacts takes place at approximately 650 and 900 Kbar, respectively.) This approach resulted in the same impact pressures as the analysis presented in Section 4.3.2 and Appendix A. Of particular interest in Figure 4-4, are those materials that generate high impact pressures (above the pressure necessary to produce melting of an aluminum projectile) at the lowest density. Ceramics are good bumper candidates by this analysis, especially boron carbide since it produces a 35 percent greater shock pressure with a density 10 percent less than aluminum, but also alumina and silicon carbide.

4.2.3 Bumper Thickness to Projectile Diameter Ratio

Although the state of the projectile is important for assessing the effectiveness of various bumpers in protecting underlying structures, the debris plume that strikes the second wall also contains significant amounts of bumper materials. In some investigations, 75 percent of the debris cloud was projectile material (25), but a recent study on graphite/-composite and aluminum thin targets found that only 5-10 percent of the debris plume was projectile (42). The difference is partly due to the different shield thickness to projectile diameter ratios (t_S/d) used in the studies (0.25 for Ref. 25 vs. 1.4 for Ref. 42). It is not too surprising that as t_S/d increases, the amount of bumper material in the debris plume also increases. Because the shield material dominates as the size of the projectiles impacting the dual-wall structure decrease, the state of the bumper material in the debris plume becomes more important in assessing protective ability at higher t_S/d ratios.

4.2.4 Fusion Energy and other Thermodynamic Properties

Thermodynamic properties of the bumper determine the phase of the bumper material in the debris cloud to a large extent. The most important is heat of fusion; others include melting temperature, vaporization energy, and vaporization temperature. The lower these properties are, the more likely the debris cloud will contain molten or vaporized bumper particles, which are far less damaging to the protected surfaces than solid fragments. Section 4.3.1 and Appendix B evaluate different materials based on these properties.

4.2.5 Density of Solid Fragments in the Debris Cloud

No matter what materials are used for the bumper, there is no question that solid bumper fragments will be produced in many collisions during its orbital lifetime because there are many more orbital debris and meteoroid particles smaller than the design particle. Substantial portions of the bumper will remain unshocked in these collisions. Bumper materials which produce low density, finely-divided fragments are preferred in this case to reduce the ability of these fragments to penetrate the second wall. Certain fiber-reinforced composites exhibit these characteristics. For instance, graphite/epoxy targets, due to their brittleness, produce a multitude of epoxy powder and fine fibers upon impact (25, p.51; 42; 61) and impacts into Kevlar composites generate low density conglomerates of fibers or "fluff" (8, 36). Since a typical criterion for determining inner wall thickness is based on resisting penetration from fragments generated in non-optimal collisions, bumpers which generate less threatening fragments can conceivably reduce inner wall thickness.

4.2.6 Impact Velocity

As mentioned in Section 3.3, over a fifth of all orbital debris particles intersecting the Space Station orbit have velocities below 7 km/sec, insufficient to generate shock waves intense enough to completely melt the particle (assuming the projectiles are aluminum and using Table 3-1). Collisions between these particles and an aluminum bumper will produce a spray of solid projectile and bumper fragments, similar to Figure 2-1a, having serious damage potential to the module hull. As explained in Section 3.1 and shown in Figure 3-2, solid fragments are more damaging to underlying structures than liquid or vapor particles.

One approach to decreasing the destructiveness of these fragments is to substitute bumper materials, such as ceramics, which produce more intense shock waves and a greater likelihood of melting the projectile (Table 4-1). Borrowing from conventional armor techniques, the ceramics would be backed by an appropriate material to contain the ceramic, or toughened by adding appropriate reinforcements to prevent it from shattering too quickly. Aluminum is widely applied as a backing material; graphite/epoxy would also be a prime candidate because of its low potential to produce large, damaging fragments. Note that the ceramic bumper debris will most likely not be melted but should be highly disrupted. The backing for the ceramic will reduce the hazard from these solid fragments by reducing the number of ceramic fragments ejected toward the inner wall.

Another approach is to use composites of high-density fibers, fabrics, or dispersed phases (chopped fibers, whiskers, platelets, etc.) in a low-density matrix. The high density component, having a large shock compressibility ratio (particle velocity to shock velocity ratio), would produce impact pressures high enough to melt or disrupt the projectile. The low density matrix would produce less-damaging debris particles. For instance, graphite/epoxy composites with a density of 1.58 g/cc have exhibited advantages over aluminum bumpers under some impact conditions (62). These findings seem to clash with the assumption, drawn from some literature sources (5, 31, 34), that materials having a density of less than 2 g/cc do not make good bumpers. Presumably, the explanation is that graphite fibers produce strong enough shock waves to melt or substantially disrupt projectiles in the velocity range of the experiments (5-7 km/sec) because of their relatively high density of 1.83 g/cc and good shock compressibility characteristics. Data in Marsh (14) suggests that graphite fibers are highly compressible; compressing 10-20 percent until they attain theoretical graphite density.

Other possible candidates for improving low velocity bumper performance while maintaining good high velocity protection are fiberglass, fiberglass graphite/epoxy hybrids, other ceramic reinforced materials, and laminates of ceramics and fiber reinforced composites. To maximize initial shock pressures and reduce the debris hazard to the second wall, the high density material should face toward the oncoming projectile, while the low density material faces the second wall. Although laminates are proposed here for testing as bumpers, the best application of laminates may be for the module pressure hull (38, 39).

Shock wave dynamics must be considered to understand potential applications of laminated materials. An impact induced compressive shock wave that moves into a laminated structure will be partially transmitted and partially reflected at the laminate interface. The relative amounts transmitted and reflected depends on the difference in shock impedance of the two materials, a characteristic which is related to density differences between layers. More of the shock wave is transmitted as this difference narrows (12, p.474). In a bumper, the portion of the compressive shock wave reflected at the laminate interface will attenuate the compressive shock wave in the projectile sooner than the rarefaction from the rear surface of the bumper. Thus, for the over-designed condition (i.e., at low projectile velocities and/or at projectile diameters less than the design particle), which normally results in large fragments of bumper material projected at high speeds toward the second wall, the top laminate now acts more nearly like an "optimal bumper" by reflecting the shock wave sooner and dispersing the projectile in a nearly optimal fashion. Since the transmitted shock wave is less intense, the bumper fragments are projected at a lower velocity and are therefore less damaging.

Although a laminated bumper should perform better for non-optimal conditions, it will not shock a design-size projectile as well as a non-laminated bumper and will therefore allow larger projectile fragments through for this relatively infrequent case. Thus, laminated bumpers are not expected to perform as well as monolithic structures, unless the density difference between the two materials is small. If the density difference is small, a properly designed laminated bumper has potential advantages over an equal areal density monolithic bumper by improving low velocity impact protection while providing equal high velocity protection.

4.2.7 Density Effects on Debris Cloud Dispersion Angle

As explained in more detail in Appendix B, the dispersion angle of the debris cloud is expected to be a function of the bumper thickness to projectile diameter ratio (t_S/d), as well as the impact velocity to target acoustic velocity ratio. The dispersion angle should be narrow for targets having a low t_S/d ratio (12, p.118). Thus, for a constant areal density bumper and given design particle size, low density bumpers will have higher t_S/d ratios and a greater potential for a wider debris dispersion angle. The benefits of a wider dispersion angle are analogous to a greater standoff distance without the additional weight of longer supports or internal volume trades.

Table 4-1. Peak Shock Pressures for Bumper Materials Impacted by Aluminum (1100) Projectiles at 7 km/sec--calculated using one-dimensional approximation (see Appendix C)

	Material	Density (g/cc)	Impact Pressure (Mbar)
1	Platinum	21.44	1.95
2	Tantalum	16.66	1.90
3	Gold	19.24	1.86
4	Tungsten Carbide	15.02	1.85
5	97% Uranium 3% Mo	18.45	1.79
6	Copper	8.93	1.53
7	Stainless Steel 304	7.90	1.51
8	Steel (Vascomax 250)	8.13	1.50
9	Lead	11.35	1.50
10	Iron	7.86	1.47
11	Cadmium	8.64	1.44
12	Boron Carbide B_4C	2.40	1.36
13	Alumina - Hot Pressed	3.94	1.29
14	Alumina-Coors-15% Silica	3.66	1.17
15	High Density Glass-Shott	5.09	1.12
16	Titanium	4.53	1.12
17	Silicon Carbide SiC	3.12	1.11
18	Al 7075	2.80	0.99
19	Al 2024	2.79	0.99
20	Al 1100	2.71	0.98
21	Al 6061	2.70	0.98
22	Mullite	2.67	0.87
23	Teflon	2.15	0.84
24	Quartz	2.65	0.82
25	Graphite, Pyrolytic	2.21	0.77
26	Pyrex	2.23	0.75
27	Carbon-Phenolic Composite	1.35	0.73
28	Mg Alloy AZ31B	1.78	0.73
29	Graphite	1.88	0.73
30	Magnesium	1.74	0.72
31	Glass SiO2	2.20	0.70
32	Teflon	2.15	0.66
33	Hi Density Polyethylene	0.95	0.63
34	Silastic Rubber RTV521	1.37	0.61
35	PVC (Boltron)	1.38	0.58
36	Polyimide	1.41	0.57
37	Graphite 3D Weave	1.52	0.56
38	Epoxy	1.20	0.56
39	Acrylic	1.19	0.55
40	Nylon	1.15	0.53
41	Polycarbonate Plastic	1.19	0.51
42	Water	1.00	0.47
43	Water Ice	0.91	0.43
44	Douglas Fir Wood	0.54	0.26

Figure 4-4. Peak Shock Pressure as function of Target Density for Aluminum (1100) Projectiles at 7 km/sec.

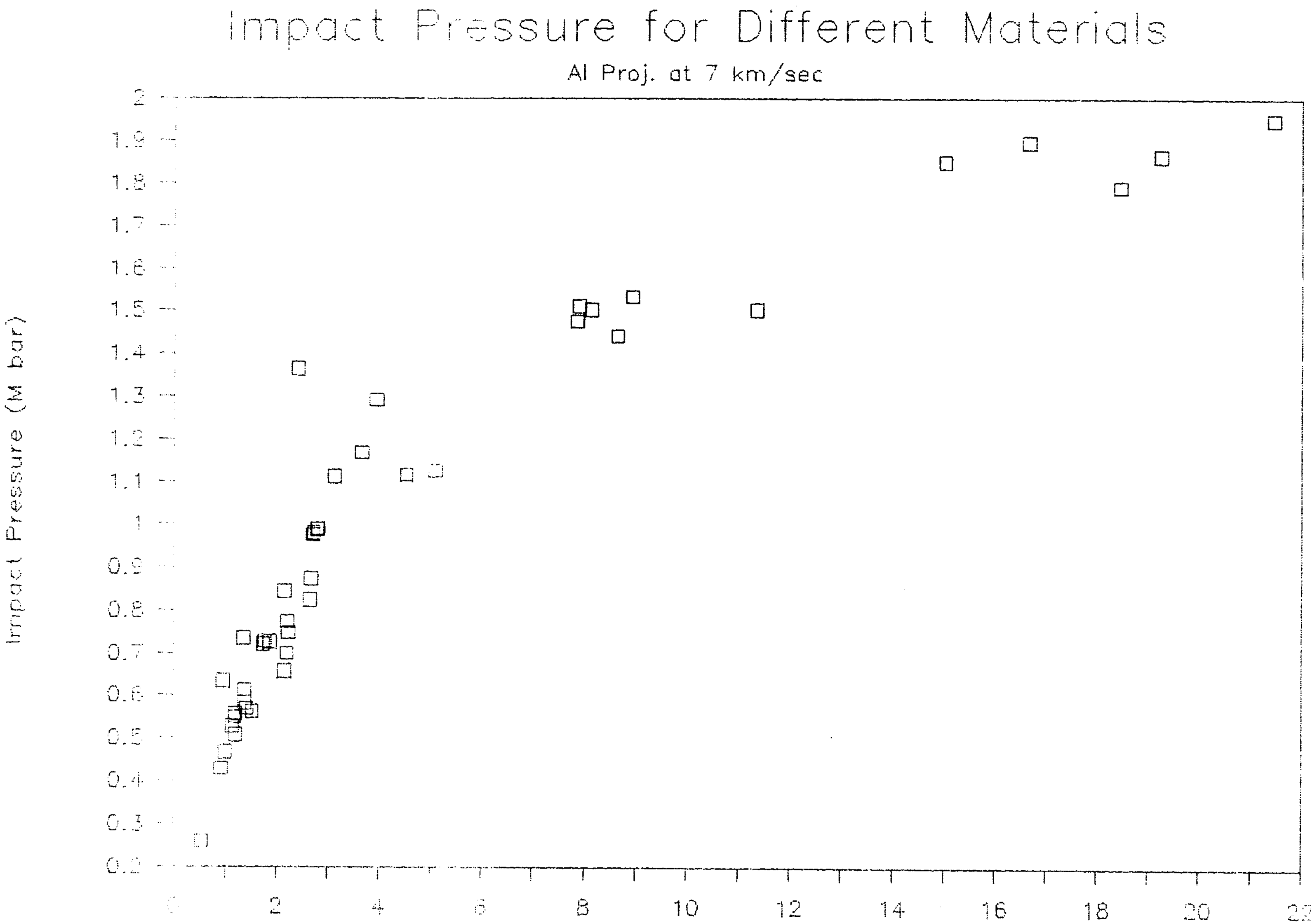

ORIGINAL PAGE IS
OF POOR QUALITY

4.3 Analysis of Shielding Materials

Early in this study, analytical tools were developed in the form of models and computer programs to assist in selecting candidates for a test program of meteoroid/orbital debris shield materials. Two models are discussed in the following sections. The first compares materials based on a figure-of-merit constructed from material properties and empirical correlations found in literature sources. The second compares materials based on peak shock pressures generated in the impact, energy partition and the resulting state of the projectile material, and optimal bumper areal density as a function of velocity that results in shocking the entire projectile at the peak shock pressure. This second model was developed from one-dimensional analysis using Rankine-Hugoniot relationships and linear approximations to equations-of-state.

4.3.1 Empirical (Figure-of-Merit) Model Results

An empirical model was developed for evaluating the performance of candidate bumper materials using a selection criterion based on material property relationships derived from References 2-6.

For space applications, it is desired to compare the efficiencies of various shielding materials for a constant weight launched to orbit. Thus, the model assumes that the shielding areal density (mass per unit area) is kept constant by varying the thickness of the shielding for materials of different density. The model was designed to quickly select appropriate bumper candidates based on their physical properties. No attempt was made to include parameters other than bumper properties that are also important in evaluating the effectiveness of the entire passive protection system such as spacing, inner-wall properties, or projectile properties. Appendix B contains a detailed discussion of the model; a summary of the approach follows.

Although the primary purpose of the bumper is to disrupt (fragment, melt, vaporize, disperse) a projectile through shock processes, it does possess some penetration resistance of its own. Thus, impacts below a certain threshold will not penetrate it. The model calculates a factor, R, that expresses the ability of a fixed areal-density bumper to resist penetration in terms of the bumper's speed of sound (C), hardness (BH), and density (p):

$$R = C^{0.67} * BH^{0.25} * p^{0.5}$$

This equation is based on empirical penetration equations into semi-infinite targets. The model assumes that resistance to penetration into thick targets is a useful gauge to differentiate the ability of various thin target materials to breakup projectiles.

The model includes thermodynamic properties of the bumper, which determine to a great extent the phase of the particles in the debris plume projected behind the bumper. For bumper materials sufficiently dense to produce shock waves intense enough to melt or vaporize the impacting projectile, Swift and Hopkins (5) found that bumper materials that melted in the collision required less second-wall thickness than materials that only fragmented. Bumper materials that vaporized required less second-wall thickness than materials that melted. Therefore, to maximize the probability that the bumper material melts or vaporizes from the impact, the shield material should have a low melting temperature, T_m, and latent heat of fusion, H_m, as well as low vaporization temperature, T_v, and latent heat of vaporization, H_v.

Because aluminum (6061-T6) is the current baseline candidate for Space Station module shielding, ratios of the thermodynamic properties of candidate bumper materials and aluminum were determined and a figure-of-merit, FOM, that combines thermodynamic and mechanical properties was developed ("(al)" stands for aluminum property):

$$FOM = \{Tm\ (al)/Tm * [Hm\ (al)/Hm]^{.5} * [Tv\ (al)/Tv]^{.1} *$$

$$[Hv\ (al)/Hv]^{.1} + 0.25 * R\}\ p(al)/p$$

The purpose of the figure-of-merit was to suggest possible alternate bumper materials, but it should be regarded as arbitrary until a complete series of impact tests has been done to evaluate its predictive ability. Details of the factors involved in formulating the FOM is given in Appendix B. A number of materials were evaluated using this expression to determine their effectiveness as bumpers. A list of these materials in order of overall effectiveness is given in Table 4-2. One of the limitations of the empirical model is that it is primarily useful in selecting only metallic materials. Composites are anisotropic; it is not possible to specify a single value for many of their material properties because they vary throughout the structure. Therefore, another model was developed to analyze the potential effectiveness of a wider range of bumper materials, including composites.

Table 4-2. Bumper Material Comparison by Empirical Figure-of-Merit

(from material properties in Appendix B)

Rank	Material	Figure-of-Merit
1	Mg and Mg alloys	2.03
2	Lead	1.90
3	Cadmium	1.89
4	Al (6061-T6)	1.25
5	Antimony	0.91
6	Iron/Steel	0.69
7	Titanium	0.67
8	Nickel	0.65
9	Copper	0.52
10	Tungsten	0.46
11	Tantalum	0.29
12	Platinum	0.29

4.3.2 Analytical Model Results

A technique utilizing one-dimensional shock theory was developed for evaluating the performance of candidate bumper systems. The approach is intended to screen a large number of potential bumper materials with a minimum amount of calculation. The procedure provides analytical closed form solutions to determine three items:

1. Peak shock pressure experienced by the bumper and shield.

2. The amount of internal energy left in the projectile after collision, in effect the temperature and phase of the projectile.

3. The minimum thickness of shield necessary to produce the peak shock pressure in the entire projectile.

Conventional hypervelocity impact theory is applied with Rankine-Hugoniot relations for materials on either side of a shock front and linearized equations of state relating shock velocity and particle velocity. The procedure assumes that the criteria for a successful bumper is one that subjects the entire mass of a threatening projectile to a pressure sufficient to thermally decompose or melt it. The calculated optimum bumper thickness can then be used to select candidate test materials.

Any projectile/target material combination having the requisite hugoniot constants available in literature can be selected. The optimum bumper thickness is determined as a function of projectile velocity, as illustrated in Figure 4-5. At a typical experimental velocity of 7 km/sec, the optimal areal density was used to catalog a number of materials as given in Table 4-3. A detailed discussion of the model, calculations, and program user's guide is given in Appendix A.

Figure 4-5. Impact Pressure, Fraction of Projectile that Melts, and Optimum Bumper Areal Density as a function of Projectile Velocity

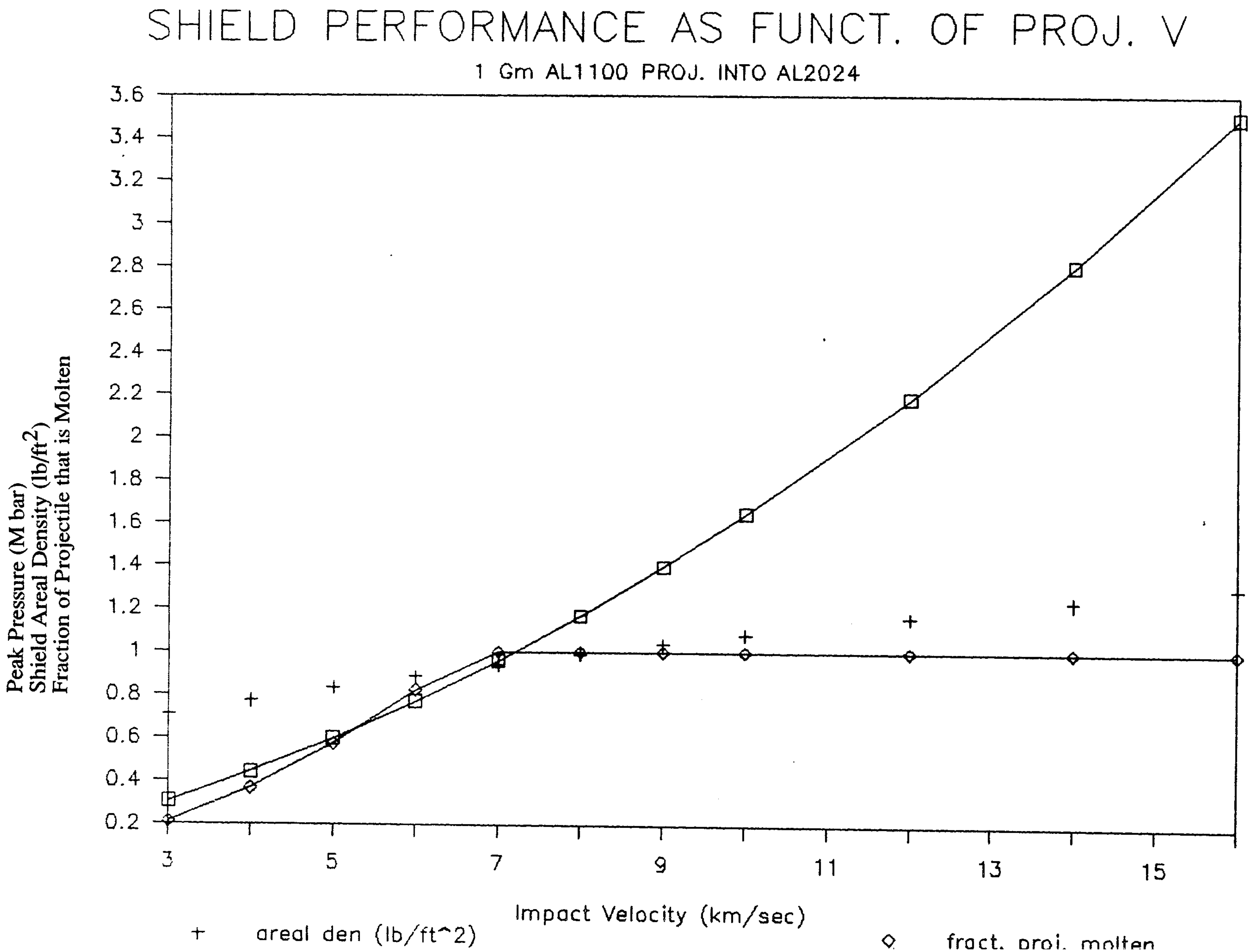

Table 4-3. Results of Analytical Model

Material Selection Based on Fraction of Projectile that Melts and Optimal Bumper Areal Density
(Calculations based on one-dimensional impact approximation
with a 1 gm, Al 1100, projectile at 7 km/sec)

Rank	Material	Density (g/cc)	Impact Pressure (Mb)	Opt. Areal Density (lb/ft^2)	State of Al Proj.
LIGHTER THAN BASELINE (IMPACT PRESSURES HIGH ENOUGH TO MELT PROJ.)					
1	Composite C-Phen.	1.35	0.72	0.606	Partially Molten
2	Magnesium	1.74	0.71	0.612	Partially Molten
3	Mg AZ31B alloy	1.78	0.72	0.621	Partially Molten
4	Glass Silica	2.20	0.69	0.630	Partially Molten
5	Glass Pyrex	2.23	0.74	0.670	Partially Molten
6	Mullite Al6Si2O13	2.67	0.86	0.812	Molten
BASELINE					
7	Al 6061	2.70	0.95	0.929	Molten
HEAVIER THAN BASELINE					
8	Aluminum 1100	2.71	0.96	0.934	Molten
9	Aluminum 2024	2.78	0.96	0.940	Molten
10	Aluminum (Ref.10)	2.75	0.97	0.944	Molten
11	Aluminum 7075	2.80	0.97	0.950	Molten
12	Aluminum 921T	2.83	0.98	0.961	Molten
13	Silicon Carbide	3.12	1.09	1.137	Molten
14	Titanium	4.53	1.10	1.195	Molten
15	Glass High Dens.	5.09	1.10	1.229	Molten
16	Alumina Coors	3.66	1.15	1.247	Molten
17	Alumina Hot press	3.94	1.27	1.468	Molten
18	Cadmium	8.64	1.40	1.871	Molten
19	Iron (Ref.10)	7.86	1.44	1.930	Molten
20	Steel 1018	7.85	1.46	1.985	Molten
21	Lead	11.35	1.47	2.088	Molten
22	Steel-Vasco250	8.13	1.47	2.007	Molten
23	Steel S/S 304	7.90	1.48	2.026	Molten
24	Copper	8.93	1.50	2.102	Molten

4.4 Candidate Bumper Materials

A list of candidate bumper materials proposed for the initial screening tests at JSC is given in Table 4-4. Justifications for considering some of these materials were given in previous sections. Basically we should consider an all-metallic baseline; low-density, fiber reinforced composites, ceramics, laminates and hybrids; dual-bumper systems; and allow testing of several unspecified materials. The composite laminate materials that have been specified are designed to create large peak shock pressures which will vaporize or fragment the projectile into fine particles. The resulting shield particles should be in vapor or molten form, or in a finely divided solid form (dust) to minimize damage to the inner wall.

The Space Station module design baseline that was available at the start of this study consisted of a 0.063 inch aluminum (6061-T6) bumper, 4.5 inch standoff (from outside surface bumper to inside inner-wall), and 0.125 inch aluminum (2219-T87) inner wall (69). A 30-layer section of insulation installed against the inner wall was also part of this configuration.

The following alternate bumper configurations and materials were selected for testing based on their potential to save weight while providing increased protection to the Space Station crew.

<u>Metallic Candidates</u>. Besides the baseline aluminum alloy (6061-T6), aluminum wire cloth could potentially produce nearly the same impact shock pressure to disrupt the projectile with less areal density.

In addition, a corrugated aluminum bumper will be tested. A normal impact on the inclined face of a corrugated bumper will result in wider dispersion of the debris plume expanding behind the bumper. Previous tests of oblique angle impacts on plates has demonstrated that the projectile material tends to expand behind the bumper along its original flight path while the bumper material is released normal to the plate. Thus, oblique angle impacts spread the debris across a larger area of the backwall, producing essentially the same dispersive effect as a larger standoff distance. But oblique impacts on flat plates are more damaging to underlying surfaces than normal impacts because larger more destructive fragments are commonly produced. This is due to lower normal peak shock pressure and to a higher t_s/d ratio (12, p.495). Thus, the corrugated bumper must be thinner; both to have the same areal density as a flat plate, and to have the correct t_s/d ratio since the projectile is traveling at an angle through the bumper. The projectile should "see" the same amount of material with an inclined impact on the corrugation as it would in a normal impact on an equal areal density flat plate. If a corrugated bumper is impacted by a critical design size projectile striking at what would be an oblique angle for a flat plate (essentially hitting at a normal angle to the corrugation), the projectile will not be as completely disrupted as it would be for a normal impact on a flat plate. However, the resulting solid projectile fragments will be traveling at an oblique angle to the backwall (along their original flight path) and would need to traverse a thicker section of the backwall to completely penetrate it. Thus, a properly designed corrugated bumper could potentially protect equally well against all angles of impacts.

Another material proposed for testing consists of metallic microspheres dispersed in a polymeric matrix. The dense metallic material would disrupt the projectile without itself producing large damaging fragments because it starts out as a collection of microspheres. The matrix would be needed to hold the microspheres in place. A tungsten/silicone rubber material was available for the first testing phase. This material contains 77 weight percent tungsten microspheres (randomly shaped, 2-4 micron diameter) bound in a silicone (type VMQ) matrix. A light (3.7 oz/yd^2) Nomex pajama-check cloth backs the material. Other metals could potentially be substituted for tungsten, such as titanium (quarter the density of tungsten), aluminum, or magnesium.

The empirical and analytical models indicated magnesium alloys were potentially better bumper materials than Al 6061-T6 (Tables 4-2 and 4-3). Magnesium alloys have always been prohibited from applications in spacecraft interiors due to the corrosive environment within the cabin (65). However, an external application such as a magnesium bumper would only require protection against corrosion prior to launch, such as exposure to salt-water environment at the Cape. The thermal protection coating could probably be designed to protect against pre-launch corrosion as well. AZ31B, a candidate magnesium alloy, is a weldable alloy containing aluminum (3%) and zinc (1%) available in a wide variety of shapes including plate and sheet. Magnesium will be tested in the next phase of the study.

Dual Bumper Systems. This study tested three wall configurations containing a dual bumper system. During Apollo, multiple wall structures were tested, but it was concluded that more than two walls offered no increased protection. In fact, in some cases the addition of a third sheet increased the vulnerability of the structure (12, p.481). The intermediate bumper tends upon failure to cause a restriction in the spread of the debris. This causes a higher load per unit area upon the backwall than would occur if the debris were allowed to spread.

In this study, an aluminum mesh was used as the outer bumper to disrupt the projectile into fine fragments without substantially slowing the fragments. The intermediate bumper then only had to disrupt/vaporize these relatively small fragments, made more possible by not slowing the fragments. A solid plate of the same thickness as the wire gauge could have been substituted for the mesh, but with a substantial weight penalty and with the possibility of substantially slowing the resultant fragments, making it more difficult for the intermediate bumper to melt or vaporize them. Alternatively, a thinner solid plate of the same mass as the wire could have been used as the outer bumper, but it is unlikely the projectile would have been fragmented as successfully as with the mesh.

The thickness of the mesh wire and the mesh opening were sized to break the projectile into fragments no greater than the mesh opening. The intermediate bumper thickness was then determined by this maximum expected fragment size.

The distance between the outer and intermediate bumpers was set at a quarter of the standoff distance between outer bumper and backwall. This distance was selected because it was thought that the debris from the initial impact on the outer bumper would have a relatively low dispersion angle because of the low t_s/d ratio (see Section 4.2.3). A larger distance would thus not allow sufficient expansion of the debris plume from the intermediate bumper before it struck the backwall. Fragments from the outer bumper impact will not strike the intermediate bumper at precisely the same time due to differences in velocity and initial spatial location. Therefore, a minimum spacing between outer and intermediate bumper seemed required to allow the fragments to separate and strike the intermediate bumper somewhat independently; too small a spacing and a concentrated impulse load from the outer bumper might plug-out a small area in the intermediate bumper allowing later fragments through unimpeded. To make comparative assessments meaningful, the standoff distance between the outer bumper and backwall for three wall configurations must stay the same as the standoff distance in dual wall tests.

Metal Matrix Composites. A combination of aluminum (6061-T6) and ceramic whiskers (SiC) could potentially produce higher impact pressures and greater disruption of an impacting projectile than just Al 6061-T6. The whiskers are tiny, typically 8 to 20 μin (20 to 51 nm) in diameter and about 0.0012 in (0.03 mm) long. Thus, the whiskers would not themselves be expected to result in destructive debris fragments upon impact. Also, less aluminum would be in the debris plume impacting the second wall. Therefore, at a given projectile velocity, greater projectile disruption and less damaging bumper debris is expected for the Al-SiC metal matrix composite than a pure Al 6061-T6 bumper. Metal matrix materials were tested to verify this hypothesis.

Ceramics and Ceramic Composites. Ceramics produce greater impact pressures and are thus capable of disrupting an impacting projectile to a greater extent than pure Al 6061-T6 (Table 4-1). As explained in Section 4.1, alumina is a standard material in ceramic armors and is therefore proposed for testing. The alumina would be backed by a suitable material, such as graphite/epoxy or aluminum, which would support the ceramic while producing minimally destructive debris particles. Other candidates include lower density ceramics, such as B_4C and SiC, which result in lower optimum areal density bumpers (Table 4-3). Recent ceramic armor work is in the area of ceramic-ceramic composites, such as SiC whisker or fiber reinforced SiC, which improves penetration resistance and provides multiple impact protection. These new materials are quite expensive, however, and will be reserved for the next phase of testing.

Graphite Composites. The highest rated material in Table 4-3 was a graphite/phenolic composite. Hugoniot data for other composite materials was not available so other graphite composites (graphite/epoxy (G/E), graphite/thermoplastic, etc.) were not evaluated but are expected to have similar or improved impact properties as discussed in Section 4.2. Thus, graphite fiber reinforced plastics are proposed for evaluation. Other hybrids with graphite composites are also proposed which should increase peak shock pressures and greater projectile disruption, such as fiberglass-G/E laminate and bonded aluminum-G/E. Graphite cloth is proposed to evaluate the hypervelocity impact protection offered by a low areal density structure of graphite alone.

Organic Polymers. Evaluation of polymeric materials such as Kevlar and Spectra (polyethylene) cloth is proposed based on their use in ballistic protection for personnel and vehicles, as well as the results of analytical model evaluations. As explained in Appendix A, an energy balance indicated that these low-density materials may result in total projectile melting, whereas when considering just shock wave heating, they would not result in projectile melting (Al 1100 at 7 km/sec). If the projectile is completely disrupted, these materials could result in significant weight savings by virtue of their low density. This hypothesis was tested.

Inner Wall. The Space Station module baseline material, Al 2219-T87, is the first choice for the backwall in the evaluation testing. Other materials and structures (laminates for instance), or liners to suppress spall from the interior wall, could potentially provide more protection for less weight. They were not evaluated during this phase of testing, however, which focused on evaluating bumper materials.

Table 4-4. List of Target Materials for Bumper Evaluation Test

Metals

1. Al 6061-T6 (S/S baseline)
2. Aluminum mesh or aluminum wire cloth
3. Magnesium alloy
4. Tungsten/Silicone material
5. Others

Dual Bumper Combinations (first bumper separated by standoff from following bumper)

1. Aluminum mesh and aluminum plate
2. Aluminum mesh and graphite/epoxy plate
3. Ceramic material and aluminum plate
4. Others

Metal Matrix Composites

1. 30-35 vol.% SiC whiskers with Al 6061-T6 matrix
2. Others

Ceramics and Ceramic Composites

1. Alumina - Coors AD-85
2. Alumina and Graphite/Epoxy bonded composite
3. Monolithic SiC or B_4C
4. Reinforced SiC or B_4C
5. Others

Graphite Composites

1. Graphite/Epoxy (G/E) with and without graphite cloth
2. Graphite/Thermoplastic
3. G/E - Fiberglass hybrid (Gr cloth, G/E outer layers, Gl/E inner layers)
4. G/E - Kevlar/Epoxy hybrid (Kevlar outer layers both sides, G/E inner layers)
5. Graphite cloth or fabric
6. Al 6061-T6 and G/E bonded composite
7. Others

Polymeric Materials

1. Kevlar
2. Spectra - Ballistic protection cloth
3. Others

Inner Wall

1. Al 2219-T87 (S/S baseline) or Al 2024-T3

5.0 Test Plan

This section describes the test plan for the experimental stage of this study, including its purpose and scope, approach, target types, and capabilities of the JSC hypervelocity impact research laboratory that carried out the tests.

5.1 Objectives

The principal test objective was to evaluate the hypervelocity impact protection afforded by a broad range of shield materials that were carefully selected after applying analytical assessments. This experimental evaluation proceeded by (1) selecting a series of material candidates for shielding applications on Space Station, (2) procuring test materials with specific areal densities, and (3) conducting the initial material evaluation and screening tests with the JSC hypervelocity impact test facility.

In the phase after this study, scaled-up versions of a few of the best candidates identified in these screening tests will be tested at other impact facilities. These tests would be designed to simulate a Space Station module shield application and would be directly comparable to existing ballistic limit data for the Space Station module wall baseline. In addition, screening tests at JSC will continue on materials and configurations not tested in this phase of the program.

A general objective was to develop the methods and required baseline database to reliably and quickly compare the relative effectiveness of new and advanced materials and structures to resist hypervelocity impact damage. The results of the testing can be used by NASA to specify for a vendor the typical sample parameters (number, areal density, length and width dimensions, etc.) that are necessary to allow evaluation through comparison to known baseline results. The results of this study also provide insight into the best method of evaluating shield materials sent to JSC from various sources that differ widely from the baseline study materials in areal density and other physical properties.

5.2 Groundrules

Since this phase of the program was essentially an evaluation and screening study of candidate bumper materials, it was not important to test typical Space Station wall configurations with the JSC gun lab. Initial screening tests were performed on materials that did not have the same shield or backwall areal density or standoff distance as the baseline Space Station wall structure. These parameters did remain constant during the tests for comparative purposes. Other gun facilities will be required to validate the results of the screening tests using larger projectiles and full-scale Space Station backwalls and standoff.

Bumper material candidates were studied in this phase of the program, while inner-wall material candidates (laminates, etc.) will be studied later.

Besides continuing screening and material evaluation, subsequent phases of the shielding program will focus on the few most promising materials identified in this and other studies. Variables that could be studied include optimization of shield/backwall areal density split, oblique impact effects, projectile density and shape effects, alternative inner-wall design assessments such as liner options to minimize spall, alternative shielding configurations, and low temperature testing. The precise ballistic limits of a small number of candidate dual-wall designs could be experimentally determined by a series of shots in a later study.

5.3 Approach

The primary objective of a passive bumper/inner wall protection system is to provide the maximum protection to personnel and equipment on-orbit with the minimum mass. Thus, one method to evaluate candidate bumper materials is to compare the effectiveness of equal areal density bumpers.

The baseline for the tests used Al 6061-T6 as the shield material (same as Space Station baseline) and consisted of a bumper/inner wall optimally designed for a particular projectile energy. The optimum bumper produces the least damaging cloud of projectile and shield debris for a particular projectile energy. The optimum backwall prevents complete perforation (but not spall) with the lowest mass. (Perforations were detected optically in this study, either by microscope and/or back-light.) Thus, no lower mass bumper/inner wall configuration which prevents perforation is possible than the optimal baseline. A thinner bumper or backwall will result in perforation of the backwall.

After determining the baseline bumper and inner wall thicknesses, screening tests were performed on materials with the same areal density (mass per area) as the baseline bumper, the same standoff distance, the same impact conditions, and a thinner inner wall. Thus, any bumper materials that prevent spall and/or perforation of the backwall obviously performed better than baseline Al 6061-T6. Subsequent tests at progressively thinner backwalls can verify and quantify the improvement.

Certainly additional tests at other projectile velocities could and probably should be conducted. However, for screening as many candidate shielding materials as possible with the fewest shots (and thus at the minimum time, materials, and costs), this procedure will reliably find materials that do shield better than the aluminum baseline for at least one projectile velocity. The result is a list of promising shield materials that would form the basis for subsequent testing at a variety of velocities as well as scaled-up verification tests with a Space Station design particle (larger projectile). The list of materials can be prioritized by comparing the extent of damage to the backwall and witness plate (mounted behind the backwall to catch spall particles). Several other comparative techniques were presented in another report (66, pp.56-61).

Note, (for those whose favorite material does not perform as well as expected) the candidate materials that fail this type of screening test are not necessarily less effective as aluminum. It may mean that the bumper was just not optimized, i.e., it may be too thick, and a thinner bumper would be more effective. If Hugoniot data existed for all bumper materials proposed for testing, an optimum bumper thickness could be calculated using the method described in Section 4.2.2. Since it does not, the best alternative is to compare the materials based on the relative protection afforded by equal areal density bumpers.

5.4 Target Parameters

To define the thickness of the screening test materials, the test projectile was selected to be a 1/8" diameter Al 1100 sphere at 6 to 7 km/sec. As determined in a previous report (66, based on refs. 3 & 33), an optimal all-aluminum bumper/backwall configuration consists of a 0.032" thick Al 6061-T6 bumper, 2" standoff, and 0.063" Al 2024-T3 backwall for the chosen projectile conditions. The areal density of the aluminum shield is 0.22 g/cm^2 (0.45 lb/ft^2). Experimental testing verified that the test projectile was at the ballistic limit for this bumper/backwall combination. A detailed description of the results of tests is given in Section 6. Subsequent testing was conducted on bumper materials having a 0.22 g/cm^2 areal density, 2" standoff, and 0.05" Al 2024-T3 backwall.

The following shield materials were evaluated in this study:

1. Al 6061-T6
2. Al 5056 mesh
3. Al 3003-0 corrugated at 60° angle
4. Tungsten microspheres imbedded in silicone rubber
5. Metal Matrix (Al 6061-T6 and 35 vol. percent SiC whiskers)
6. Alumina bonded to Al 3003-0
7. Alumina
8. Silicon Carbide (SiC) cloth
9. Shuttle Tile (foamed silica with borosilicate glass coating)
10. Graphite/Epoxy
11. Al 3003-0 bonded to graphite/epoxy
12. Al 5056 mesh & Al 3003-0 plate dual bumper (w/ spacing)
13. Al 5056 mesh & graphite/epoxy dual bumper (w/ spacing)
14. Kevlar cloth
15. Classified materials

The thickness, density, and type of all unclassified materials tested in this study are indicated in Table 5-1. A more detailed description of each material is given in Section 6. Classified materials are discussed in the classified addendum to this report.

5.5 Materials for Later Screening Tests

Several other materials looked like promising candidates in our analytical assessments but were not tested in this phase of the program due to study funding limitations. They include ceramic/ceramic and graphite composites which could be included in follow-on screening tests. In addition, the results of this study indicated that dual-bumper systems incorporating a mesh as the outer bumper offered advantages over single bumpers. Alternative dual-bumper systems should also be studied.

A ceramic material that is highly recommended for inclusion in a later study is boron carbide (B_4C) reinforced with B_4C whiskers and platelets. As given in Table 4-1, B_4C produces a 35 percent greater peak shock pressure in an impacting projectile with a density approximately 10 percent less than aluminum. By adding a reinforcement to toughen the ceramic, it is less likely to shatter on impact. Because the screening tests required a bumper of a specific areal density and therefore thickness, the cost for a set of 4 reinforced B_4C test plates was estimated as $2,500 (rough-order-of-magnitude or ROM costs are given in Appendix E). Procuring materials of often non-standard thicknesses becomes prohibitively expensive. However, budgeting for material procurement must be included in planning screening tests, as the success of such tests depends on acquiring the most promising material candidates.

The results of this study indicated that graphite/epoxy was an effective intermediate bumper and we recommend further testing of graphite composites as the second shield in dual-bumper systems. A number of graphite composite materials suitable for later screening tests is given in Appendix E. Costs for these materials are in the $700-$900 range without acquiring any test spares. The preliminary results of an earlier study indicated that a graphite/epoxy balsa-core sandwich material performed better than 2219 aluminum as a backwall or pressure hull (62). Later assessments of alternative backwall configurations could include the graphite-balsa sandwich and a graphite-balsa-aluminum sandwich (a thin aluminum interior surface would minimize off-gassing and flammability concerns intrinsic with use of graphite composites for pressure hulls).

Silicon carbide (SiC) cloth should be tested as the outer bumper in alternative dual-bumper follow-on tests.

5.6 Hypervelocity Impact Research Laboratory

JSC's Hypervelocity Impact Research Laboratory (HIRL) contains two light gas launchers. The small light gas gun has a 1.7 mm launch tube bore and is capable of launching 5 mg nylon slugs (L/D = 1) at 8.5 km/sec. The medium light gas gun has a 4.3 mm bore and is capable of launching saboted 1/8" aluminum spheres (45 mg) at over 7 km/sec or 73 mg nylon slugs (L/D = 1) at 7.4 km/sec. Additional details of the capabilities for these two launchers are described in another report (76). Only the medium light gas gun was used in this study.

In screening tests of this kind (i.e., only one shot per material), it is critical that the shots be "clean". If anything but the projectile hits the target (such as sabot pieces, shear plate fragments, or even gun powder debris), the data can be seriously compromised and must be repeated (with financial, time, and limited target penalties). Fortunately, over the past several years, the JSC HIRL personnel have developed techniques and equipment that are quite reliable in producing clean shots; perfect for materials screening studies.

The lab offers other advantages. The shot-to-shot turn around time is low because of the relatively small scale of HIRL's launchers and because operating procedures have become greatly refined over the years. For instance, during this study, two and sometimes three shots per day were performed. This was also partly the result of not having to alter launcher conditions.

A valuable diagnostic tool at JSC's HIRL is a Model 330 IR, high-speed framing camera manufactured by the Cordin Company. This rotating-mirror camera operates at one million frames per second with a 5 nanosecond exposure time. It is used to verify that a shot is "clean", and provides clues to the problem for the infrequent times it is not. The real value of the camera is in assessing the state of the debris cloud (whether it contains large fragments or far less damaging smaller particles), determining ejecta and debris cloud dispersion angles and velocities, and as a cross-check of projectile velocity. Further details can be found in another paper (77).

Table 5-1. Bumper Materials for Screening Test (Phase I)

Shot	Bumper Material	BUMPER Width (in)	Length (in)	Thickness (in)	Mass (g)	Bumper Areal Dens. (g/cm^2)	Density (g/cc)	Al 2024-T3 Backplate Thickness (in)	Combined Bumper & Backplate Areal Dens. (g/cm^2)	Witness Plate Al 3003-0 Thickness (in)	PROJECTILE Al 1100 Sphere Proj. Mass (mg)	Proj. Dia. (mm)	Proj. Vel. (km/s)	Proj. Energy (J)
Aluminum Baseline (Normal Impact)														
A151	Al 6061-T6	6.0	6.0	0.032	50.60	0.22	2.713	0.05	0.56	-	45.25	3.17	6.60	986
A228	Al 6061-T6	5.5	6.0	0.032	46.53	0.22	2.713	0.05	0.57	0.008	45.09	3.17	6.39	921
A231	Al 6061-T6	5.5	6.0	0.032	46.18	0.22	2.713	0.05	0.57	0.016	45.18	3.17	6.73	1023
A150	Al 6061-T6	6.0	6.0	0.032	50.43	0.22	2.713	0.063	0.66	-	45.25	3.17	6.45	941
A236	Al 6061-T6	5.4	6.0	0.032	45.19	0.22	2.713	0.063	0.66	0.016	45.23	3.17	6.48	950
Aluminum and other Metallic Bumper Configurations														
A161	Al mesh (Al 5056)	6.0	6.0	0.120	47.20	0.20	0.66	0.05	0.55	0.008	45.29	3.17	6.50	957
A223	Corrugated Al (Al 3003-0)	5.0	12.0 (6" corrugated)	0.016	41.69	0.22	2.74	0.05	0.57	0.008	45.27	3.17	6.32	903
A226	Tungsten/ Silicone	3.75	3.75	0.04	31.11	0.34	3.38	0.05	0.70	0.008	45.13	3.17	6.56	971
A230	Tungsten/ Silicone	4.0	4.0	0.04	35.50	0.34	3.38	0.04	0.62	0.016	45.03	3.16	6.70	1011
Metal Matrix Composites (Al 6061-T6 and 35 v% SiC)														
A152	Metal Matrix	4.0	4.0	0.032	22.70	0.22	2.75	0.063	0.66	-	45.25	3.17	6.52	963
A157	Metal Matrix	4.0	4.0	0.032	22.70	0.22	2.75	0.05	0.57	0.008	45.17	3.17	6.71	1017
A220	Metal Matrix	4.0	4.0	0.032	22.64	0.22	2.74	0.05	0.57	0.008	45.34	3.17	6.46	946
Ceramics and Ceramic Composites														
A159	Alumina & Al	4.5	4.5	0.030	27.79	0.21	2.77	0.05	0.56	0.008	45.33	3.17	6.56	976
A221	Alumina bonded to Aluminum	4.5	4.5	0.030	27.79	0.21	2.77	0.05	0.57	0.008	45.22	3.17	6.30	897

Table 5-1 (Cont). Bumper Materials for Screening Test (Phase I)

Shot	Bumper Material	BUMPER Width (in)	Length (in)	Thickness (in)	Mass (g)	Bumper Areal Dens. (g/cm^2)	Density (g/cc)	Al 2024-T3 Backplate Thickness (in)	Combined Bumper & Backplate Areal Dens. (g/cm^2)	Witness Plate Al 3003-0 Thickness (in)	PROJECTILE Al 1100 Sphere Proj. Mass (mg)	Proj. Dia. (mm)	Proj. Vel. (km/s)	Proj. Energy (J)
A237	Alumina	4.5	4.5	0.020	24.93	0.19	3.79	0.05	0.55	0.008	45.25	3.17	6.40	925
A222	SiC	5.1	5.1	0.349	38.32	0.23	0.26	0.05	0.58	0.008	45.16	3.17	6.64	996
A219	Shuttle Tile	5.25	6.0	0.44	45.79	0.23	0.20	0.05	0.58	-	45.29	3.17	6.52	964
Graphite Composites														
A225	Graphite/Epoxy	6.0	6.0	0.058	53.14	0.23	1.56	0.05	0.58	0.016	45.23	3.17	6.61	988
A158	Al bonded to G/E	6.0	6.0	0.063	62.23	0.27	1.68	0.05	0.62	0.008	45.24	3.17	6.18	864
Dual Bumpers														
A224	Al mesh - Aluminum plate	5.4 5.4	5.6 6.0	0.030 0.016	10.16 22.63	0.05 0.11	0.67 2.74	0.05	0.51	0.008	45.30	3.17	6.39	925
A238	Al mesh - G/E	5.3 5.3	6.0 6.0	0.030 0.052	10.42 41.77	0.05 0.20	0.66 1.54	0.05	0.61	0.008	45.09	3.17	6.31	898
Organic Polymers														
A163	Kevlar	6.0	6.0	0.138	51.90	0.22	0.64	0.05	0.57	0.008	45.30	3.17	7.07	1131

6.0 Test Results

The following sections report the results of impact tests for the major categories of materials tested: aluminum plate, metallic configurations, metal matrix, ceramics, graphite composites, dual-bumpers, and organic polymers. All impact tests used a 1/8" (3.17 mm) diameter aluminum (type 1100) projectile weighing approximately 45 mg at a velocity of 6.2-7.1 km/sec. Each section includes a description of the material tested, the significant results of the test(s), and further tests (if any) which should be considered for the material. Later sections compare the relative effectiveness of each shield and characterize the secondary ejecta particles from the various materials.

6.1 Baseline Aluminum Bumper

A 0.032" thick Al 6061-T6 aluminum plate with an areal density of 0.22 g/cm^2 was used as the baseline bumper for the screening tests. Aluminum 6061-T6 was used since it is the baseline material for shielding the Space Station habitat and laboratory modules. The 0.032" thick bumper results in a near-optimum thickness for breaking up a 0.125" diameter test projectile in the 6-7 km/sec velocity range of the tests (66). The second wall material was aluminum 2024-T3 which was mounted 2" behind the bumper. Tests were conducted using 0.05" thick second walls that by calculation would definitely be perforated with the test projectile, and 0.063" thick second walls which were just at the perforation ballistic limit. Areal densities for the two bumper/second wall combinations are 0.57 g/cm^2 and 0.66 g/cm^2, respectively. For comparison purposes, subsequent testing of different bumper materials primarily occurred with areal densities approximately equal to 0.57 g/cm^2, although a few tests were carried out with the higher combined bumper/-backwall areal density. The standoff distance in all subsequent testing was held constant at 2".

6.1.1 Normal Impacts

With the projectile impact perpendicular to the bumper (normal impact), baseline target damage was determined in a series of three tests using a 0.05" Al 2024-T3 second wall (shot no. A151, A228, and A231) and two tests with a 0.063" Al 2024-T3 second wall (shot no. A150 and A236). Damage to the bumper, second wall, and witness sheet (mounted

4" behind the second wall) is summarized in Table 6-1; details are given in Appendix D; and photo documentation in Figures 6-1 and 6-2.

For each of these shots, the 1/8" Al 1100 spherical projectile caused a circular hole in the bumper that was consistently 2.1-2.2 times greater than the projectile diameter. A slight lip (0.5 mm wide) also formed around the hole on front and back sides of the bumper. A bright spray pattern covered the back of each bumper which was resolved by microscope as fine splash marks made by molten aluminum droplets. This, along with the increase in bumper mass after impact (Appendix D), indicated that the impact melted a substantial part of the aluminum projectile which consequently rebounded from the backwall to strike the back of the bumper.

A nearly circular area of concentrated cratering and blast loading occurred on the backwall. For all shots with the 0.05" thick backwall, a somewhat irregular hole was produced in the center of the backwall (shape varied from circular to rectangular) having an average equivalent circular hole diameter of 4.1 mm (30 percent greater than the projectile diameter). Several 3-8 mm long through cracks usually emanated from the hole. The 1.9-6.6 mm variability in hole diameter for the three 0.05" tests was due in part to these cracks because they tended to cause relatively large pieces of the backwall to fail.

The impacts were at the ballistic limit threshold for the 0.063" backwall; one impact perforated the backwall while the other did not, although it did result in a 11 mm long through crack. A 0.5" wide circular spall zone detached from the backs of the second walls in all 5 shots (with both 0.05" and 0.063" backplates). Spall fragments had in several places completely penetrated an aluminum (Al 3003-0) witness plate (both 8 and 16 mils thick) mounted 4" behind the second wall, and also left numerous craters. This demonstrates the destructive nature of spall fragments from aluminum pressure hulls, and indicates the need and potential beneficial role a liner could play in suppressing spall damage.

6.1.2 Oblique Impacts

Although the material screening tests did not involve evaluation of oblique impact effects, two shots were carried out at a 45° oblique angle to a 0.032" Al 6061-T6 plate (shot no.

A315 and A316). The primary purpose of these shots was to collect data for a more accurate representation of the trajectory of ejecta particles from an oblique impact (Figure 3-9). An ejecta catcher, U-shaped 0.008" Al 3003-0 plate placed in front of the bumper, and high-speed camera film were used for this purpose.

These shots also illustrated that oblique impacts can produce more damage to a backwall. The impacts were performed with the second wall 2" behind and parallel to the bumper. As given in Appendix D, 7 holes occurred in a 0.05" Al 2024-T3 second wall (shot #A315) with a maximum diameter of 5.5 mm (equivalent circular diameter) and 4 holes occurred in a 0.063" Al 2024-T3 second wall (shot #A316) with a maximum diameter of 5 mm; significantly more damage than occurred on the baseline normal shots.

6.2 Metallic Bumpers

As described in the following sections, screening tests included other metallic bumper configurations besides the baseline Al 6061-T6 flat plate: an aluminum mesh, a corrugated aluminum bumper, and a tungsten/silicone rubber material.

6.2.1 Aluminum Mesh

The bumper consisted of four sheets of aluminum mesh (Al 5056) containing a square 30 x 30 (per square inch) pattern of 0.012" wire. The purpose was to determine if a metallic fabric had any advantage over a plate, but mesh was substituted because aluminum cloth was unavailable. The four sheet combination did not have significant straight through openings (most light transmission was blocked) although no attempt was made to rotate the mesh sheets; the wires in the sheets were either parallel or orthogonal to each other.

The all-mesh bumper did a poor job of protecting the backwall as shown in the photographs of Figure 6-3. Although the fine aluminum spray on the backwall and witness plate was evidence that a significant portion of the projectile melted in the impact, fragments perforated the backwall in a dozen places as given in Table 6-1. The combined hole area in the backwall was equivalent to a 9 mm diameter circle. There was no large detached spall from the backwall; consequently, witness plate hole size was less than for baseline Al 6061-T6, although the number of witness plate holes increased with the number of backwall perforations. Although more data would be needed for confirmation, a preliminary conclusion from this test is that mesh or cloth material would by itself perform less satisfactorily than a single solid plate of the same material.

6.2.2 Corrugated Aluminum Bumper

A 6" x 12" piece of 0.016" thick Al 3003-0 was folded every 1" at a 60° angle to form a 6" square corrugated aluminum bumper with the same areal density as the baseline bumper. The purpose of the corrugations was to produce a wider dispersion of the bumper/projectile debris plume than possible with a flat plate. As explained in Section 4.4, an impact on the corrugated face of this bumper ("normal" to the plane of the bumper) will cause the projectile and shield debris to separate because projectile particles follow along their original flight path while bumper particles are released normal to the shield. A wider dispersion angle provides essentially the same protective influence as a greater standoff distance without added support structure weight and complexity.

Projectile and bumper debris separation was apparent by the back plate damage pattern as shown in Figure 6-4. However, in this case, greater separation of these components was not particularly significant as the impact also produced a large backwall hole (but no spall). Positional evidence suggests the scalloped hole (nearly 10 mm in equivalent circular diameter) was made by projectile fragments, and fragments from the bumper created the craters sprayed out to the left of the hole. The results of this test strongly resemble the 45° oblique shots described in Section 6.1.2. As in those impacts, the projectile velocity component into the bumper decreases by the cosine of the impact angle. Impact pressures decrease in oblique impacts (12, p.495); thus, a simplifying assumption is to use the velocity cosine as the effective impact velocity. Whereas the effective projectile velocity for the 45° impacts was 4.2-4.3 km/s, the effective velocity for this 60° impact was only 3.1 km/s. As described in Section 3.1, the most damaging velocity range for two wall structures is in the low velocity region (2-3 km/s) when the projectile is still in relatively large, solid fragments. Also, increasing the standoff distance in this region is ineffective because the failure mechanism is governed more by penetration of solid fragments than by blast loading. Thus, most of the backwall damage is due to insufficient shock pressure at the impact velocity of the test to fully fragment the projectile.

Ejecta from the front surface of the bumper tore an essentially round 20 mm hole in an adjacent corrugation due to the high obliquity of the shot. Although this secondary impact created havoc to the bumper, it only deposited fine particles on the backwall (to the right of the hole) that did not significantly add to its damage.

From this test, it is not expected that corrugated bumpers will improve the protection from hypervelocity impacts having velocity cosines of less than 6-7 km/sec. This eliminates all but flatter corrugations from consideration as candidate bumper alternatives; the average orbital debris velocity of 9 km/sec means the corrugation angle should be nearly 90° to keep the velocity cosine above 6 km/sec. If another corrugated bumper is tested later, the folds should be made at 90° or greater, and they need to be sharp and precise. Extensive backwall damage occurred in this shot partly because the projectile struck near an edge of a corrugation that was rounded. Thus, some of the projectile impacted at a more normal angle where the bumper is too thin to shock the projectile completely.

6.2.3 Tungsten/Silicone

The tungsten/silicone rubber material tested is a combination of randomly shaped, 2-4 micron diameter tungsten microspheres (77 weight percent) bound in a silicone (type VMQ) matrix. A light (3.7 oz/yd^2) Nomex, pajama-check style, cloth backs the material. Because this material has a relatively high areal density (Table 5-1), the damage resulting to a 0.05" backwall (Shot #A226) should be compared to the baseline Al 6061-T6 with 0.063" backwall. The combined areal density of the baseline Al 6061-T6 bumper and 0.05" backwall is slightly less than the tungsten/silicone bumper with a 0.04" backwall; therefore, compare other shot results on a 0.05" backwall with shot number A230 for tungsten/silicone (Table 6-1).

Photographic documentation of the backwall and witness plate damage for shot number A226 and A230 is presented in Figure 6-5 and 6-6, respectively. Because the 0.05" backwall in shot number A226 showed no holes, through cracks, or significant detached spall, tungsten/silicone clearly performed better than aluminum 6061-T6 in the heavier combined areal density category (0.66-0.70 g/cm^2). A 1.9 mm circular hole was found in shot number A230's 0.04" backwall. But because this is equal to the smallest of three comparable Al 6061-T6 bumper shots, and no significant detached spall from the backwall or witness plate damage was visible, tungsten/silicone performance is still rated superior to the aluminum baseline.

The recognizable characteristics that play a role in producing this result are: (1) the high density of tungsten which shocks the aluminum projectile to a greater extent than aluminum (Figure 4-4), (2) the dispersion angle for tungsten/silicone's debris plume was 25 percent wider than aluminum's (55° vs. 40° as given in Appendix D), and (3) the nature of the tungsten phase. A solid tungsten plate is not expected to perform as well as aluminum from thermodynamic considerations described in Section 4.3.1, because an impact on tungsten is more apt than aluminum to produce damaging solid fragments. However, a bumper containing tungsten will not suffer from this problem if the tungsten phase is already in a finely divided state, as it is with the microspheres in the tungsten/-silicone material.

The next step in testing this material would be to scale it up for an appropriate Space Station scale test. An aluminum comparison shot should be made as part of the tests. As given in Figure 3-1, a 1/3" diameter Al 1100 sphere (0.86 g) at 6 km/s should perforate a 1/8" Al 2219-T87 backwall at a 4" standoff from a 0.063" Al 6061-T6 bumper (with no MLI). Keeping the projectile conditions, standoff distance, and backwall constant, a 0.05" thick tungsten/silicone material would have the same bumper areal density (0.43 g/cm^2). However, to keep the bumper/backwall areal density split nearly the same as in the original screening tests, a 0.06" tungsten/silicone bumper with a 1/9" Al 2219-T87 backwall should also be considered for testing.

Later screening tests should consider substituting other metallic microspheres for tungsten, such as magnesium, aluminum, or titanium (in that order of preference). These lower density metals could potentially reduce the bumper areal density while still sufficiently shocking the projectile.

6.3 Metal Matrix Composites

The metal matrix composite tested in this study was generously provided by Rockwell International Corporation. The material consisted of 30-35 volume percent silicon carbide (SiC) whiskers in a Al 6061-T6 matrix. Bumper target parameters are given in Table 5-1 and a summary of damage conditions following screening tests is given in Table 6-1.

This material performed marginally better than aluminum. In shot number A152 using a 0.063" backplate, surface damage patterns and detached spall were similar to Al 6061-T6 results (Figure 6-7). However, unlike the Al 6061-T6 shots, no hole or through crack was detected. In two shots (A157 and A220) with a 0.05" backwall, complete penetrations were evident, but were approximately 30 percent smaller than the aluminum baseline. Although its damage reduction ability is not significantly greater than Al 6061-T6, SiC/Al metal matrix does have the advantage that it is brittler than aluminum alone and tends to produce smaller ejecta particles on impact (although they are more numerous) as described in more detail in Section 6.9. Smaller secondaries are presumably less damaging if they impact other Space Station structures.

6.4 Ceramics and Ceramic Composites

Given the potential advantages ceramics have over aluminum (Section 4.1), several ceramic materials were included in the screening tests: alumina epoxy-bonded to aluminum, monolithic alumina, Nicalon SiC fabric, and a trimmed Shuttle tile.

6.4.1 Alumina bonded to Aluminum

This target consisted of a 0.015" alumina (aluminum oxide--Al_2O_3) bonded to 0.008" Al 3003-0. The alumina used in this study was donated by the Coors Ceramics Company (type ADS-96R). A generic epoxy glue was used as the bonding agent. Properties of this composite are given in Table 5-1.

The results of two shots (A159, A221) on this material are given in Table 6-1. In shot number A159, a small secondary particle also struck the bumper (see comments in Appendix D); therefore, the shot was repeated. The epoxied laminate did not debond; in fact, both shots were performed on the same 4.5" square target. The laminate was impacted on the alumina side, resulting in a clean hole and no cracking or shattering of the ceramic. However, the aluminum was more severely deformed, peeling back from the impact 2-3 times the alumina hole diameter. The surface ejecta was far less damaging to the Al 3003-0 ejecta-catcher witness plate than the aluminum baseline.

Damage to the 0.05" backwall for both shots resembled the metal matrix pattern. Each shot resulted in a single backwall hole and a relatively large spalled zone. Although it is encouraging to note the backwall hole size averaged 2.1 mm, 50 percent less than the aluminum baseline, the protection afforded by this bumper can not be classified as significantly superior.

6.4.2 Alumina

Because the results of the alumina/aluminum laminate were favorable, it was thought that alumina alone should be tested. The target consisted of 0.020" Coors alumina with no backing or coating. As indicated in Figure 6-8, the alumina broke into several large pieces. Apparently, the bumper shattered before completely shocking the projectile, as several perforations of the backwall occurred. An area surrounding the holes in the backwall was coated by an aluminum spray and no detached spall was evident.

Because this bumper performed remarkably well in melting the projectile before shattering, it is recommended that a toughened ceramic be included in a later screening test. A good candidate is boron carbide reinforced with boron carbide whiskers or platelets (see Section 5.5).

6.4.3 Silicon Carbide Cloth

Nicalon silicon carbide (SiC) cloth in a 8 harness satin weave (M sizing) was procured from Dow Corning Company, Inc. From the damage documented in Figure 6-9 and Table 6-1, it is apparent that this material by itself does not perform as well as aluminum. However, high shock pressures were encountered by some of the projectile as evident by the splash of fine aluminum droplets surrounding the holes in the backwall. Apparently, the weave of the cloth produces variable shock pressures in the projectile. A solid SiC plate would probably perform better. But the real advantage with this material may be in combining SiC cloth with a second solid bumper that shocks any remaining fine solid debris. This concept is explained in more detail in Section 6.6.

6.4.4 Shuttle Tile

A Shuttle tile represents a porous class of ceramics, consisting of foamed silica (SiO_2) and a borosilicate glass coating. A tile was sectioned to the correct areal density (0.44" thick) for this test as given in Table 5-1. Figure 6-10 shows the bumper and backwall after impact. The projectile impact formed a clean hole on the front borosilicate glass side, expanded in a cone shape into the low density foamed silica, and exited with a hole 4 times the entry hole diameter (Appendix D). Solid projectile fragments produced the large (10 mm) hole in the backwall. Performance was obviously substandard.

6.5 Graphite Composites

A graphite/epoxy plate and a laminate of graphite/epoxy and aluminum were included in the screening tests.

6.5.1 Graphite/Epoxy

A generic graphite/epoxy (G/E) plate was impacted in shot number A225. The G/E plate had a cloth surface covering that prevented peeling of the surface laminae. As indicated by Figure 6-11, G/E did not shock the projectile enough to prevent a large scalloped hole (28 mm) to be punched out by projectile fragments. This was somewhat of a surprise because a previous study (62) indicated favorable shielding characteristics for G/E. That study, however, generally used nylon projectiles having a density slightly lower than G/E. In this study, the aluminum projectiles (density 80 percent greater than G/E) at the velocity range of the tests did not generate adequate shock pressures to completely disrupt the projectile. Although it is possible that G/E would perform better than aluminum at higher impact velocities, the effectiveness of G/E in this test was clearly less than aluminum.

6.5.2 Aluminum bonded to Graphite/Epoxy

A laminate was made by epoxy bonding a generic G/E plate to 0.008" Al 3003-0. Physical parameters of this combination are given in Table 5-1. Damage, summarized in Table 6-1, compares favorably with the aluminum baseline. The backwall suffered three small (1.8 mm max.) perforations and insignificant spall.

However, the bumper practically debonded completely. The shock reflection at the laminate interface was particularly strong due to the difference in density and impedance mismatch of the laminates (12, p.474), causing the aluminum front surface to peel away from the impact point. If this material is re-tested, new bonding material and techniques are necessary.

6.6 Dual Bumpers

The dual bumper considered in this study consisted of a first bumper that would break up the projectile into fragments without slowing them down, and a second that would completely shock the remaining small fragments. The distance between the bumpers was selected to generate the largest possible dispersion of the debris plume. A mesh or fabric best fulfills the requirements for the outer (or first) bumper at a minimum areal density, while the second bumper had to be a solid sheet. An aluminum mesh was used in this study, other materials could be substituted. Two second bumpers were tested: aluminum plate and graphite/epoxy.

6.6.1 Aluminum Mesh and Aluminum Plate

This dual bumper consisted of a sheet of Al 5056 mesh (see Section 6.2.1) at a 0.5" spacing from a 0.016" Al 3003-0 second bumper. The distance from the mesh to backwall remained at 2". Damage to the bumpers, backwall, and witness plate is summarized for shot number A224 in Table 6-1 and Appendix D. As indicated, the dual bumpers effectively broke up and melted the projectile (see also Figure 6-12). Most of the impacts on the backwall were from molten aluminum particles. The solid fragments that remained are the likely cause of the 2 small backwall perforations (0.8 mm and 0.7 mm in diameter). There was no backplate spall or witness plate perforations. The results are clearly superior to the aluminum baseline.

6.6.2 Aluminum Mesh and Graphite/Epoxy Plate

An alternative second bumper material, a generic (cloth covered) graphite/epoxy plate, was used in shot number A238. Other materials remained the same as shot number A224 (Section 6.6.1).

The condition after impact of the backplate and witness plate improved over A224. Figure 6-13 shows that there were no perforations or detached spall from the backwall. The witness plate was clean (no holes or craters).

These results indicate the highly desirable characteristics of a dual bumper configuration utilizing a mesh as the outer bumper. A series of shots should be included in later screening tests to confirm these dual bumper results, optimize the spacing distance between dual bumpers, and test alternative dual bumper materials. Specific impact tests are proposed below. They are divided between screening shots at JSC's Hypervelocity Impact Research Laboratory and other shots requiring a larger gun facility. The proposed shots are not an exhaustive list, but merely indicate some that should get early priority because they help us understand and better define the potential protective capabilities of dual bumpers.

Proposed Shots at JSC

1. A good alternative candidate for the outer bumper is SiC cloth. The test would use 2-3 sheets of the SiC for the outer bumper, 0.5" spacing, 0.016" Al 3003-0 second bumper, 1.5" spacing, and 0.05" Al 2024-T3 backwall.

2. Several shots are needed to study the optimum spacing between bumpers. Tests should use the aluminum mesh and aluminum plate configuration, stepping through higher and lower spacings.

Proposed Testing at Another Impact Facility

After completing screening work at JSC that will develop confidence in a dual bumper system, it is strongly recommended that a scaled up version of that system, whether it is the aluminum mesh/aluminum second wall configuration or an alternative bumper material, be tested at another gun lab. The tests should use the same projectile conditions described in Section 6.2.3 (1/3" Al 1100 sphere at 6 km/s), and the mesh size should be increased. The test could be set up as follows:

1. Establish a baseline: the test projectile should penetrate a 0.032" Al 6061-T6 bumper, 4" standoff, and 0.125" Al 2219-T87 backwall.

ORIGINAL PAGE IS
OF POOR QUALITY

2. With the same projectile conditions, test an alternative dual bumper system consisting of a Al 5056 mesh sheet (14 x 14 wires per in.^{2}, 0.028" wire thickness, 0.043" opening, and 0.12 g/cm^2), 1" spacing, 0.045" aluminum second bumper (Al 6061-T6), 3" standoff, and 0.125" Al 2219-T87 backwall. All spacings to be measured from the back surface of one plate to the back surface of the other.

6.7 Organic Polymers

Both Kevlar and Spectra (polyethylene ballistic protection cloth) were procured but only Kevlar was included in this study.

6.7.1 Kevlar

The Kevlar cloth tested was a plain weave material (style #095) having 1000 denier strands in a 31 x 31 construction. The impact on 8 sheets of Kevlar resulted in the damage shown in Figure 6-14 and summarized in Table 6-1. The impact shock pressures were too low to completely shock the projectile allowing fragments to impact the second wall. The backwall perforations matched to some extent the square pattern of the cloth.

Follow-on shots may look at the possibility of using Kevlar or Spectra as a intermediate bumper (either second or third).

6.8 Materials Comparison

Table 6-2 ranks the bumper materials tested in this study based on the number of damage points accumulated by each (better bumpers have fewer damage points). The top group of three materials in Table 6-2 compares the heavier areal density class of materials, while the bottom group is for the lighter category (usually using a 0.05" backwall).

In the lighter category ($\approx$ 0.6 g/cm^2), the two dual bumper combinations were ranked highest because the backwalls for these materials had practically no penetrations and no spall. The tungsten/silicone material and aluminum/graphite epoxy laminate were ranked next highest because they protected from spall, although their backwalls did have pene-

ORIGINAL PAGE IS
OF POOR QUALITY

trations (smaller than aluminum baseline). The alumina/aluminum laminate and metal matrix were rated slightly higher than aluminum because they had smaller backwall holes although backwall spall was essentially the same as aluminum. Seven materials were ranked lower than the Al 6061-T6 baseline.

Points are assigned by a formula allocating a maximum 75 points to backwall damage and 25 points to witness plate damage. An implicit assumption in the formulation is that hazards to occupants and equipment come primarily from complete penetration of the pressure hull (leading to decompression, fragments, heat, light, overpressure and other interior effects associated with a penetration), but may also come from spall particles which cause many of the same interior effects as a perforation. Thus, primarily backwall hole size (perforation), but also the amount of witness plate damage (spall & perforation) are important in assessing the potential hazards from damage.

Points are calculated relative to the maximum damage in the group (Table 6-3). For the lighter areal density group, the largest backwall hole was for the graphite/epoxy bumper followed by the Shuttle tile. Because the G/E backwall hole was over twice the size of any other, the G/E shot collected the maximum 75 points for backwall damage and the formula calculated points for the other bumpers by relating damage to the Shuttle tile (ST) backwall hole size, i.e.,

Hole Points = Total Hole Dia./ST Hole Dia * 75

Witness plate damage was assigned 25 points which was divided between the size of holes in the witness plate (10 points), the number of holes in the witness plate (12.5 points), and the size of craters in the witness plate (2.5 points). This split was rather arbitrarily settled on after a brief assessment of what will cause more interior damage; many small penetrating fragments or a few large ones. Since the risk that something important is going to get hit by a fragment goes up with the number of fragments, the largest point weighting went to the number of holes. The 10 points for witness plate hole size was divided equally between the maximum hole and the total hole size (total hole size is the equivalent diameter of the sum of hole areas). The calculation of witness plate (WP) points was made relative to the maximum damage in these subdivisions. For the lighter areal density group, Al 6061-T6 (Al) witness plate had the largest maximum

ORIGINAL PAGE IS
OF POOR QUALITY

hole diameter and crater diameter, while the Corrugated aluminum (CA) witness plate had the largest total hole diameter and number of holes. WP points were calculated by:

WP points = (Max. Hole/Al * 5) + (Tot. Hole/CA * 5) + (No. Holes/CA * 12.5) + (Tot. Crater/Al * 2.5)

The sum of backwall and witness plate damage points equals the total points shown in Table 6-2. The break down of points into the various damage categories is given in Table 6-3. This formulation did not compensate for any difference in projectile energy or bumper/backwall areal density. The tests were designed to keep these parameters constant, but of course they did vary. Certainly, some changes in ranking are possible if a new bumper comparison equation was developed, but the general conclusion that there are materials with better shielding performance than Al 6061-T6 will remain valid.

6.9 Secondary Ejecta

Ejecta particles (size, shape, mass, velocity) produced by hypervelocity impact are of interest to some because of the potential these particles have to damage other structures (42). An ejecta catcher made from 0.008" Al 3003-0 was used to examine some of the characteristics of ejecta from various materials. The catcher was mounted 4" in front of the bumper and a hole drilled in the catcher prior to impact allowed the projectile to pass through without damage.

Visual examination of the ejecta catchers after impacts on Al 6061-T6 and SiC/aluminum metal matrix indicated that aluminum ejecta was larger in size but smaller in number than metal matrix ejecta (see Figure 6-15). A particle count for the metal matrix ejecta from shot number A152 is included in Appendix D. A hole count was made, diameters measured, and particle size calculated from penetration equations (43, 44). This activity was not continued due to funding and time constraints; however, it did indicate the feasibility of gaining useful data on particle size and number from these ejecta catchers.

Maximum ejecta velocity was determined from high speed film for shots A150 (Al - 6.7 km/s), A157 (metal matrix - 5.2 km/s), A158 (Al & G/E - 3.9 km/s), A159 (alumina & Al - 4.2 km/s), A161 (Al mesh - 2.1 km/s), and A163 (Kevlar - 2.4 km/s). The high speed camera data for these shots is also included in Appendix D.

ORIGINAL PAGE IS
OF POOR QUALITY

Although a quantitative assessment was not made, visual inspection showed that the number and size of perforations in the ejecta catcher increased in the following order: Kevlar and aluminum mesh (neither ejecta catcher had any holes at all), alumina/aluminum laminate (no holes, just etched), aluminum/graphite epoxy laminate (few holes), metal matrix (many small holes), Al 6061-T6 (many large holes). It therefore seems possible that an aluminum mesh or other surface treatment could potentially decrease or eliminate the secondary impact problem.

Table 6-1. Bumper, Backwall, and Witness Plate Damage Summary

Shot	Bumper Material	Bumper Areal Dens. (g/cm^2)	Al 2024-T3 Backplate Thickness (in)	Bumper & Backplate Areal Dens. (g/cm^2)	Al 1100 Sphere (45 mg) Proj. Vel. (km/s)	BUMPER Hole Dia. (mm)	Hole to Proj Dia. Ratio	Al 2024-T3 BACKPLATE Number Holes	Hole Dia. (mm)	Avg. Total Hole Dia. (mm)	Detached Spall Dia. (mm)	WITNESS PLATE Al 3003-0 Witness Plate Thickness (in)	Number Holes	Max. Hole Dia. (mm)	Avg. Hole Dia. (mm)	Avg. Total Hole Dia. (mm)	Number Craters	Max. Crater Dia. (mm)	Approx. Avg. Crater Dia. (mm)	Avg. Total Crater Dia. (mm)
Aluminum Baseline (Normal Impact)																				
A151	Al 6061-T6	0.22	0.05	0.56	6.60	7.0	2.2	1	2.0		14	-								
A228	Al 6061-T6	0.22	0.05	0.57	6.39	6.9	2.2	1	6.6		12.4	0.008	8	9.3	3.9		35	4.1	1.7	
A231	Al 6061-T6	0.22	0.05	0.57	6.73	6.9	2.2	1	1.9		12.7	0.016	2	6.6	4.8		30	4.1	1.9	
Average	Al 6061-T6	0.22	0.05	0.57	6.57	6.9	2.2		4.1			0.008	8	9.3		11.0				9.8
A150	Al 6061-T6	0.22	0.063	0.66	6.45	6.8	2.1	0			13	-								
A236	Al 6061-T6	0.22	0.063	0.66	6.48	6.6	2.1	1	0.7		12.4	0.016	1	3.2	3.2		20	5.1	1.5	
Average	Al 6061-T6	0.22	0.063	0.66	6.47	6.7	2.1		0.5			0.016	1	3.2		3.2				6.8
Aluminum and other Metallic Bumper Configurations																				
A161	Al mesh	0.20	0.05	0.55	6.50	5.6	1.8	12	2.6 (avg)	9.0		0.008	36	2.0	0.5	3.0	30	0.8	0.5	2.8
A223	Corrugated Al	0.22	0.05	0.57	6.32	7.0	2.2	1	9.8			0.008	260	3.3	1.1	17.2	80	1.3	0.6	5.0
A226	Tungsten/ Silicone	0.34	0.05	0.70	6.56	8.4	2.7	0		0		0.008	0				8	0.8	0.4	1.1
A230	Tungsten/ Silicone	0.34	0.04	0.62	6.70	8.8	2.8	1	1.9			0.016	0				12	0.7	0.3	0.9
Metal Matrix Composites (Al 6061-T6 and 35 v% SiC)																				
A152	Metal Matrix	0.22	0.063	0.66	6.52	6.3	2.0	0			10.9	-								
A157	Metal Matrix	0.22	0.05	0.57	6.71	6.1	1.9	1	1.2		13	0.008	4	4.2	3.4		21	3.3	2	
A220	Metal Matrix	0.22	0.05	0.57	6.46	6.1	1.9	1	3.8		11.9	0.008	6	4.1	3.0		18	4.1	1.5	
Average	Metal Matrix	0.22	0.05	0.57	6.59	6.1	1.9		2.8			0.008	5	4.1		7.1				8.0

Table 6-1 (Cont). Bumper, Backwall, and Witness Plate Damage

Shot	Bumper Material	Bumper Areal Dens. (g/cm^2)	Al 2024-T3 Backplate Thickness (in)	Bumper & Backplate Areal Dens. (g/cm^2)	Al 1100 Sphere (45 mg) Proj. Vel. (km/s)	BUMPER Hole Dia. (mm)	Hole to Proj Dia. Ratio	Al 2024-T3 BACKPLATE Number Holes	Hole Dia. (mm)	Avg. Total Hole Dia. (mm)	Detached Spall Dia. (mm)	WITNESS PLATE Al 3003-0 Witness Plate Thickness (in)	Number Holes	Max. Hole Dia. (mm)	Avg. Hole Dia. (mm)	Avg. Total Hole Dia. (mm)	Number Craters	Max. Crater Dia. (mm)	Approx. Avg. Crater Dia. (mm)	Avg. Total Crater Dia. (mm)
Ceramics and Ceramic Composites																				
A159	Alumina & Al	0.21	0.05	0.56	6.56	6.6	2.1	1	0.9		12	0.008	1	3.8	3.8		17	5.3	2.3	
A221	Alumina & Al	0.21	0.05	0.57	6.30	8.9	2.8	1	2.8		11.2	0.008	5	3.8	3.3		18	3.0	1.5	
Average	Alumina bonded to Aluminum	0.21	0.05	0.57	6.43	7.7	2.4		2.1			0.008	3	3.8		5.9				8.1
A237	Alumina	0.19	0.05	0.55	6.40	6.6	2.1	7	1.9 (avg)	5.0		0.008	29	1.3	0.6	3.4	100	2.0	0.6	6.4
A222	SiC	0.23	0.05	0.58	6.64	5.3	1.7	9	2.9 (avg)	8.6		0.008	125	3.0	0.9	9.9	120	3.3	0.5	5.6
A219	Shuttle Tile	0.23	0.05	0.58	6.52	5.6	1.8	2	10.3 1.4	10.4		-								
Graphite Composites																				
A225	Graphite/Epoxy	0.23	0.05	0.58	6.61	6.4	2.0	2	28.2 1.3	28.2		0.016	1	0.4	0.4	0.4	70	3.3	1.1	9.6
A158	Al bonded to G/E	0.27	0.05	0.62	6.18	7.1	2.2	3	1.8 0.8 0.1	2.0		0.008	0			0	11	0.5	0.3	0.8
Dual Bumpers																				
A224	Al mesh - Al	0.16	0.05	0.51	6.39	6.6	2.1	2	0.8 0.7	1.0		0.008	0			0	12	0.3	0.1	0.4
A238	Al mesh - G/E	0.25	0.05	0.61	6.31	6.1	1.9	0		0		0.008	0			0	0			0
Organic Polymers																				

Table 6-1 (Cont). Bumper, Backwall, and Witness Plate Damage

						BUMPER		AL 2024-T3 BACKPLATE				WITNESS PLATE								
Shot	Bumper Material	Bumper Areal Dens. (g/cm^2)	Al 2024-T3 Backplate Thickness (in)	Bumper & Backplate Areal Dens. (g/cm^2)	Al 1100 Sphere (45 mg) Proj. Vel. (km/s)	Hole Dia. (mm)	Hole to Proj Dia. Ratio	Number Holes	Hole Dia. (mm)	Avg. Total Hole Dia. (mm)	Detached Spall Dia. (mm)	Al 3003-0 Witness Plate Thickness (in)	Number Holes	Max. Hole Dia. (mm)	Avg. Hole Dia. (mm)	Avg. Total Hole Dia. (mm)	Number Craters	Max. Crater Dia. (mm)	Approx. Avg. Crater Dia. (mm)	Avg. Total Crater Dia. (mm)
A163	Kevlar	0.22	0.05	0.57	7.07	2.8	0.9	9	2.7 (avg)	8.1		0.008	102	3.0	0.6	6.4	46	2.3	0.4	2.6

Table 6-2. Bumper Comparison

Bumper Material	Bumper Areal Dens. (g/cm^2)	Bumper & Backplate Areal Dens. (g/cm^2)	Proj Energy (J)	Al2024-T3 Backplate Thickness (in)	Total Points
1. Tungsten/Silicone	0.34	0.70	971	0.05	0.4
2. Metal Matrix	0.22	0.66	963	0.063	25.0
3. Al 6061-T6	0.22	0.66	945	0.063	100.0
1. Al mesh - G/E	0.25	0.61	898	0.05	0.0
2. Al mesh - Al	0.16	0.51	925	0.05	7.6
3. Tungsten/Silicone	0.34	0.62	1011	0.04	14.0
4. Al & G/E	0.27	0.62	864	0.05	14.5
5. Alumina & Al	0.21	0.57	936	0.05	21.0
6. Metal Matrix	0.22	0.57	981	0.05	27.2
7. Al 6061-T6	0.22	0.57	976	0.05	40.9
8. Alumina	0.19	0.55	925	0.05	41.0
9. Kevlar	0.22	0.57	1131	0.05	67.5
10. Al mesh	0.20	0.55	957	0.05	69.4
11. SiC	0.23	0.58	996	0.05	73.7
12. Graphite/Epoxy	0.23	0.58	988	0.05	77.8
13. Corrugated Al	0.22	0.57	903	0.05	91.3
14. Shuttle Tile	0.22	0.58	964	0.05	100.0

Table 6-3. Damage Point Breakdown

Averages for Shots	Bumper Material	Bumper Areal Dens. (g/cm^2)	Bumper & Backplate Areal Dens. (g/cm^2)	Al 1100 Spherical Proj Proj. Mass (mg)	Proj. Vel. (km/s)	Proj. Energy (J)	Al 2024-T3 Backplate Thickness (in)	Damage Scale 1 = Hole & Spall 2 = Hole, no spall 3 = Crack (thru) & Spall 4 = Spall, no hole or thru-crack 5 = No spall or hole	Avg. Total Hole Dia. (mm)	Hole Points	Al 3003-0 Witness Plate Thickness (in)	Avg. Max. Hole Dia. (mm)	Avg. Total Hole Dia. (mm)	Avg. No. of Holes	Avg. Total Crater Dia. (mm)	Witness Max. Hole Dia. Points	Witness Tot. Hole Dia. Points	Avg. No. of Holes Points	Witness Tot. Crater Dia. Points	Tot. Witness Points	Total Points
A150,A236	Al 6061-T6	0.22	0.66	45.24	6.47	945	0.063	3,1	0.5	75.0	0.016	3.2	3.2	1	6.8	5.0	5.0	12.5	2.5	25.0	100.0
A152	Metal Matrix	0.22	0.66	45.25	6.52	963	0.063	4	0	0.0						5.0	5.0	12.5	2.5	25.0	25.0
A226	Tungsten/Silicone	0.34	0.70	45.13	6.56	971	0.05	5	0	0.0	0.008	0	0	0	1.1	0.0	0.0	0.0	0.4	0.4	0.4
A151,A228,A231	Al 6061-T6	0.22	0.57	45.17	6.57	976	0.05	1	4.1	29.8	0.008	9.3	11.0	8	9.8	5.0	3.2	0.4	2.5	11.1	40.9
A157,A220	Metal Matrix	0.22	0.57	45.26	6.59	981	0.05	1	2.8	20.6	0.008	4.1	7.1	5	8.0	2.2	2.1	0.2	2.1	6.6	27.2
A158	Al & G/E	0.27	0.62	45.24	6.18	864	0.05	2	2.0	14.3	0.008	0	0	0	0.8	0.0	0.0	0.0	0.2	0.2	14.5
A159,A221	Alumina & Al	0.21	0.57	45.28	6.43	936	0.05	1	2.1	15.1	0.008	3.8	5.9	3	8.1	2.0	1.7	0.1	2.1	6.0	21.0
A161	Al mesh	0.20	0.55	45.29	6.50	957	0.05	2	9.0	65.0	0.008	2.0	3.0	36	2.8	1.1	0.9	1.7	0.7	4.4	69.4
A163	Kevlar	0.22	0.57	45.30	7.07	1131	0.05	2	8.1	58.5	0.008	3.0	6.4	102	2.6	1.6	1.9	4.9	0.7	9.1	67.5
A219	Shuttle Tile	0.22	0.58	45.29	6.52	964	0.05	2	10.4	75.0											100.0
A222	SiC	0.23	0.58	45.16	6.64	996	0.05	2	8.6	61.8	0.008	3.0	9.9	125	5.6	1.6	2.9	6.0	1.4	12.0	73.7
A223	Corrugated Al	0.22	0.57	45.27	6.32	903	0.05	2	9.8	70.8	0.008	3.3	17.2	260	5.0	1.8	5.0	12.5	1.3	20.5	91.3
A224	Al mesh - Al	0.16	0.51	45.30	6.39	925	0.05	2	1.0	7.5	0.008	0	0	0	0.4	0.0	0.0	0.0	0.1	0.1	7.6
A225	Graphite/Epoxy	0.23	0.58	45.23	6.61	988	0.05	2	28.2	75.0	0.016	0.4	0.4	1	9.6	0.2	0.1	0.0	2.4	2.8	77.8
A230	Tungsten/Silicone	0.34	0.62	45.03	6.70	1011	0.04	2	1.9	13.8	0.016	0	0	0	0.9	0.0	0.0	0.0	0.2	0.2	14.0
A237	Alumina	0.19	0.55	45.25	6.40	925	0.05	2	5.0	36.3	0.008	1.3	3.4	29	6.4	0.7	1.0	1.4	1.6	4.7	41.0
A238	Al mesh - G/E	0.25	0.61	45.09	6.31	898	0.05	5	0	0.0	0.008	0	0	0	0	0.0	0.0	0.0	0.0	0.0	0.0

Figure 6-1. Photographic Documentation for Shot #A231

.032" Al 6061-T6 bumper, 2" standoff, .050" Al 2024-T3 backwall, 4" spacing, .016" Al 3003-0 witness plate
.125" Al 1100 spherical projectile, 45.18 mg, 6.73 km/sec

FRONT BACK

BUMPER

BACKWALL

WITNESS

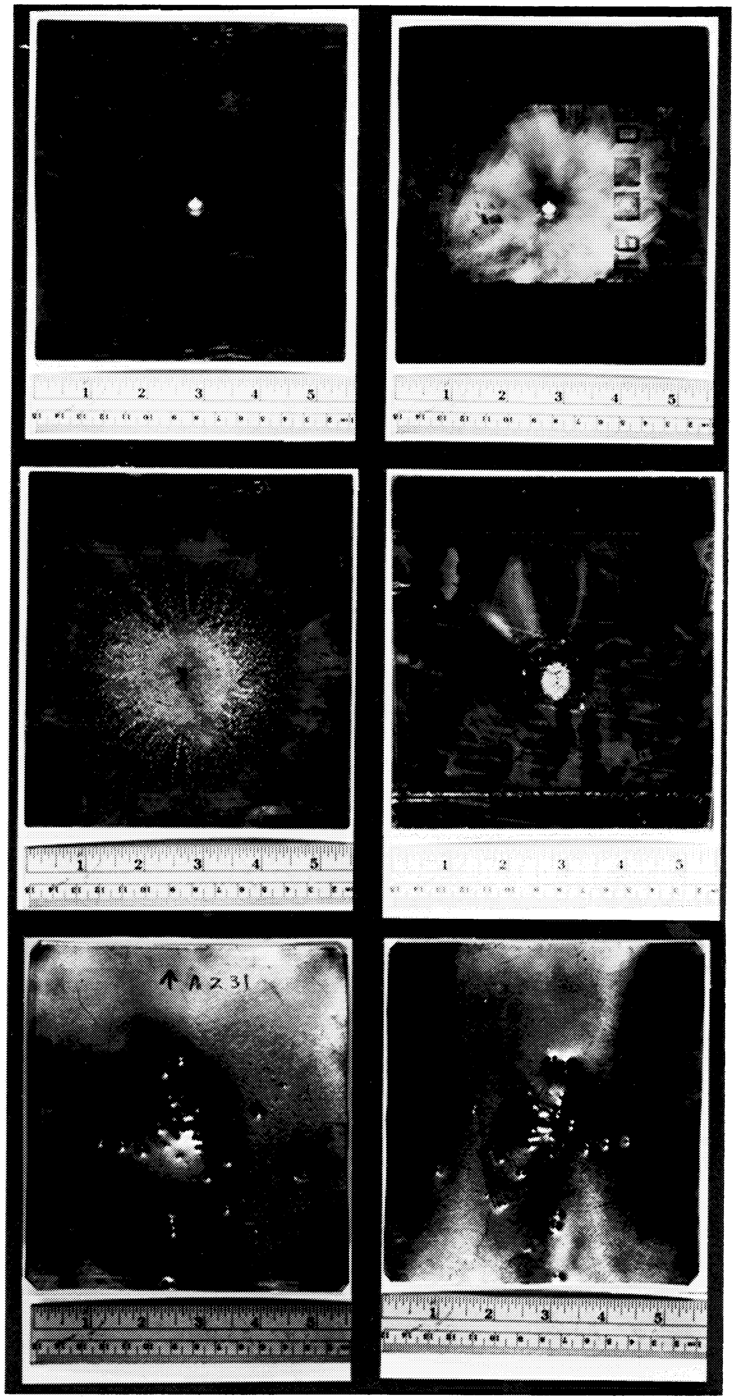

ORIGINAL PAGE
COLOR PHOTOGRAPH

Figure 6-2. Photographic Documentation for Shot #A236

.032" Al 6061-T6 bumper, 2" standoff, .063" Al 2024-T3 backwall, 4" spacing, .016" Al 3003-0 witness plate
.125" Al 1100 spherical projectile, 45.23 mg, 6.48 km/sec

FRONT BACK

BUMPER

BACKWALL

WITNESS

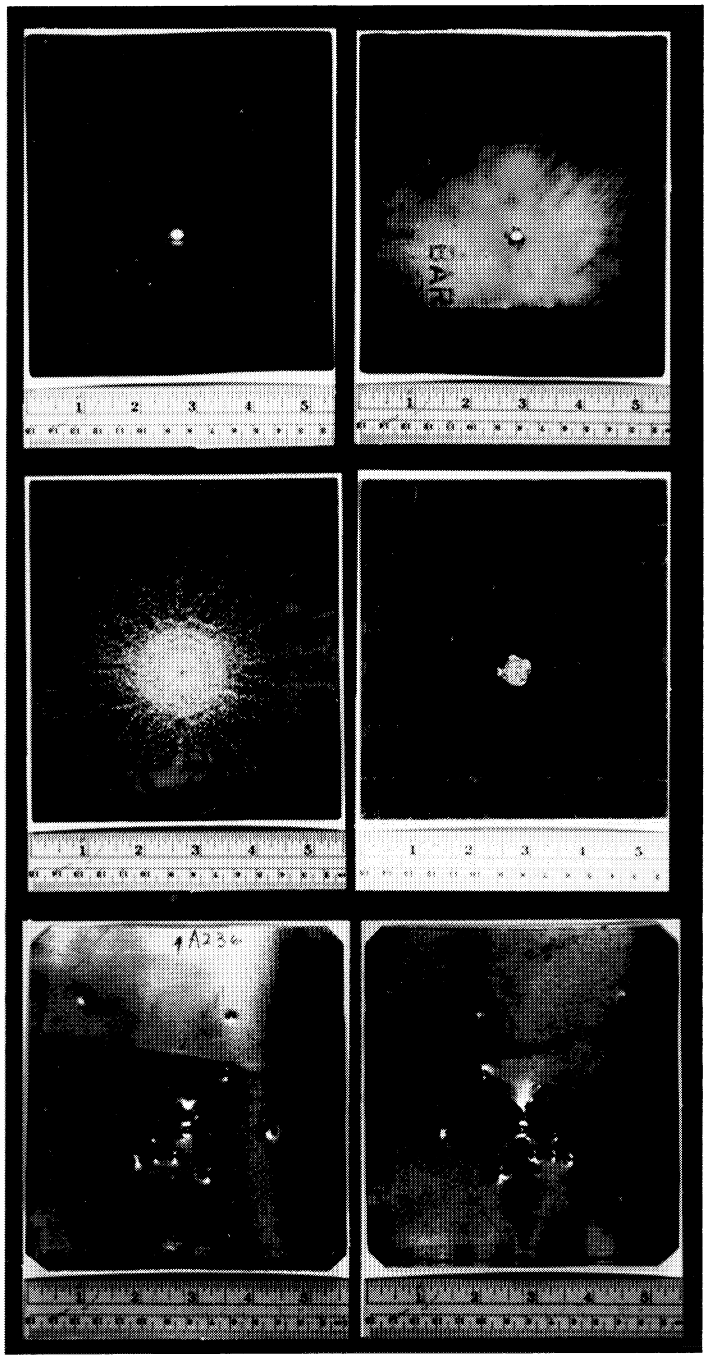

ORIGINAL PAGE
COLOR PHOTOGRAPH

Figure 6-3. Photographic Documentation for Shot #A161

.12" Al mesh bumper, 2" standoff, .050" Al 2024-T3 backwall, 4" spacing, .008" Al 3003-0 witness plate
.125" Al 1100 spherical projectile, 45.29 mg, 6.50 km/sec

FRONT BACK

BUMPER

BACKWALL

WITNESS

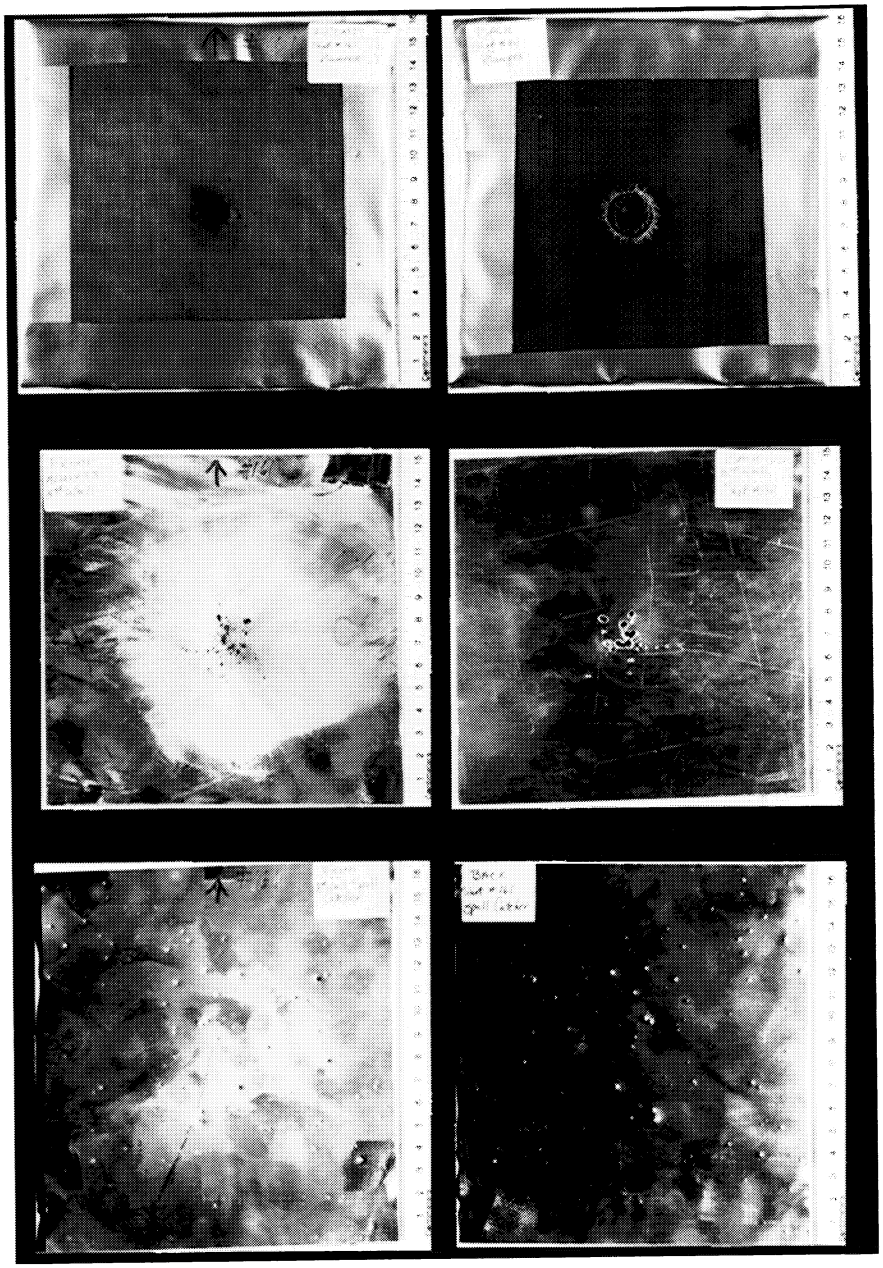

ORIGINAL PAGE
COLOR PHOTOGRAPH

Figure 6-4. Photographic Documentation for Shot #A223

.016" Al 3003-0 corrugated bumper, 2" standoff, .050" Al 2024-T3 backwall, 4" spacing, .008" Al 3003-0 witness plate
.125" Al 1100 spherical projectile, 45.27 mg, 6.32 km/sec

FRONT BACK

BUMPER

BACKWALL

WITNESS

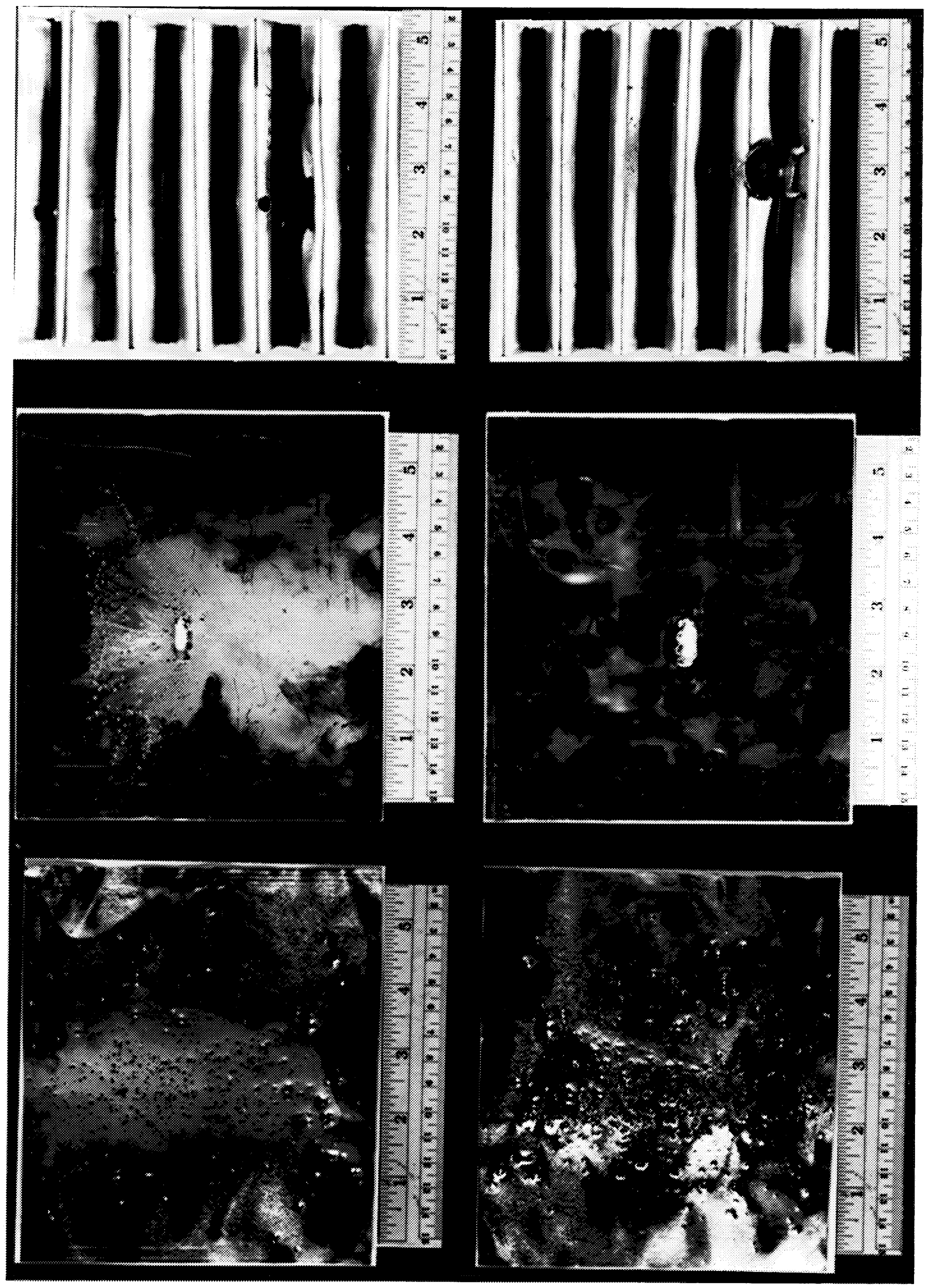

ORIGINAL PAGE
COLOR PHOTOGRAPH

Figure 6-5. Photographic Documentation for Shot #A226

.04" Tungsten/Silicone rubber, 2" standoff, .050" Al 2024-T3 backwall, 4" spacing, .008" Al 3003-0 witness plate
.125" Al 1100 spherical projectile, 45.13 mg, 6.56 km/sec

FRONT BACK

BUMPER

BACKWALL

WITNESS

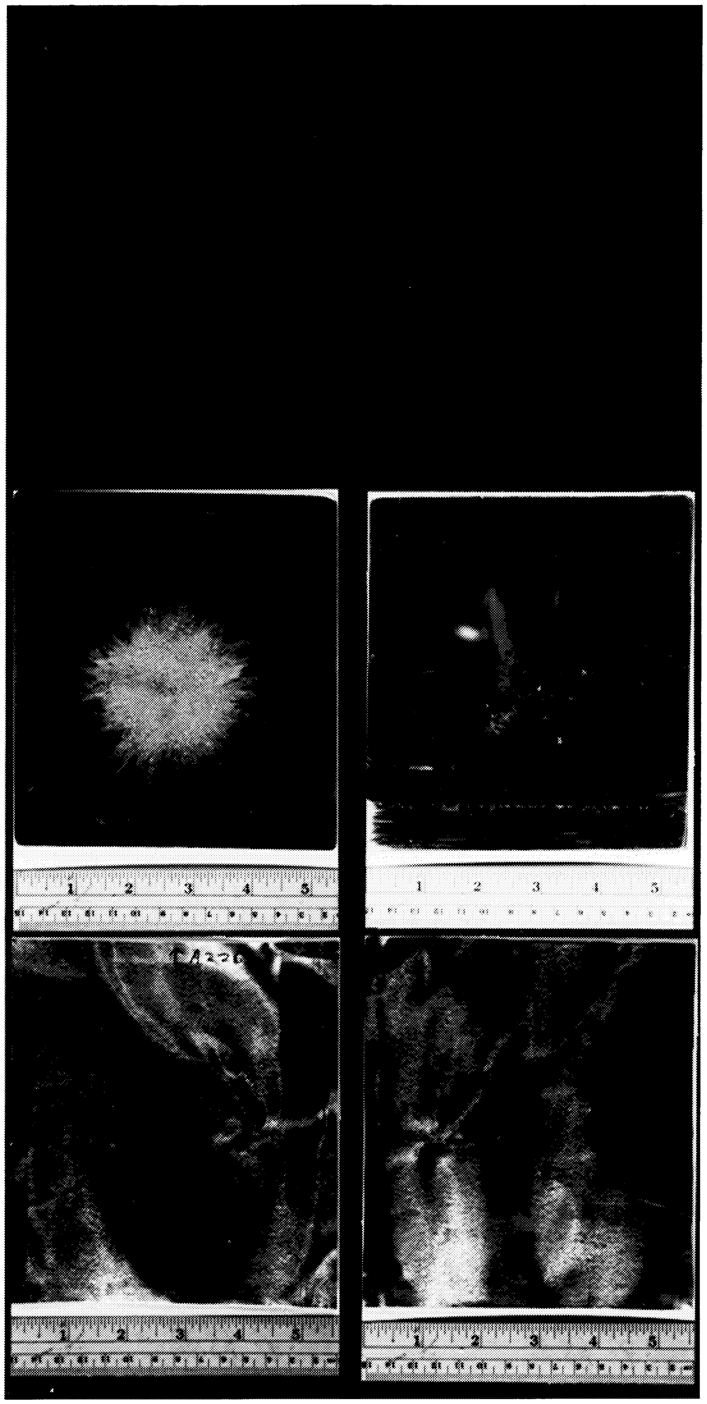

ORIGINAL PAGE
COLOR PHOTOGRAPH

Figure 6-6. Photographic Documentation for Shot #A230

.04" Tungsten/Silicone rubber, 2" standoff, .040" Al 2024-T3 backwall, 4" spacing, .016" Al 3003-0 witness plate
.125" Al 1100 spherical projectile, 45.03 mg, 6.70 km/sec

FRONT BACK

BUMPER

BACKWALL

WITNESS

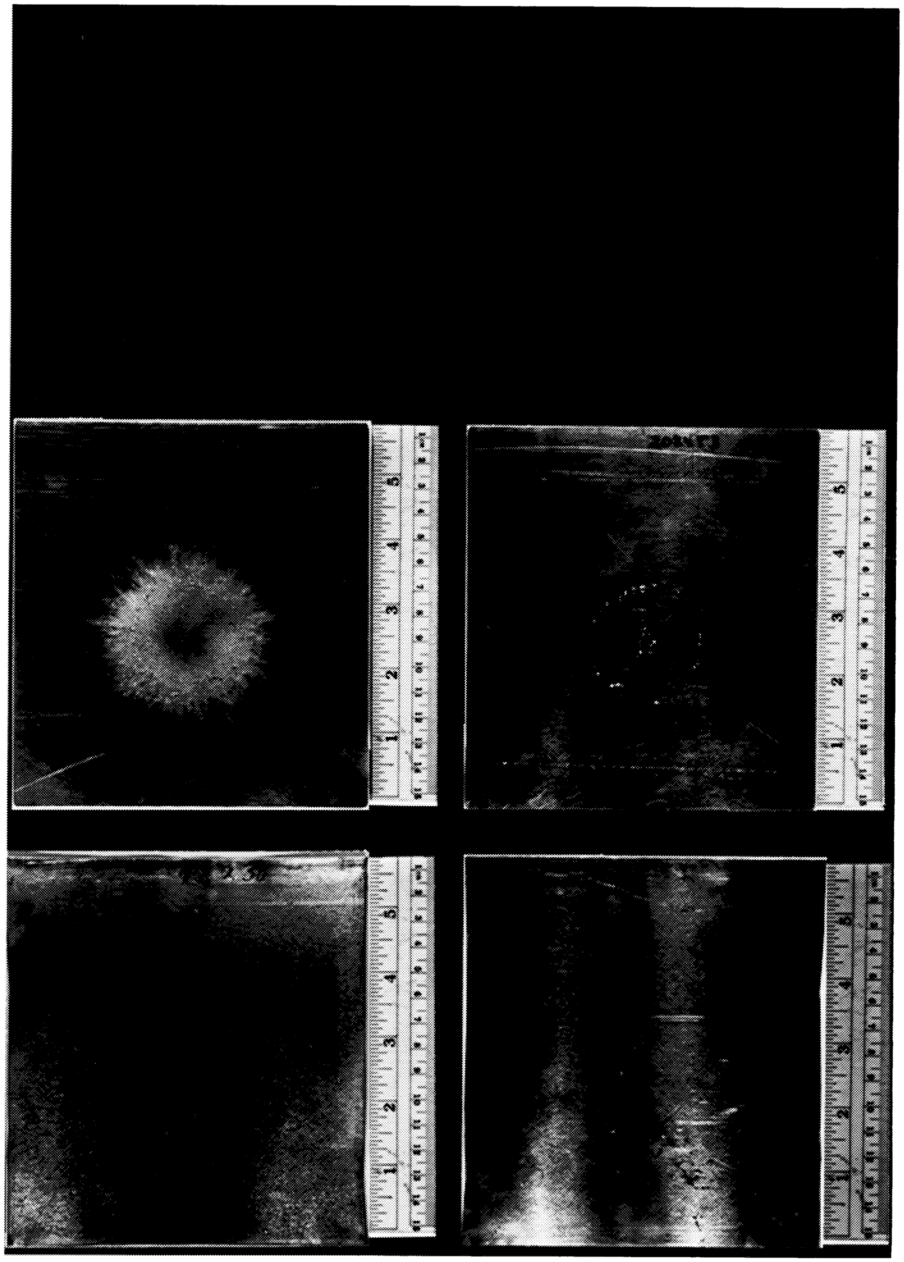

ORIGINAL PAGE
COLOR PHOTOGRAPH

Figure 6-7. Photographic Documentation for Shot #A152

.032" Metal Matrix, 2" standoff, .063" Al 2024-T3 backwall
.125" Al 1100 spherical projectile, 45.25 mg, 6.52 km/sec

FRONT BACK

BUMPER

BACKWALL

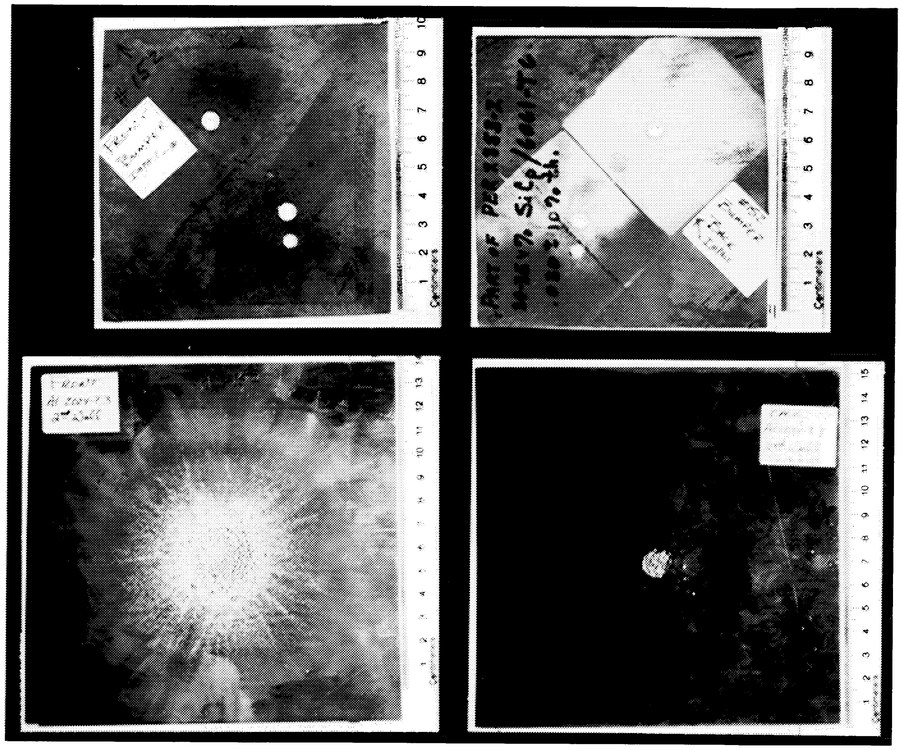

ORIGINAL PAGE IS
COLOR PHOTOGRAPH

Figure 6-8. Photographic Documentation for Shot #A237

.020" Alumina, 2" standoff, .050" Al 2024-T3 backwall, 4" spacing, .008" Al 3003-0 witness plate
.125" Al 1100 spherical projectile, 45.25 mg, 6.40 km/sec

FRONT BACK

BUMPER

BACKWALL

WITNESS

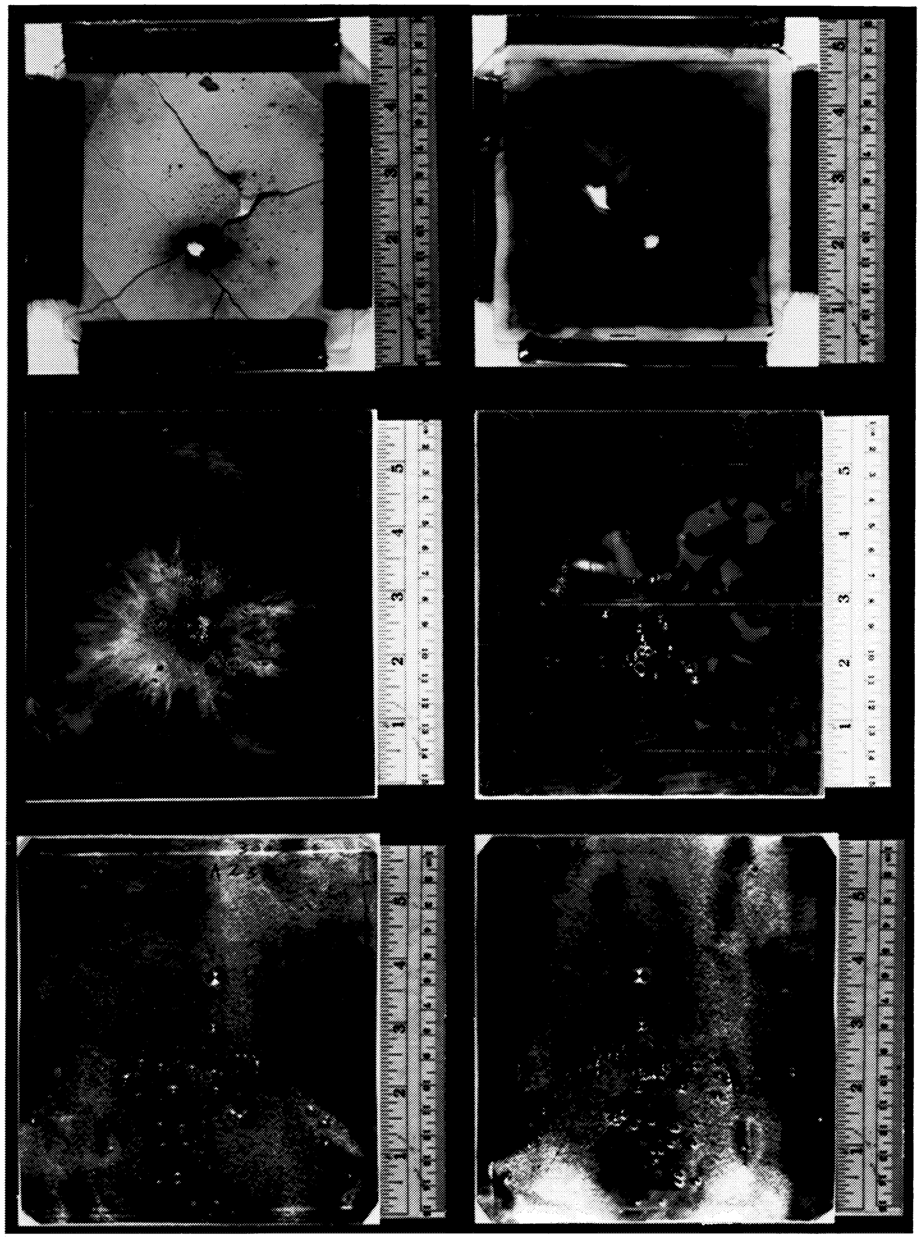

ORIGINAL PAGE
COLOR PHOTOGRAPH

Figure 6-9. Photographic Documentation for Shot #A222

.035" Silicon Carbide cloth, 2" standoff, .050" Al 2024-T3 backwall, 4" spacing, .008" Al 3003-0 witness plate
.125" Al 1100 spherical projectile, 45.16 mg, 6.64 km/sec

FRONT BACK

BUMPER

BACKWALL

WITNESS

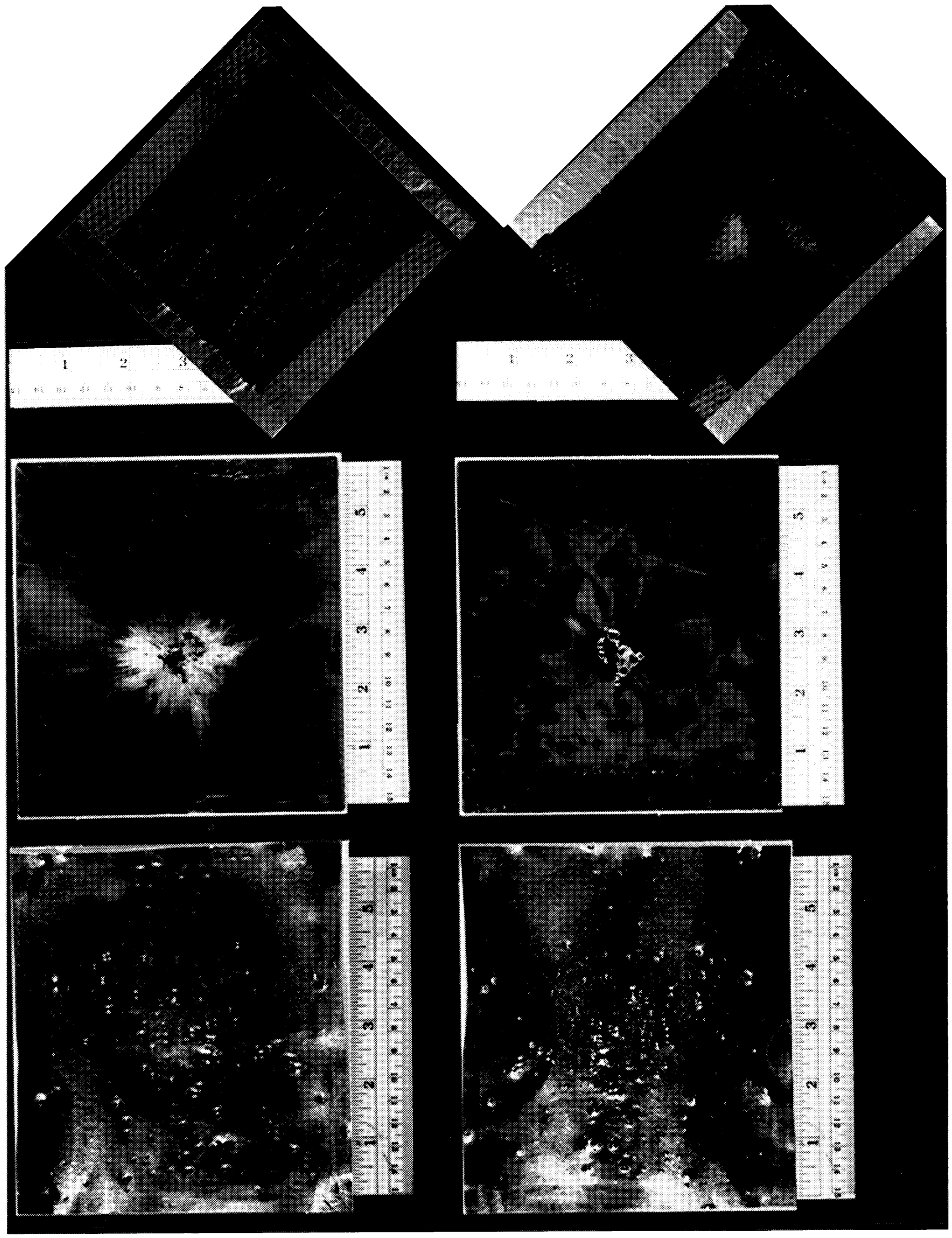

ORIGINAL PAGE
COLOR PHOTOGRAPH

Figure 6-10. Photographic Documentation for Shot #A219

.44" Shuttle Tile, 2" standoff, .050" Al 2024-T3 backwall
.125" Al 1100 spherical projectile, 45.29 mg, 6.52 km/sec

FRONT BACK

BUMPER

BACKWALL

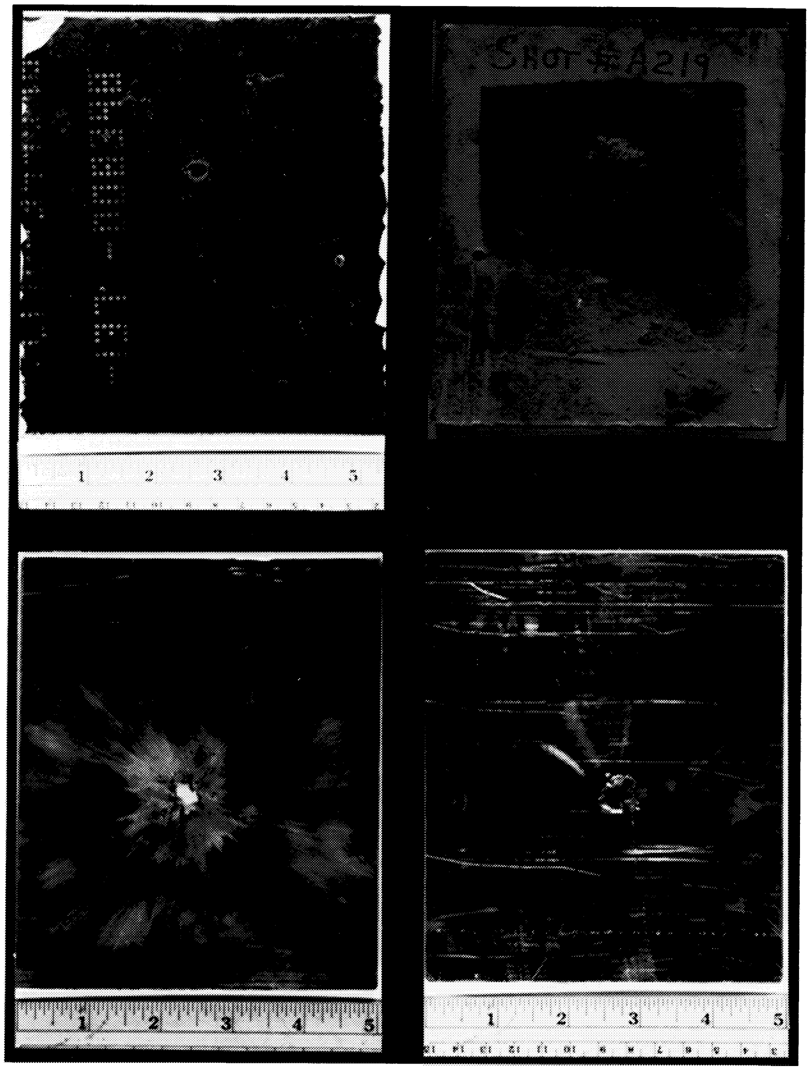

ORIGINAL PAGE
COLOR PHOTOGRAPH

Figure 6-11. Photographic Documentation for Shot #A225

.058" Graphite/Epoxy, 2" standoff, .050" Al 2024-T3 backwall, 4" spacing, .016" Al 3003-0 witness plate
.125" Al 1100 spherical projectile, 45.23 mg, 6.61 km/sec

FRONT BACK

BUMPER

BACKWALL

WITNESS

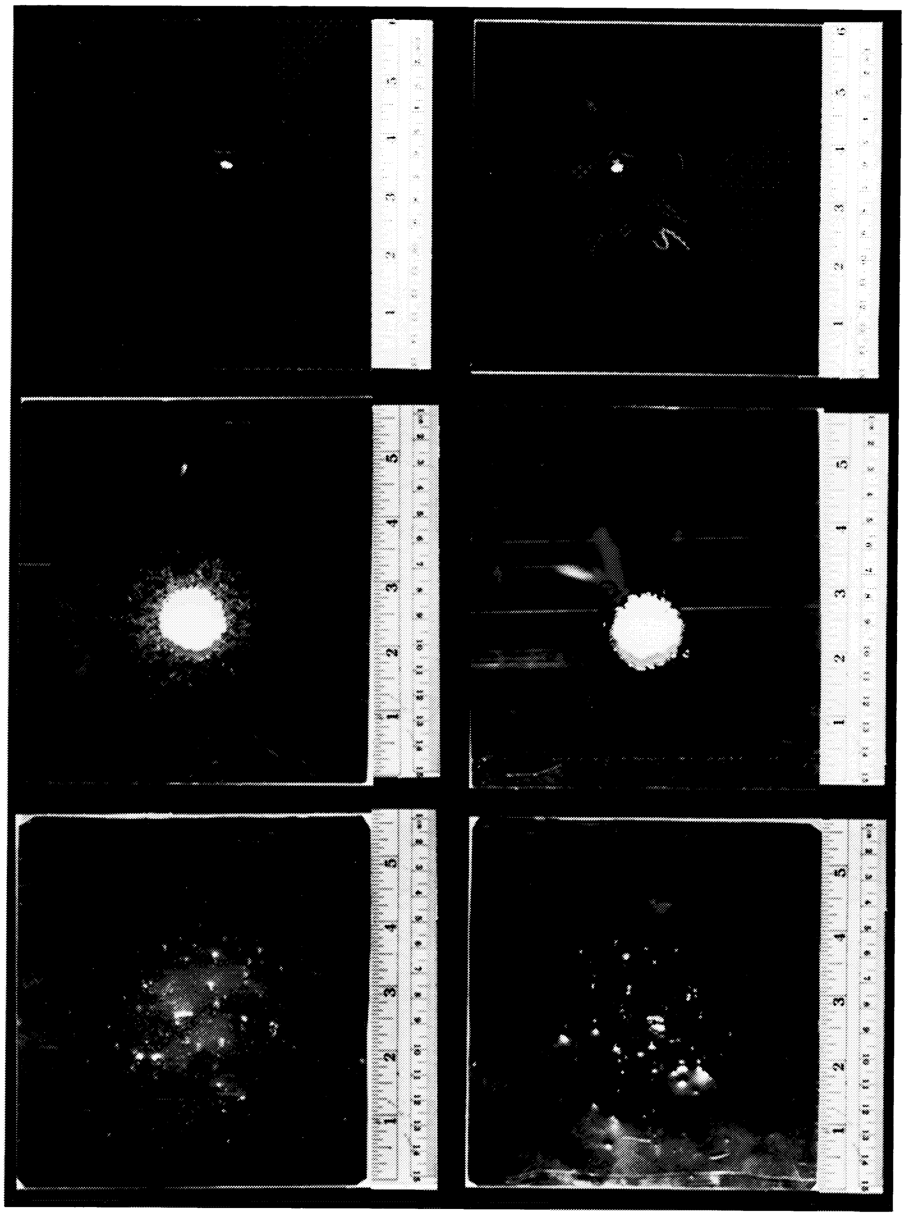

ORIGINAL PAGE
COLOR PHOTOGRAPH

Figure 6-12. Photographic Documentation for Shot #A224

.03" Aluminum mesh, 0.5" spacing, .016" Al 3003-0 plate, 1.5" standoff, .050" Al 2024-T3 backwall
.125" Al 1100 spherical projectile, 45.30 mg, 6.39 km/sec

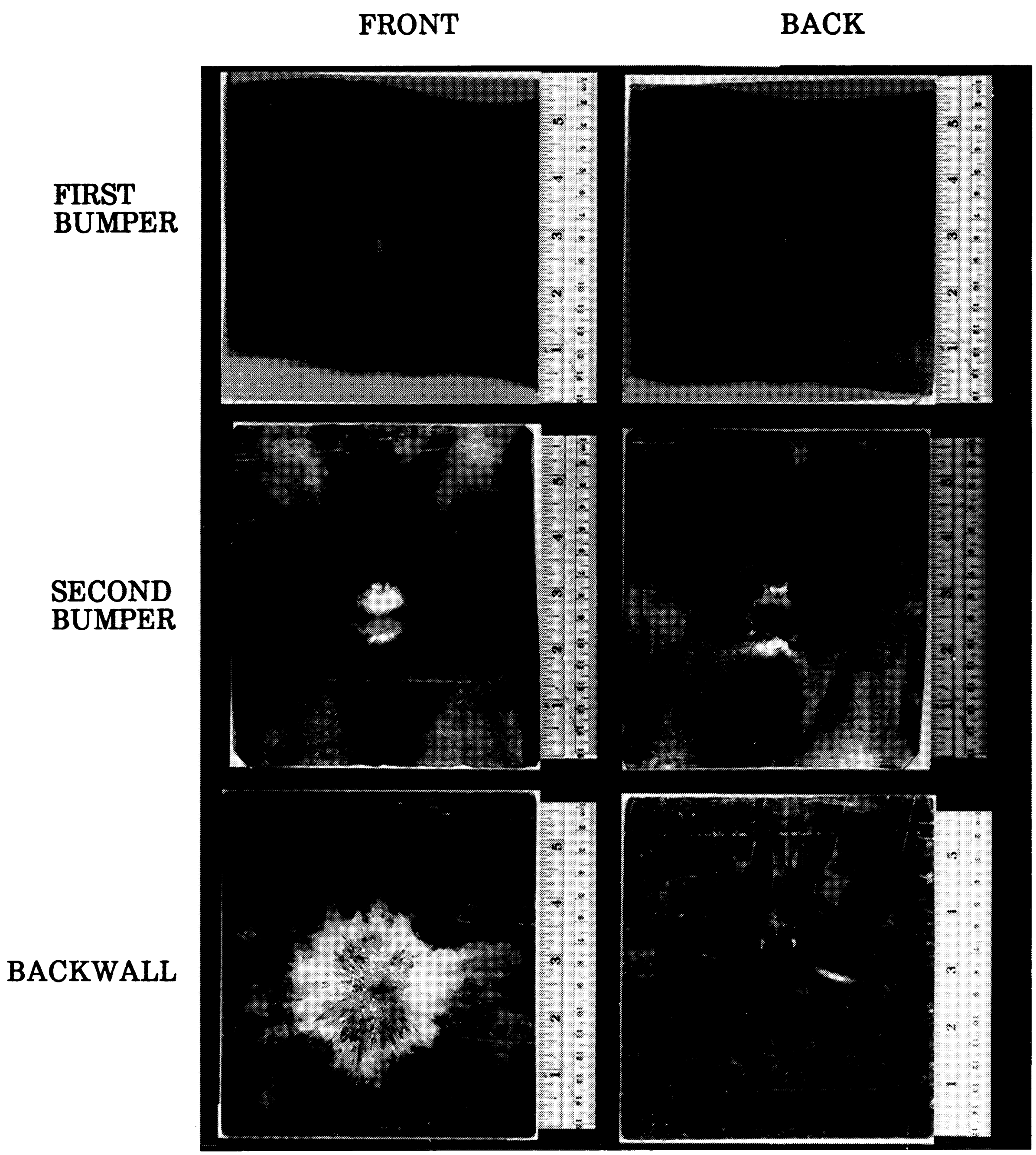

ORIGINAL PAGE
COLOR PHOTOGRAPH

Figure 6-13. Photographic Documentation for Shot #A238

.03" Aluminum mesh, 0.5" spacing, 0.052" Graphite/epoxy plate, 1.5" standoff, .050" Al 2024-T3 backwall
.125" Al 1100 spherical projectile, 45.09 mg, 6.31 km/sec

FRONT | BACK

FIRST BUMPER

SECOND BUMPER

BACKWALL

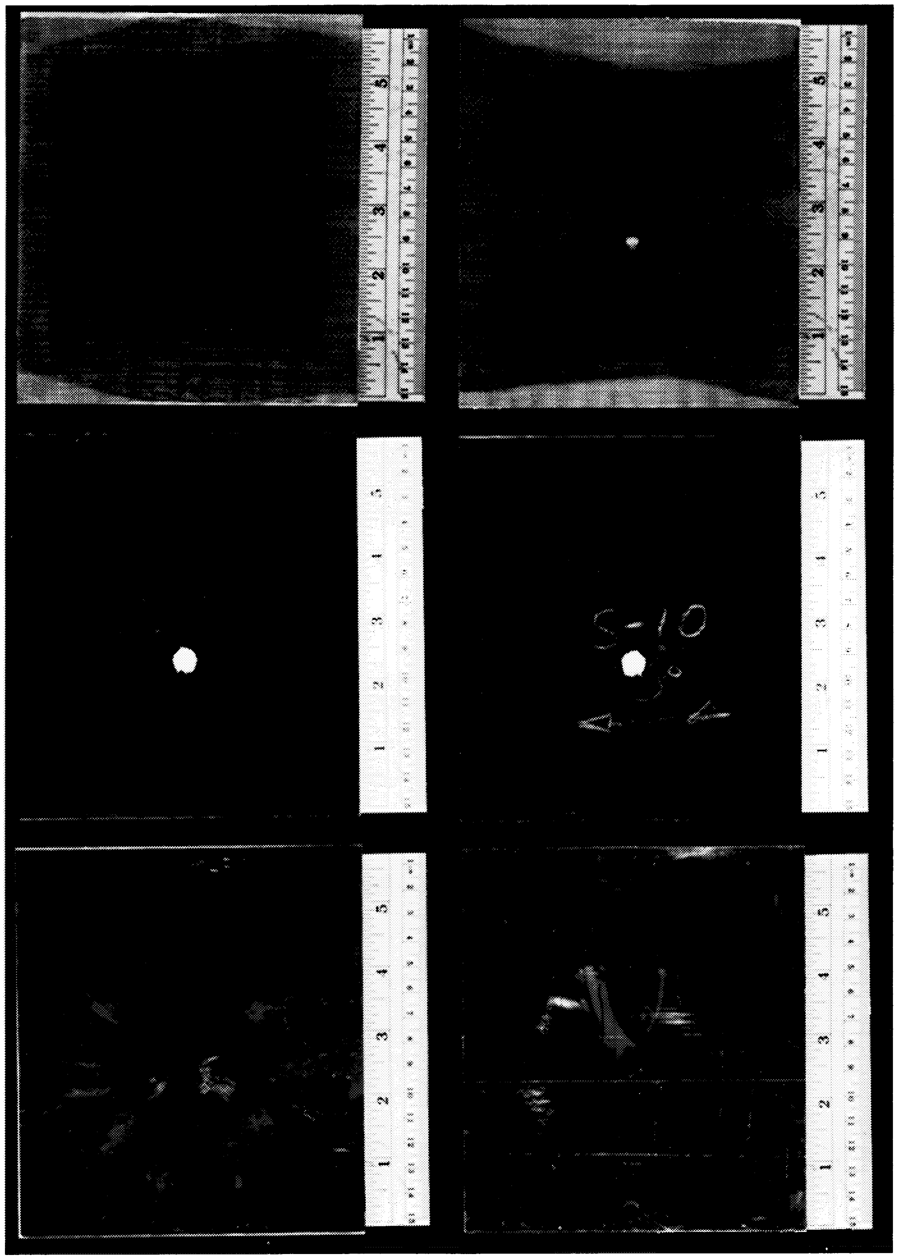

ORIGINAL PAGE
COLOR PHOTOGRAPH

Figure 6-14. Photographic Documentation for Shot #A163

.14" Kevlar cloth, 2" standoff, .050" Al 2024-T3 backwall, 4" standoff, .008" Al 3003-0 witness plate
.125" Al 1100 spherical projectile, 45.30 mg, 7.07 km/sec

FRONT BACK

BUMPER

BACKWALL

WITNESS

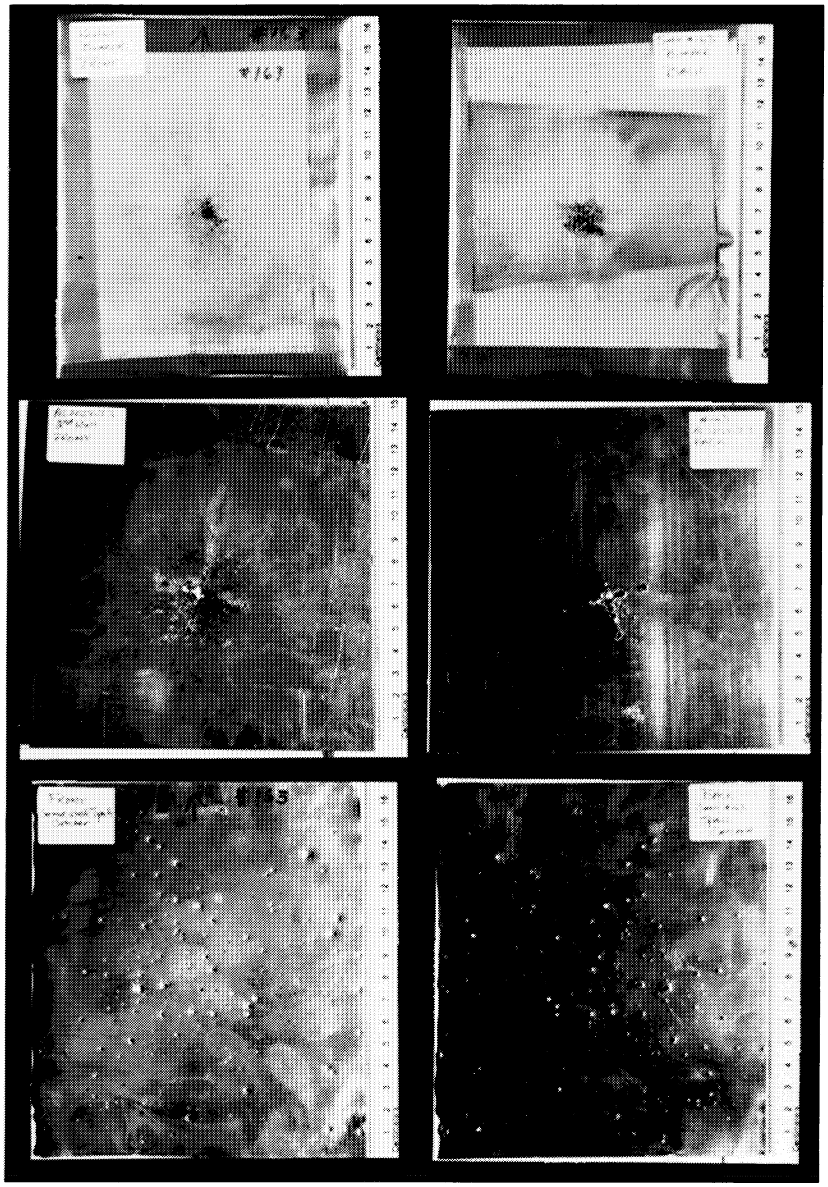

ORIGINAL PAGE
COLOR PHOTOGRAPH

Figure 6-15. Ejecta Catchers for Aluminum (Shot #A151) and Metal Matrix (Shot #A152)

.008" Al 3003-0 plate ejecta catcher, 4" spacing from bumper
Proj.: #A151 45.25 mg, 6.60 km/s; #A152 45.25 mg, 6.42 km/s
#A161 45.29 mg, 6.50 km/s

FACING BUMPER | BACK SIDE

SHOT #A151

SHOT #A152

SHOT #A161

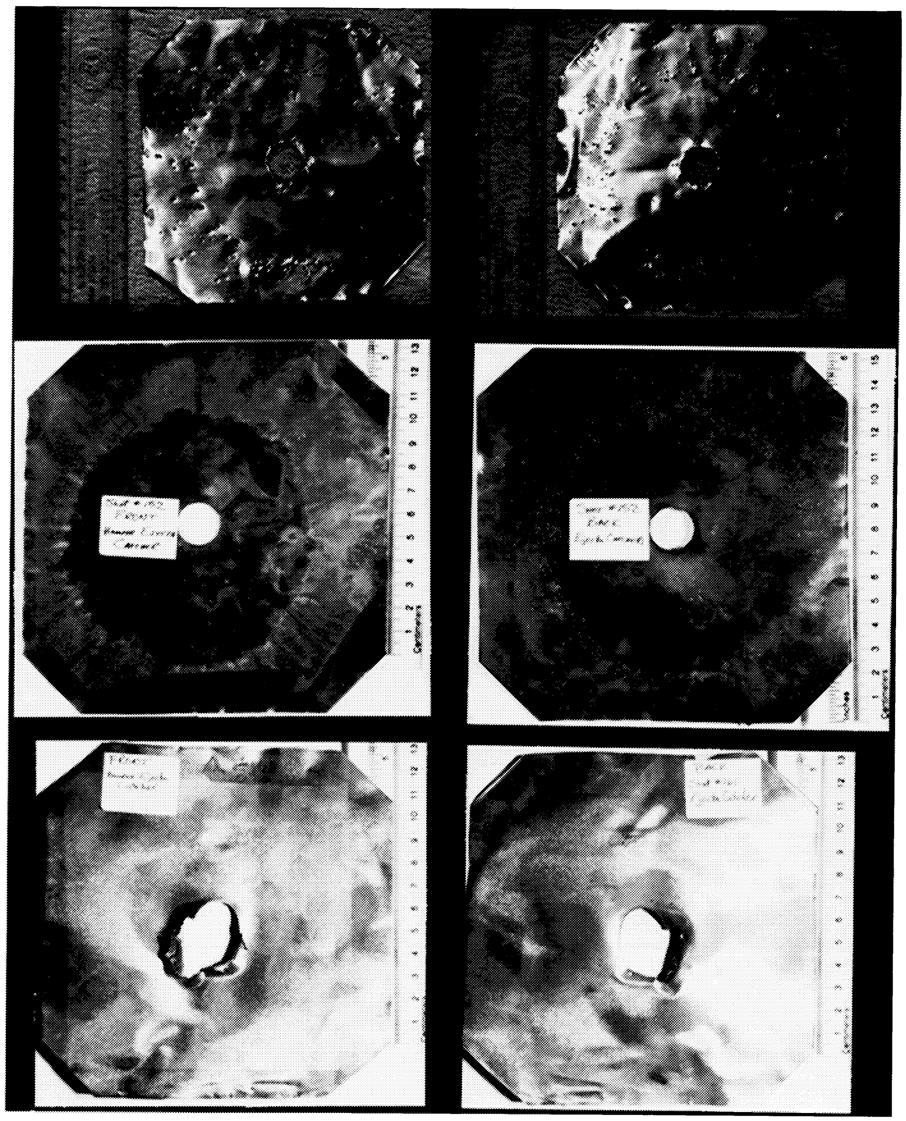

ORIGINAL PAGE
COLOR PHOTOGRAPH

7.0 Conclusions

Major conclusions of the shielding requirements study (Section 3):

- From consideration of no-penetration criteria, module geometry (including self-shielding), and the orbital debris environment, the modules would need to be designed to protect against a 1.1 g (0.92 cm) debris particle at a minimum. It appears that the baseline (0.063" Al 6061-T6 shield, 4.5" standoff, multilayer insulation, and 0.125" Al 2219-T87 backwall) will not offer sufficient protection from a particle of this size (at any velocity) and will therefore require additional protection to prevent critical damage, especially if both detached spall and perforation is to be prevented.

- Methods to achieve additional protection without a mass penalty include (1) alternative shielding materials or concepts, and (2) deployable shields to increase the standoff distance between bumper and inner wall. This study focused on screening alternative shield materials. Deployable shield concepts should also be studied.

- Protection can also be augmented by deploying additional shielding some time (years) after the pressurized modules have been on orbit. Such augmentation can allow module design to proceed without great change as long as augmentation techniques are developed and experimentally verified early and scars are added to the module exterior to accept additional shielding.

7.1 Summary of Findings

Several shielding configurations were rated superior to an aluminum (6061-T6) bumper based on hypervelocity impact testing; particularly, (1) double bumpers utilizing an aluminum mesh outer shield and an aluminum or graphite/epoxy second shield, and (2) a tungsten microsphere/silicone rubber material.

Other conclusions derived from testing and analysis include:

- Spall fragments can cause substantial damage, even when the backwall is not perforated. Spall was produced with aluminum (6061-T6) shields but was not with the double bumpers and tungsten/silicone material.

- Mesh, fabric, or porous materials do not make good shields by themselves, but are good low mass candidates for the outer shield in dual bumper systems.

- Corrugated bumpers do not perform as well as flat plates. The advantage of corrugated shields in dispersing debris plume particles over a wider area is more than outweighed by reduced projectile disruption from lower peak shock pressures.

- Graphite/epoxy alone did not shield as well as aluminum, however, its protective capability as a second bumper in dual bumper systems was rated superior.

- Laminated shields in this study (aluminum/graphite epoxy and alumina/aluminum) protected marginally better than aluminum. However, the aluminum layer was severely deformed, particularly for the Al - G/E laminate, due to strong shock reflection (caused by density differences) at the interface. From analysis, the performance of laminates as bumpers should suffer because shock waves reflect at the layer interface. This, however, is an advantage for the inner wall because it can suppress spall. Laminated inner walls and/or inner wall liners should be considered for Space Station module hulls to reduce spall.

- Ceramic plates need to be backed, supported or toughened in some way to avoid complete shattering. Toughened ceramics by reinforcing with ceramic whiskers and platelets should be experimentally evaluated.

- Al 6061-T6 had the most damaging ejecta particles. Brittler targets (alumina, metal matrix), or less dense materials (Kevlar) had less damaging ejecta. Ejecta from aluminum mesh was not damaging at all.

7.2 Recommendations

This study has determined that certain shielding concepts offer the promise of greater protection at less weight than aluminum. Additional testing in the JSC Hypervelocity Impact Research Laboratory is recommended to provide a larger database on these materials, to screen additional shield materials, and to test alternative inner wall concepts designed to suppress spall. Specific tests include:

1. Substituting SiC cloth for the aluminum mesh in a dual bumper study. To be comparable to earlier results, the test should use 2-3 sheets of SiC, 0.5" spacing, 0.016" Al 3003-0 second bumper, 1.5" standoff, and 0.05" Al 2024-T3 backwall.

2. Determining the optimal spacing between dual bumpers by using the aluminum mesh/-aluminum plate configuration tested in this study as a baseline, and stepping through higher and lower spacings.

3. Determining if a less ductile aluminum second bumper such as Al 6061-T6 (0.016" thickness) would perform better by reducing the channeling of front sheet debris.

4. Screening additional candidate bumper materials, particularly boron carbide ceramic reinforced with boron carbide whiskers or platelets, graphite composites (as second plate in dual bumper configuration), and magnesium alloy AZ31B.

5. Testing the ability of a backplate liner to prevent spall. Polyethylene is one candidate liner but flammability issues should be considered. Candidate backplate/liner combinations should be tested at the same areal density as the baseline backplate for comparative purposes.

Testing is recommended at another impact facility capable of launching 1/3" Al 1100 spherical projectiles at 6 km/sec. The purpose of these tests would be to verify that materials identified in subscale screening tests operate the same way with a larger particle. Tests should include shots on an aluminum baseline for comparative purposes. From the results of this study, the following shots are proposed to confirm that dual bumpers and tungsten/silicone materials can be successfully scaled. However, the materials proposed for testing at another facility are likely to change after further screening tests at JSC.

1. Establish an aluminum baseline with a 1/3" Al 1100 projectile at 6 km/sec: 0.032" Al 6061-T6 bumper, 4" standoff (no MLI), and 0.125" Al 2219-T87 backwall.

2. At the same impact conditions, test an Al 5056 mesh (14 x 14 wires per in^2, 0.028" wire thickness) outer bumper, 1" spacing, 0.045" Al 6061-T6 second bumper, 3" standoff, and 0.125" Al 2219-T87 backwall.

3. At the same impact conditions, test a 0.06" tungsten/silicone material bumper, 4" standoff, and 0.11" Al 2219-T87 backwall. If 1/9" Al 2219-T87 is unavailable, test a 0.05" tungsten/silicone bumper, 4" standoff, and 0.125" Al 2219-T87 backwall.

8.0 References

1. Christiansen, E.L.: "Space Station Meteoroid/Debris Bumper Study Test Planning and Setup," Eagle Engineering, July 17, 1986.

2. Wilkinson, J.P.D.: "A Penetration Criterion for Double-Walled Structures Subject to Meteoroid Impact," AIAA Journal, pp. 1937-1943, October, 1969.

3. Cour-Palais, B.G.: "Space Vehicle Meteoroid Shielding Design," ESA SP-153, pp. 85-92, April, 1979.

4. Johnston, R.H., Knapton, D.A., and Lull, D., "Meteoroid Bumper Protection for Space Vehicles, Tentative Design Criteria," NASA Technical Report 65008-05-01, 1963.

5. Swift, H.F. and Hopkins, A.K.: "Effects of Bumper Material Properties on the Operation of Spaced Meteoroid Shields," Journal of Spacecraft, vol. 7, no. 1, pp. 73-77, 1970.

6. Wilbeck, J.S., Anderson, C.E., Wenzel, A.B., Westine, P.S., and Lindholm, U.S. (instructors), "A Short Course on Penetration Mechanics," Southwest Research Institute, 1985.

7. Perry, R.H. (ed): Engineering Manual, 3rd Edition, Tables 3-1 and 3-41, 1976.

8. Elfer, N. and Kovacevic, G.: "Design for Space Debris Protection," Proceedings of the Third Annual AIAA Aerospace Technology Symposium, 14 pages, 1985

9. Garg, S.K. and Kirsch, J.W.: "Hugoniot Analysis of Composite Materials," J. Composite Materials, vol. 5, pp. 428-445, 1971.

10. Gault, D.E. and Heitowit, E.D.: "The Partition of Energy for Hypervelocity Impact Craters formed in Rock," Sixth Symposium on Hypervelocity Impact, Cleveland Ohio, pp. 419-456, 1963.

11. Kieffer, S.W. and Simonds, C.H.: "The Role of Volatiles and Lithology in the Cratering Process," Rev. Geophysics and Space Physics, vol. 18, pp. 143-181, 1980.

12. Kinslow, R. (ed): High-Velocity Impact Phenomena, Academic Press, New York, 1970.

13. Maiden, C.J., Gehring, J.W., and McMillan, A.R.: "Investigation of Fundamental Mechanism of Damage to Thin Targets by Hypervelocity Projectiles," Final Report NASA TR 63-225, 81 pages, 1963.

14. Marsh, S.P.: LASL Shock Hugoniot Data, University of California Press, Berkeley, California, 1980.

15. Maxwell, D.E.: "Simple Z model of Cratering, Ejection, and the Overturned Flap," Impact and Explosion Cratering, ed. D. J. Roddy, R. O. Pepin, and R. B. Merrill, pp. 1003-1008, Pergamon, New York, 1977.

16. Munson, D.E. and Schuler, K.W.: "Steady Wave Analysis of Wave Propagation in Laminates and Mechanical Mixtures," J. Composite Materials, vol. 5, pp. 286-304, 1971.

17. Nysmith, C.R.: "An Experimental Impact Investigation of Aluminum Double Sheet Structures," AIAA Paper 69-375, AIAA Hypervelocity Impact Conference, 5 pages, Cincinnati, Ohio, 1969.

18. Nysmith, C.R.: "A Discussion of the Modes of Failure of Bumper-Hull Structures with Application to the Meteoroid Hazard," NASA TN D-6039, 11 pages, 1970.

19. Richardson, A.J.: "Theoretical Penetration Mechanics of Multisheet Structures Based on Discrete Particle Modeling," J. Spacecraft and Rockets, April, 1970.

20. Richardson, A.J. and Sanders, J.P.: "Development of Dual Bumper Wall Construction for Advanced Spacecraft," AIAA paper 71-339, 7 pages, 1971.

21. Rinehart, J.S.: Stress Transients in Solids, Hyperdynamics, Santa Fe, 230 pages, 1975.

22. Rinehart, J.S.: "Compilation of Dynamic Equation of State Data for Solids and Liquids," U.S. Navel Ordnance Test Station, TN3798, 1965.

23. Ruoff, A.L.: "Linear Shock-Velocity-Particle-Velocity Relationship," Jour. Appl. Physics, vol.38, pp.4976-4980, 1967.

24. Swift, H.F.: Hypervelocity Impact Mechanics, Wiley Interscience, 1982.

25. Swift, H.F., Bamford, R., and Chen, R.: "Designing Dual Plate Meteoroid Shields- A New Analysis," JPL Publication 82-39, 85 pages, 1982.

26. Tsou, F.K. and Chou, P.C.: "Shock Hugoniot in Composite Materials - A Finite Control Volume Approach," AIAA Hypervelocity Impact Conference, AIAA Paper 69-359, 8 pages, 1969.

27. Tsou, F.K. and Chou, P.C.: "Analytical Study of Hugoniot in Unidirectional Fiber Reinforced Composites," J. Composite Materials, vol. 3, pp. 500-514, 1969.

28. Van Thiel, M.: Compendium of Shock Wave Data, UCRL-50108, vol. 1 and 2, Lawrence Radiation Laboratory, University of California, 1965.

29. Whipple, F.L.: "Meteorites and Space Travels," Astronomical Journal, no. 1161, p.131, 1947.

30. Yew, C.H., Kendrick, R.B., and Wang, C.Y.: "A Study of Damage in Composite Panels Produced by Hypervelocity Impact," Paper prepared for 1986 Hypervelocity Impact Symposium, May 1986.

31. Swift, H.F. and Hopkins, A.K.: "The Effects of Bumper Material Properties on the Operation of Spaced Hypervelocity Particle Shields," Air Force Materials Laboratory, AFML-TR-68-257, 1968.

32. "Comet Halley Micrometeoroid Hazard Workshop," ESA SP-153, Proceedings of an ESA International Workshop, Noordwijk, The Netherlands, 1979.

33. Cour-Palais, B.G.: "Meteoroid Protection by Multiwall Structures," AIAA Paper 69-372, AIAA Hypervelocity Impact Conference, 10 pages, Cincinnati, Ohio, 1969.

34. Hopkins, A.K., Lee, T.W., and Swift, H.F.: "Material Phase Transformation Effects Upon Performance of Spaced Bumper Systems," Journal of Spacecraft and Rockets, Vol. 9, pp. 342-345, May 1972.

35. Swift, H.F.: "Notes on the Further Development of Two Element Meteoroid Shield Response to a Realistic Meteoroid Threat," International Applied Physics Inc., December 1980.

36. Swift, H.F.: "Use of Kevlar Cloth/Epoxy Panels in Meteoroid Shield of Halley Comet Intercept Vehicle," International Applied Physics Inc., July 1981.

37. Bless, S.J. and Green, J.E.: "Micrometeoroid Evaluation of Galileo Spacecraft Structures," Final Report for JPL P.O. 955828, December 1980.

38. Kinslow, R.: "Bumper-Protected Laminated Spacecraft Mainwalls," NAS 1-10967, NASA CR-2262, May 1973.

39. DiBattista, J.D. and Humes, D.H.: "Multimaterial Lamination as a Means of Retarding Penetration and Spallation Failures in Plates," NASA Langley Research Center, NASA TN D-6989, November 1972.

40. Swift, H.F., Turpin, W.C., and Cunningham, J.H.: "Characterization of Debris Clouds Behind Impacted Meteoroid Bumper Plates," Wright-Patterson AFB, AF Contract F33615-67-C-1712.

41. Wilkins, M.L.: "Mechanics of Penetration and Perforation," Int. J. Engineering Science, Vol. 16, pp. 793-807, Pergamon Press, 1978.

42. Stump, W.R. and Christiansen, E.L.: "Secondary Impact Hazard Assessment," Eagle Engineering Report No. 86-128, June 1986.

43. Cour-Palais, B.G.: "Hypervelocity Impact Investigations and Meteoroid Shielding Experience Related to Apollo and Skylab," Orbital Debris, NASA Conference Publication 2360, pp.247-275, 1985.

44. Duke, M.B.: "Hazard Assessment of the Candidate 8 psi Space Suit," NASA-JSC memo SN3-85-158, November 1984.

45. Simpkin, R.: "Tactical Aspects of Active and Reactive Armours," Military Technology-MILTECH, pp. 18-28, April 1986.

46. "Reinforced Ceramics - Materials for Light and Heavy Armor," Avco Specialty Materials IRAD document, Division of Textron Inc., 1985.

47. E.E. Engler: "Space Station Advanced Development," Presentation at the Marshal Space Flight Center, March 1986.

48. Kessler, D.J.: "Orbital Debris Environment for Space Station," JSC20001, 1984.

49. Vaughan, W.W. and Green, C.E.: "Natural Environment Design Criteria Guidelines for the Space Station Definition and Preliminary Design (Second Revision)," NASA TM-86498, 1985.

50. Haines, C.D., Craig, M.K., and Aaron, J.: "Baseline Meteoroid/Debris Damage Tolerance Probabilities," SSCB Directive, Revision to Section 3 of JSC 30000, Space Station Systems Requirements, Paragraphs 2.1.3.1.1.B.2 and 2.1.3.1.1.C.1, November 5, 1986.

51. "IRR - Common Module Structures Definition," MSFC Presentation documents, January 1986.

52. "Baseline Configuration Document," Space Station Program Office, JSC 30255, November 18, 1986.

53. Leger, L.J.: "Oxygen Atom Reaction with Shuttle Materials at Orbital Altitudes," NASA TM-58246, May 1982.

54. Leger, L.J.: "Oxygen Atom Reaction with Shuttle Materials at Orbital Altitudes," AIAA-83-0073, AIAA 21st Aerospace Sciences Meeting, January 1983.

55. Visentine, J.T., Leger, L.J., Schomburg, C., and Jones, W.B.: "Atomic Oxygen Effects on Surfaces in Low Earth Orbit," Second Solar Dynamic Power Systems Workshop, JSC, August 1984.

56. Leger, L.J., Visentine, J.T., and Schliesing, J.A.: "A Consideration of Atomic Oxygen Interactions with Space Station," AIAA-85-0476, AIAA 23rd Aerospace Sciences Meeting, January 1985.

57. Whitaker, A.F., Burka, J.A., Coston, J.E., Dalins, I., Little, S.A., and DeHaye, R.F.: "Protective Coatings for Atomic Oxygen Susceptible Spacecraft Materials - STS 41G Results," AIAA Shuttle Environment and Operations II Conference, November 1985.

58. "Space Station Preliminary Analysis and Design Document, Book 4, Assembly Truss and Structure, Material Trade Study," McDonnell Douglas Astronautics Company-Huntington Beach, December 1985.

59. "Architectural Control Document, Thermal Control System," Space Station Program Office, JSC 30258, December 1, 1986.

60. "Boeing Wings it with Thermoplastics," Aerospace America, p. 54, November 1986.

61. Carson, J.M. and Hopkins, A.K.: "Impact Response of High Strength, Carbon Fiber/-Epoxy Composite Materials," Air Force Materials Laboratory, AFML-TR-71-178, October 1971.

62. Crews, J.L. and Stump, W.R.: "Preliminary Comparison of Aluminum and Composite Habitation Module Walls and Bumpers Subjected to Hypervelocity Impact," NASA JSC and Eagle Engineering, January 1984.

63. Kavanaugh, H.C. and Miller, G.J.: "Preliminary Structural Design and Analysis of a Shuttle Launched Space Station Manned Habitable Module," Space Station Subsystem White Paper, June 1984.

64. "Space Station Advanced Development Data Book - Volume 2," JSC-30232, November 1986.

65. "Space Station Requirements for Materials and Processes," JSC-30233, May 30, 1986.

66. Christiansen, E.L.: "Assessment of Space Station Meteoroid/Debris Shielding Materials," Eagle Engineering Report No. 86-149, December 1986.

67. "Space Station Projects Requirements Document," JSC-31000, Rev. C, March 6, 1987, Change Package No. 1, April 22, 1987.

68. "Space Station Definition and Preliminary Design, WP-01, Book 2, Common Module, Data Requirement No. DR-02, Rev.A," Martin Marietta Aerospace, Denver, Colorado, NAS8-36525, SSP-MMC-00031, June 30, 1986.

69. Engler, E.E.: Personal Communication. NASA, Marshall Space Flight Center, Code EP13, August 22, 1986.

70. "Common Module, End Item Data Book, Rev. B, Boeing FSCM No. 81205, DR-02 Data Package - WP-01," Boeing Aerospace Company, Huntsville, Alabama, NAS8-36526, June 30, 1986.

71. Cour-Palais, B.G.: "Hypervelocity Impact in Metals, Glass, and Composites," Proceedings of the 1986 Hypervelocity Impact Symposium, International Journal of Impact Engineering, Vol. 5, pp. 221-237, Pergamon Press, 1987.

72. Eichhorn, G.: "Analysis of the Hypervelocity Impact Process from Impact Flash Measurements," Planetary Space Science, Vol. 24, pp. 771-781, Pergamon Press, 1976.

73. Cour-Palais, B.G.: "Hypervelocity Impact Investigations and Meteoroid Shielding Experience Related to Apollo and Skylab," from Minutes of the NASA Workshop on Space Debris and Meteoroid Technology and Implications to Space Station, September 5-6, 1984.

74. Kessler, D.J. and Cour-Palais, B.G.: "Collision Frequency of Artificial Satellites: the Creation of a Debris Belt," Journal of Geophysical Research, Vol. 83, No. A6, p. 2637, June 1978.

75. Su, S.Y. and Kessler, D.J.: "Contribution of Explosion and Future Collision Fragments to the Orbital Debris Environment," Advanced Space Research, Vol. 5, No. 2, pp. 25-34, 1985.

76. Yew, C.H. and Wang, C.Y. (University of Texas), and Crews, J.L. (NASA JSC): "A Phenomenological Study of the Effect of Hypervelocity Impacts on Graphite-Epoxy Plates," NASA Johnson Space Center, 1987.

77. Parker, V.C. (Cordin Co.) and Crews, J.L. (NASA JSC): "Hypervelocity Impact Studies Using a Rotating Mirror Framing Laser Shadowgraph Camera," Paper 832-13, presented at the Optical and Optoelectronic Applied Science and Engineering Technical Symposium, San Diego, California, August 16-21, 1987.

78. Morrissey, R.J. and Dreiband, S.: "Army Materials Lab Works with Small Business to Lighten the Force," Defense Science & Electronics, pp.38-39, August, 1987.

Appendix A

Description of Analytical Model Calculations

INTRODUCTION

This appendix presents a "quick look" technique for evaluating the performance of candidate bumper systems when subjected to hypervelocity impact. The criteria for a successful bumper are: 1) that impact with the shield material will deposit enough internal energy in the projectile to cause it to melt or vaporize and 2) that the shield is thick enough to subject all of the projectile to peak shock pressures.

The technique uses one dimensional shock theory to determine the minimum impact velocity required to melt a variety of projectiles by comparing the internal energy required to melt or vaporize the projectile with the amount of internal energy increase in the projectile following impact. The procedure assumes that the criteria for a successful bumper is considered to be that it subjects the entire mass of a threatening projectile to a pressure sufficient to melt it. Calculated peak shock pressures may be directly compared to the established peak shock pressures required to melt materials. If a shield is too thin, the rarefaction wave emanating from the back of the shield catches up with the compressive pulse emanating from the projectile shield interface before the entire projectile is subjected to the peak shock pressure. A calculation is done using a simple linear relation between shock and particle velocities and rarefaction wave velocity, to estimate the minimum thickness of a shield for projectiles of interest. Obviously the bumpers will be too thick for much smaller projectiles, and a threat of spall exists for the smaller projectile. The current analysis does not consider spall processes.

CALCULATIONS

The concept considered is that of the hypervelocity impact protective shield, or Whipple bumper (29). The approach used here is intended to screen a large number of potential bumper materials with a minimum amount of calculation. The models are simplified with large numbers of assumptions so that the numerical solutions are arrived at from closed form solutions to the relevant equations. The approach used is based on work from the early phases of bumper studies in the 1960's, but is supported by a much broader body of experimental data on equations of state relating shock and particle velocities, pressures, and material densities than was available during the Apollo era. The formulation of the problem follows the logic used in Gault and Heitowit (10), Maiden et. al. (13), Cour-Palais (3) and Kieffer and Simonds (11). A review of the more recent investigations to support the Comet Halley missions (32) indicates that the basic assumptions used in the analysis are still regarded as acceptable, although the solution technique lacks the geometric sophistication of the hydrodynamic code models. However the total cost of this analysis is a few percent of the cost of a hydrodynamic code calculation.

The calculations that are presented here focus on determining three items:

1. Peak shock pressure experienced by the bumper and shield.

2. The amount of internal energy left in the projectile after collision, in effect the temperature and state of the projectile.

3. The minimum thickness of shield necessary to produce the peak shock pressure in the entire projectile.

The procedure which is used here provides analytical closed form solutions to the relevant equations by following the well-trodden path of hypervelocity impact theory, using Rankine-Hugoniot relations for materials on either size of a shock front and approximating equations of state with linear relations between shock and particle velocities.

An approximate one-dimensional approach is used to allow rapid evaluation of a large number of projectile and shield materials with combinations of impact velocity, projectile size, and shield thickness. The goal of the model is to predict the fraction of the projectile that is shocked and the peak shock pressure to which the bumper and projectile are subjected. The basic criteria for a successful bumper is one which shocks 100 percent of a projectile to a pressure which will melt the projectile. An ancillary consideration is that the shield immediately in front of the projectile shock also be shocked to a level that it is melted, or at least fragmented to very small particles.

In this initial phase of the analysis, it is assumed that the impact is between two semi-infinite (half-space) masses which make contact with a planar interface. The geometry and nomenclature are shown below.

	δ_{0p}	P_{0p}	E_{0p}	μ_{0p}	
shock front		U_p ↑			PROJECTILE
	δ_p	P_p	E_p	μ_p	
Shocked Region		↓			Interface
	δ_t	P_t	E_t	μ_t	
shock front		U_t ↓			TARGET
	δ_{0t}	P_{0t}	E_{0t}	μ_{0t}	

The frame of reference for the calculations is that used by Gault and Heitowit (10) and Kieffer and Simonds (11), with velocities referred to the materials prior to the time of impact. The target velocities are determined with respect to the back of the shield and projectile velocities with respect to the back of the projectile. This convention is different from that used by Maiden et. al. (13).

PEAK SHOCK PRESSURES

This analysis of peak shock pressures follows the established practice of Gault and Heitowit (10) and Kieffer and Simonds (11) in modeling a one-dimensional impact. The starting point is the Rankine-Hugoniot equations for the conditions on either side of a shock front.

Conservation of momentum

$$P - P_0 = 10\, \delta\, U\, \mu \qquad (1)$$

Conservation of mass

$$\delta_0\, U = \delta\, (U - \mu) \qquad (2)$$

Conservation of energy

$$E - E_0 = 100\,(P + P_0)\,(V_0 - V) / 2 \qquad (3)$$

As a practical matter the initial pressures and internal energy can be assumed to be zero, thus equation 1 simplifies to

$$P = 10\,\delta\,U\,\mu \qquad (1a)$$

and equation 3 simplifies to

$$E = 100\,P\,(V_0 - V)/2 \qquad (3a)$$

or, in terms of densities:

$$E = 100\,P\,[(1/\delta_0) - (1/\delta)] \qquad (3b)$$

The equation of state used in all of the analyses is in the form of a linear relation for the shock velocity and particle velocity:

$$U = c_0 + s\,\mu \qquad (4)$$

This relation has been demonstrated as a satisfactory approximation for virtually all solids that are free of phase changes over the range of interest and of substantial initial void space (23) (see the diagrams in Reference 14 for numerous examples).

The critical assumption in the analysis is that the material within the shocked region on either side of the contact surface is at a single shock pressure and is moving as a single unit with one speed. Mathematically, this means that

$$v_i = \mu_p + \mu_t \qquad (5)$$

and

$$P_p = P_t \qquad (6)$$

Using equation 4 to eliminate the shock velocity in equation 1a

$$P = 10\ \delta_0\ (\ c_0 + s\mu)\mu \qquad (7)$$

and equation 5 to eliminate μ_p results in the expressions:

$$P_p = 10\ \delta_{0p}\ [\ c_0 + s_t\ (v_i - \mu_t)](v_i - \mu_t) \qquad (8)$$

$$P_t = 10\ \delta_{0t}\ (c_0 + s_t\ \mu_t\ )\ \mu_t \qquad (9)$$

Peak shock pressures are calculated by solving the following quadratic equation for the particle velocity in the target, μ_t.

$$\delta_p[c_{0p} + s_p\ (v_i - \mu_t)](v_i - \mu_t) = \delta_{0t}(c_{0t} + s_t\ \mu_t)\mu_t \qquad (10)$$

The standard solution for a quadratic equation is:

$$\mu_t = \frac{-b \pm (b^2 - 4ac)^{0.5}}{2a} \qquad (11)$$

where,

$$a = (\delta_{0p}\ s_p) - (\delta_{0t}\ s_t) \qquad (12)$$

$$b = -\ (2\ \delta_{0p}\ s_p\ v_i) - (\delta_{0p}\ c_{0p}) - (\delta_{0t}\ c_{0t}) \qquad (13)$$

$$c = (\delta_{0p}\ v_i\ c_{0p}) + (\delta_{0p}\ v_i^2\ s_p) \qquad (14)$$

The quadratic has two solutions. The solution selected is in the range of 0.1 to 1.0 times the impact velocity while the other solution has no physical meaning. The value of the particle velocity in the target, μ_t, is substituted into the linear shock-velocity/-particle-velocity Hugoniot (equation 4) to determine the shock velocity, U_t.

$$U_t = c_{0t} + s_t\ \mu_t$$

The shocked density of the target is calculated by substituting into the equation for conservation of mass (equation 2).

$$\delta_t = (\delta_{0t}\, U_t) / (U_t - \mu_t)$$

Finally, the shock pressure ($P=P_t=P_p$) is calculated by substituting values for shocked density, particle velocity, and shock velocity into the equation for conservation of momentum (equation 1).

$$P = 10\, \delta_t\, U_t\, \mu_t$$

The particle velocity in the projectile, μ_p, is calculated using equation 5:

$$\mu_p = v_i - \mu_t$$

and the shock velocity in the projectile from equation 4.

$$U_p = c0_p + s_p\, \mu_p$$

The projectile shocked density is determined in a manner similar to that used for the target.

$$\delta_p = (\delta_{0p}\, U_p) / (U_p - \mu_p)$$

These calculations are performed on a simple Lotus 1-2-3 spreadsheet, since all of the solutions are in closed form.

KINETIC AND THERMAL ENERGY PARTITION BETWEEN THE PROJECTILE AND SHIELD

A key calculation useful in evaluating the relative performance of different bumper materials is to compare the amount of heating, melting, and vaporization of the threatening projectile. Following the logic used in Gault and Heitowit (10) and Kieffer and

Simonds (11), the total energy retained by the projectile out of the initial kinetic energy, $0.5*10*\delta_{0p}*V_p*v_i^2$, when it has been subjected to the peak shock pressure is

$$5\,\delta_{0p}\,V_p\,[(v_i - \mu_t)^2 + \mu_t^2] \qquad (17)$$

and the retained kinetic energy of the projectile (contained in the ejecta and remaining projectile) is

$$10\,\delta_{0p}\,V_p\,\mu_t^2 / 2 \qquad (18)$$

The difference between the two is an estimate of the amount of internal energy retained in the projectile. In the spreadsheet, ratios of the retained internal energy to the energy required to melt and vaporize the projectile are calculated, yielding the estimated state of the projectile.

This calculation estimates the state of the projectile from an energy balance, not by calculation of the P-V work done by the shock process from the difference between the area under the Hugoniot compression and isentropic release curves on a P-V diagram. Projectile melting and vaporization can occur from thermal energy added during shock compression and release. As given in Table 3-1, impact pressures of approximately 650 Kbars will result in incipient melting of a aluminum projectile while 900 Kbars will completely melt an aluminum projectile. However, this calculation sets an upper bound on the temperature to which the projectile may be heated from a simple energy partition approach. The results suggest that there is enough energy to melt an aluminum (1100) projectile for many low density materials, although the melting may not be due to shock compression and release (lower half of Table A-1). This implies low density materials may disrupt projectiles to a greater extent than would be concluded from consideration of shock processes alone.

MINIMUM THICKNESS OF SHIELD

An estimate of the minimum shield thickness required to completely shock the projectile is calculated using the logic of Maiden et. al. (12, ch. 4; 13) although the results presented here differ somewhat. The basic assumption made is that the entire volume of the projectile must be swept by the compressional shock wave following impact and prior to the arrival of the rarefaction wave reflected off the back of the shield. For shield materials that are thin in comparison to the projectile, the rarefaction wave travels though compressed projectile material and thus has a shorter distance to travel than the shock wave, which travels through unshocked material.

The equation to be solved is the time for the shock to travel through the unshocked projectile, T_{0p}, equals the sum of the time for the shock to travel to the back of the unshocked shield, T_{0t}, plus the time for the rarefaction to travel back through the compressed shield, T_t, plus the time for the rarefaction to pass back through the projectile, T_p, where

$$T_{0p} = L_p / (10\ U_p) \qquad (19a)$$

$$T_{0t} = L_t / (10\ U_t) \qquad (19b)$$

$$T_t = L_t\ \delta_{0t} / (10\ \delta_t\ C_t) \qquad (19c)$$

$$T_p = L_p\ \delta_{0p} / (10\ \delta_p\ C_p) \qquad (19d)$$

The sound velocity of the rarefaction in the highly compressed material is calculated using the same relation that was used by Maiden et. al. (13).

$$C = U\ \{0.49 + [(U - \mu)/U]^2\}^{0.5} \qquad (20)$$

Combining equations 19 (a-d) and solving for ratio of shield to projectile length gives

$$L_t/L_p = \{(1/U_p) - [\delta_{0p}/(\delta_p\ C_p)]\}/\{[\delta_{0t}/(\delta_t\ C_t)] + (1/U_t)\}$$

which can be solved for the optimum shield thickness, L_t, given projectile diameter, L_p.

INPUT DATA

A variety of sources of data have been searched out to find published Hugoniot data for the constants in equation 4 (9-16, 21-23, 26-28). The most comprehensive lists are in Kinslow (12, p. 371) and Marsh (14). The values of the constants for aluminum and basalt used by Gault and Heitowit (10) are also included. The calculation procedure was verified by duplicating the results of Reference 10 for aluminum impacting basalt. For materials without significant phase transformations, the linear shock-velocity/particle-velocity parameters are appropriate for the entire data set. However, for most of the other materials, one or more phase transformations are present. In those instances, the parameters c_0 and s represent a fit to the higher pressure portions of the published data, typically with pressures above 150-200 kilobars.

Hugoniot data for composite materials is presently not abundant. None is available for graphite epoxy composites. Munson and Schuler (16) and the works referenced therein review a number of procedures for calculating Hugoniots for composites using data on the component materials and the volume proportions. However, the current analysis has not been able to fully explore the composite models and test their results against data for a number of composites for which data does exist (e.g. epoxy and paraffin combined with a number of minerals as given in Reference 14).

The spreadsheet also contains thermophysical properties for a number of the pure elements and simpler compounds. Data of particular interest is the energy content for the melted or vaporized state, because most of these simple materials may model projectiles. For orbital debris problems the values for aluminum, either the Gault and Heitowit (10) values or those for 1100 aluminum are well defined, as is the data for iron.

CALCULATION PROCEDURE

The calculation procedure follows a sequence of steps.

A. Extract physical properties data from a table.

B. Calculate properties for the target in the shocked state.

1. Particle velocity for the target, μ_t.
2. Shock velocity for the target, U_t.
3. Density of the target, δ_t.

4. Shock pressure in the target, P_t.
5. Fraction of energy deposited in the target assuming that the target is thick relative to the projectile.
6. Acoustic velocity of the rarefaction wave, C_t.

C. Calculate the properties of the projectile in the shocked state.

1. Particle velocity, μ_p.
2. Shock velocity, U_p.
3. Density, δ_p.
4. Shock pressure in the projectile, P_p, which should equal P_t.
5. Fraction of energy deposited in the projectile assuming that the target is thick relative to the projectile.
6. Acoustic velocity of the rarefaction wave, C_p.

D. Calculate the optimum shield thickness.

1. Ratio of the shield to projectile thickness.
2. Conversion of units to inches.
3. Determining weight of shield in pounds per square foot.
4. Verification time check.

OPERATING PROCEDURE

Calculations are performed for 1 gram projectiles with impact velocities of 3 to 24 kilometers per second, as given by the example spreadsheet in Figure A-1. The user can select any desired projectile or target materials given in cells B7 through B49 by entering the appropriate number in cells F56 and F57 respectively. The user can also select any desired projectile impact velocity in cell F58. The rest of the spreadsheet is protected from accidental entry. The spreadsheet calculations are performed by pressing the "Calc" function key, <F9> on IBM PC's and most compatibles. Some results of interest are impact pressure (F85), fraction energy in target (F86), fraction energy in projectile (F96), ratio of residual projectile internal energy to energy required to melt the projectile (F100), and ratio of projectile internal to required vaporization energy (F101). The spreadsheet can be printed by pressing the keys / **P P A G** in that order. A graph of the results can be viewed by pressing the "Graph" key, <F10> on IBM PC's and most compatibles.

RESULTS

The example graph given in Figure A-2 illustrates the calculated peak shock pressure in megabars (solid line through squares), the optimal shield areal density in lbs/sq. ft. (diamonds), and the fraction of projectile that melts (solid line through triangles), all as a function of impact velocity. As shown by the graph, an aluminum projectile is completely molten for the given areal density shield at an impact speed of approximately 7 km/sec. The optimal areal density shield continually increases, which differs from Maiden (13) and Cour-Palais (3, 33). It has been reported that as projectile velocity increases above the velocity necessary to melt the projectile, the bumper thickness can be decreased while still producing a molten projectile (3; 6, pp. 6-118; 12; 13). The slope of the optimal areal density curve increases with velocity because it was calculated based on shocking the entire projectile at the impact pressure. If the thickness of shield was recalculated based on just producing a totally molten projectile, the slope would decrease with increasing velocity because the available kinetic energy increases, but the projectile would not be totally shocked since the rarefaction wave overtakes the compressive shock wave moving into the projectile and weakens it.

ACCESS TO SPREADSHEET

The analytical model calculations and Hugoniot equation-of-state constants for the materials in Figure A-1 are given in the spreadsheet on the diskette at the back of this report. The spreadsheet name is IMPACT.WKS.

SYMBOLS

c	=	First term in the linear shock-velocity/particle-velocity Hugoniot, (in general the term does not equal the acoustic velocity of a material at zero pressure) (km/sec)
C	=	Acoustic velocity, or velocity of rarefaction (km/sec)
L	=	Characteristic length or thickness of projectile or shield (cm)
s	=	Second term in shock-velocity/particle-velocity Hugoniot (dimensionless)
v	=	Velocity (km/sec)
V	=	Specific volume = $1/\delta$ (cm^3/gm) in Equations 3 and 3a Volume (cm^3) in Equations 17 and 18
δ	=	Density (gm/cm^3)
P	=	Pressure (kilobars)
E	=	Internal Energy (Joule/gm)
μ	=	Particle velocity (km/sec)
U	=	Shock Velocity (km/sec)
T	=	Time (micro-sec)

Subscripts:

blank	=	shocked state
i	=	impact
0	=	rest state
t	=	target
p	=	projectile

29-Dec-86

Figure A-1. Analytical Model Spreadsheet

MATERIAL PROPERTIES

#		Density g/cm3	c0 (eff) km/s	s (eff)	K0 (eff) kbar	n	HEL	P part me	P melt	P vapor
1	Alumina Coors Al203 15%Si02	3.660	5.650	2.200	487.604	7.800				
2	Alumina Al203 Hot pressed	3.940	8.250	1.210	2681.663	3.840				
3	Aluminum 1100	2.714	5.392	1.341	789.059	4.364				
4	Aluminum 2024 Alloy	2.784	5.370	1.290	802.819	4.160				
5	Aluminum 6061 Alloy	2.703	5.350	1.340	773.066	4.360				
6	Aluminum 7075 Alloy	2.804	5.200	1.360	758.202	4.440				
7	Aluminum 921 T Alloy	2.833	5.041	1.420	719.913	4.680		600	900	
8	Aluminum (Gault&Heitowit)	2.750	5.300	1.370	772.000	4.480		600	900	
9	Anorthosite	2.730	4.170	1.120	474.717	3.480				
10	Basalt (Gault&Heitowit)	2.860	2.600	1.620	193.000	5.500				
11	Cadmium	8.639	2.480	1.640	531.333	5.560				
12	Carbon Graphite 3D fibers	1.519	2.22	1.14	96.616	3.575				
13	Composite 2D-CP C-PHEN.	1.350	2.500	2.200	205.335	7.800				
14	Copper	8.930	3.940	1.469	1386.257	4.956		1400	1800	
15	Feldspar Anorthosite NY	2.732	2.790	1.533	212.662	5.132				
16	Glass High Density (Shott)	5.085	1.513	1.611	167.142	5.444				
17	Glass Pyrex	2.230	1.730	1.550	66.742	5.200				
18	Glass Silica	2.204	3.180	0.990	222.877	2.960		250		
19	Gold	19.240	3.05	1.57	1796.850	5.288				
20	H2O Ice	0.910	1.280	1.560	15.020	5.230				
21	H2O Water	1.000	1.480	1.600	22.000	5.400				
22	Iron (Gault&Heitowit)	7.850	3.600	1.580	1135.00	5.320			2000	
23	Lead	11.346	2.030	1.470	467.557	4.880				
24	Magnesium	1.740	4.492	1.263	351.098	4.052				
25	Magnesium AZ 31 B alloy	1.775	4.516	1.256	361.998	4.024				
26	Mullite Al6Si2013	2.670	2.300	1.650	141.243	5.600				
27	Plastic Acrylic	1.185	2.527	1.536	75.671	5.144				
28	Plastic Epoxy	1.198	2.678	1.520	85.917	5.080				
29	Plastic Polyamide (Nylon)	1.146	3.910	1.180	175.202	3.720				
30	Plastic Polycarbonate	1.193	2.191	1.145	121.477	3.580				
31	Plastic Polyimide	1.414	1.615	1.490	36.880	4.960				
32	Plastic PVC (Boltron)	1.376	2.415	1.442	80.251	4.768				
33	Plastic Teflon	2.147	1.682	1.189	60.741	3.756				
34	Platinum	21.440	3.63	1.47	2829.799	4.888				
35	Silica Quartz x cut	2.650	4.030	0.990	430.384	2.960		250		
36	Silicon Carbide SiC	3.120	8.000	0.950	1995.800	2.800				
37	Steel 1018	7.850	3.357	1.920	864.853	6.680			2000	
38	Steel 304 Stainless	7.696	4.569	1.490	1648.350	4.960				
39	Steel maraging(Vascomax250)	8.129	3.993	1.576	1296.092	5.304				
40	Titanium	4.528	5.220	0.767	1233.808	2.068		>1000		
41	Tungsten Carbide WC	15.020	4.920	1.339	3635.801	4.356				
42	Uranium 97%U 3%Mo	18.450	2.565	1.531	1213.867	5.124				
43	Wood Douglas Fir	0.536	[illegible]	1.360	1.085	4.520				

#		en to mp erg/gm	en melted erg/gm	en to bp erg/gm	en vap erg/gm	T melt K	T vap K	a (cal/deg C per mole)	b	c	heat vmel cal/mole	heat v cal/mole	mol wt gm/mole
1	Alumina Coors Al203 15%Si02												
2	Alumina Al203 Hot pressed	4.08E+10	5.15E+10	7.98E+10	7.98E+10	2318	3273	22.030	0.009	-522500	26000		101.819
3	Aluminum 1100	5.04E+10	5.44E+10	4.23E+11	5.16E+11	933	2823	4.800	0.032		2550	60020	26.980
4	Aluminum 2024 Alloy												
5	Aluminum 6061 Alloy												
6	Aluminum 7075 Alloy												
7	Aluminum 921 T Alloy												
8	Aluminum (Gault&Heitowit)	5.04E+10	5.44E+10	4.23E+11	5.16E+11	933	2823	4.800	0.032		2550	60020	26.980
9	Anorthosite												
10	Basalt (Gault&Heitowit)												
11	Cadmium	1.53E+09	2.07E+09	3.64E+09	1.25E+10	594	1038	5.460	0.002		1460	23870	112.400
12	Carbon Graphite 3D fibers					3873	11273	2.673	0.003	116900			12.011
13	Composite 2D-CP C-PHEN.												
14	Copper	6.63E+09	8.68E+09	2.02E+10	6.82E+10	1356	2868	5.440	0.001		3110	72810	63.540
15	Feldspar Anorthosite NY												
16	Glass High Density (Shott)												
17	Glass Pyrex												
18	Glass Silica												60.074
19	Gold												
20	H2O Ice	5.24E+09	8.58E+09	1.05E+10	3.31E+10	273	373	8.220	0.000	0	1436	9729	18.010
21	H2O Water	5.24E+09	8.58E+09	1.05E+10	3.31E+10	273	373	8.220	0.000	0	1436	9729	18.010
22	Iron (Gault&Heitowit)	4.37E+10	4.92E+10	1.14E+11	2.46E+11	1803	3008	4.13	0.01		3560	84600	26.980
23	Lead	1.47E+08	3.79E+08	1.90E+09	1.05E+10	601	2023		0.002		1147	42471	207.190
24	Magnesium	1.18E+10	1.55E+10	2.28E+10	7.88E+10	923	1380	6.200	0.001	-67800	2160	32520	24.312
25	Magnesium AZ 31 B alloy												
26	Mullite Al6Si2013	0.00E+00	1.78E+08	1.78E+08	1.78E+08						1510		425.940
27	Plastic Acrylic												
28	Plastic Epoxy												
29	Plastic Polyamide (Nylon)												
30	Plastic Polycarbonate												
31	Plastic Polyimide												
32	Plastic PVC (Boltron)												
33	Plastic Teflon												
34	Platinum												
35	Silica Quartz x cut	3.16E+10	3.40E+10	5.93E+10	5.93E+10	1743	2503	10.870	0.009	-241200	3400		60.074
36	Silicon Carbide SiC	5.09E+10	5.09E+10			2873		8.890	0.003	-284000			40.700
37	Steel 1018												
38	Steel 304 Stainless												
39	Steel maraging(Vascomax250)												
40	Titanium	2.04E+10	2.04E+10	3.61E+10	3.61E+10	2073	3273	8.910	0.001	-433000			47.90
41	Tungsten Carbide WC					3143	6273						175.930
42	Uranium 97%U 3%Mo	1.64E+09	1.64E+09	4.77E+09	4.77E+09	1405	4091	6.640					[illegible]
43	Wood Douglas Fir												

INPUT PARAMETERS

Projectile Material	3		3.000	3.000	3.000	3.000	3.000	3.000	3.000	3.000	3.000	3.000	3.000	3.000	[illegible]	3.000	[illegible]
Target Material	4		4.000	4.000	4.000	4.000	4.000	4.000	4.000	4.000	4.000	4.000	4.000	4.000	[illegible]	4.000	[illegible]
Impact Velocity,km/sec	7.000		3.000	4.000	5.000	6.000	7.000	8.000	9.000	10.000	12.000	14.000	16.000	18.000	20.000	22.000	[illegible]
	frame of reference	frame of reference															

ORIGINAL PAGE IS OF POOR QUALITY

Figure A-1 (Cont). Analytical Model Spreadsheet

		back of shield back of projectile		back of shield															
projectile length cm	0.89	0.889		0.889	0.889	0.889	0.889	0.889	0.889	0.889	0.889	0.889	0.889	0.889	0.889	0.889	0.889	0.889	0.889
shield thickness cm		0.133		0.133	0.133	0.133	0.133	0.133	0.133	0.133	0.133	0.133	0.133	0.133	0.133	0.133	0.133	0.133	0.133
MATERIAL PROPERTIES																			
Projectile Density gm/cc		2.714		2.714															
Projectile Co km/sec		5.392		5.392															
Projectile s		1.341		1.341															
Projectile energy to melt erg/gm		5.44E+10																	
Projectile energy to vaporize erg/gm		5.16E+11																	
Target Density gm/cc		2.78		2.78															
Target Co km/sec		5.37		5.37															
Target s		1.29		1.29															
Target energy to melt erg/melt		0.00E+00																	
Target Energy to vaporize erg/gm		0.00E+00																	
TARGET CALCULATIONS																			
c		280.77		280.77	76.66	116.77	164.16	218.82	280.77	350.00	426.50	510.29	699.69	918.21	1165.85	1442.60	1748.47	2083.45	2447.55
b		-80.54		-80.54	-51.42	-58.70	-65.98	-73.26	-80.54	-87.82	-95.09	-102.37	-116.93	-131.49	-146.05	-160.61	-175.16	-189.72	-204.28
a		0.05		0.05	0.05	0.05	0.05	0.05	0.05	0.05	0.05	0.05	0.05	0.05	0.05	0.05	0.05	0.05	0.05
mu target km/sec soln #1		1670.38		1670.38	1067.24	1218.02	1368.81	1519.59	1670.38	1821.16	1971.95	2122.73	2424.30	2725.87	3027.44	3329.00	3630.57	3932.14	4233.71
mu target km/sec soln #2		3.49		3.49	1.49	1.99	2.49	2.99	3.49	3.99	4.50	5.00	6.00	7.00	8.00	9.01	10.01	11.01	12.02
mu target best km/sec		3.49	5.17	3.49	1.49	1.99	2.49	2.99	3.49	3.99	4.50	5.00	6.00	7.00	8.00	9.01	10.01	11.01	12.02
Us target km/sec		9.88	9.88	9.88	7.30	7.94	8.59	9.23	9.88	10.52	11.17	11.82	13.11	14.40	15.69	16.99	18.28	19.58	20.87
density in target gm/cc		4.31		4.31	3.50	3.72	3.92	4.12	4.31	4.49	4.66	4.82	5.13	5.42	5.68	5.93	6.15	6.36	6.56
frac compression target		0.35		0.35	0.20	0.25	0.29	0.32	0.35	0.38	0.40	0.42	0.46	0.49	0.51	0.53	0.55	0.56	0.58
P target kilobars		960.61	211.28	960.61	303.22	440.45	595.76	769.15	960.61	1170.15	1397.76	1643.46	2189.07	2806.99	3497.22	4259.75	5094.59	6001.73	6931.18
frac energy in thick target		0.50	0.50	0.50	0.50	0.50	0.50	0.50	0.50	0.50	0.50	0.50	0.50	0.50	0.50	0.50	0.50	0.50	0.50
frac kinetic energy in thick target		0.25		0.25	0.25	0.25	0.25	0.25	0.25	0.25	0.25	0.25	0.25	0.25	0.25	0.25	0.25	0.25	0.25
frac int energy in thick target		0.25		0.25	0.25	0.25	0.25	0.25	0.25	0.25	0.25	0.25	0.25	0.25	0.25	0.25	0.25	0.25	0.25
cp target		9.41		9.41	7.73	8.14	8.56	8.98	9.41	9.84	10.28	10.72	11.61	12.51	13.41	14.32	15.24	16.16	17.08
PROJECTILE CALCULATIONS																			
mu projectile km/sec		3.51	3.49	3.49	1.51	2.01	2.51	3.01	3.51	4.01	4.50	5.00	6.00	7.00	8.00	8.99	9.99	10.99	11.98
Us projectile km/sec		10.09	3.09	3.09	7.41	8.08	8.75	9.42	10.09	10.76	11.43	12.10	13.44	14.78	16.11	17.45	18.79	20.13	21.46
density in projectile gm/cc		4.16		4.16	3.41	3.61	3.80	3.99	4.16	4.32	4.48	4.63	4.90	5.16	5.39	5.60	5.80	5.98	6.15
frac compression projectile		0.35		0.35	0.20	0.25	0.29	0.32	0.35	0.37	0.39	0.41	0.45	0.47	0.50	0.52	0.53	0.55	0.56
P projectile kilobars		960.61		960.61	303.22	440.45	595.76	769.15	960.61	1170.15	1397.76	1643.46	2189.07	2806.99	3497.22	4259.75	5094.59	6001.73	6931.18
frac energy in projectile		0.50		0.50	0.50	0.50	0.50	0.50	0.50	0.50	0.50	0.50	0.50	0.50	0.50	0.50	0.50	0.50	0.50
frac int energy projectile		0.25		0.25	0.25	0.25	0.25	0.25	0.25	0.25	0.25	0.25	0.25	0.25	0.25	0.25	0.25	0.25	0.25
frac kinetic energy projectile		0.25			0.25	0.25	0.25	0.25	0.25	0.25	0.25	0.25	0.25	0.25	0.25	0.25	0.25	0.25	0.25
spec int energy projectile erg/gm		6.10E+10		6.10E+10	1.11E+10	1.98E+10	3.11E+10	4.48E+10	6.10E+10	7.98E+10	1.01E+11	1.25E+11	1.80E+11	2.45E+11	3.20E+11	4.06E+11	5.01E+11	[illegible]	[illegible]
projectile energy to energy to melt		1.12E+00			2.05E-01	3.65E-01	5.71E-01	8.24E-01	1.12E+00	1.47E+00	1.86E+00	2.30E+00	3.31E+00	4.51E+00	5.89E+00	7.46E+00	9.21E+00	1.12E+01	[illegible]
projec energy to energy to vaporize		1.18E-01			2.16E-02	3.85E-02	6.02E-02	8.68E-02	1.18E-01	1.55E-01	1.96E-01	2.42E-01	3.49E-01	4.75E-01	6.21E-01	7.86E-01	[illegible]	[illegible]	[illegible]
spec kin energy of proj erg/gm		6.15E+10			1.14E+10	2.02E+10	3.14E+10	4.52E+10	6.15E+10	8.02E+10	1.01E+11	1.25E+11	1.80E+11	2.45E+11	3.20E+11	4.04E+11	[illegible]	[illegible]	7.18E+11
ave vel of proj after impact km/sec		3.51			1.51	2.01	2.51	3.01	3.51	4.01	4.50	5.00	6.00	7.00	8.00	8.99	[illegible]	10.99	[illegible]
cp projectile		9.65		-6.17	7.86	8.30	8.75	9.20	9.66	10.12	10.59	11.05	11.99	12.94	13.90	14.86	15.82	16.79	[illegible]
OPTIMUM SHIELD CALCULATIONS																			
thickness opt shield/thickness projectile		0.19			0.14	0.15	0.16	0.17	0.19	0.20	0.20	0.21	0.23	0.24	0.26	0.27	0.28	0.29	0.30
thickness opt shield cm		0.16			0.12	0.14	0.15	0.16	0.16	0.17	0.18	0.19	0.20	0.22	0.23	0.24	0.25	0.26	0.27
thick opt shield 10,000ths inch		649.36			489.75	533.01	573.99	612.74	649.36	683.96	716.65	747.55	804.42	855.43	901.36	942.85	[illegible]	[illegible]	1045.01
weight opt shield lb/ 1000 ft^2		940.50			709.32	771.98	831.33	887.46	940.50	990.60	1037.95	1082.70	1165.07	1238.95	1305.47	1365.56	[illegible]	[illegible]	1514.57
thick candidate shield/thick opt shield		0.81			1.07	0.99	0.92	0.86	0.81	0.77	0.73	0.70	0.65	0.61	0.58	0.55	.54	0.52	[illegible]
time for Us to pass through projectile		8.81E-07			1.20E-06	1.10E-06	1.02E-06	9.44E-07	8.81E-07	8.26E-07	7.78E-07	7.35E-07	6.62E-07	6.02E-07	5.52E-07	5.10E-07	[illegible]	[illegible]	4.14E-07
time for Us to pass through shield		1.67E-07			1.71E-07	1.71E-07	1.70E-07	1.69E-07	1.67E-07	1.65E-07	1.63E-07	1.61E-07	1.56E-07	1.51E-07	1.46E-07	1.41E-07	[illegible]	[illegible]	[illegible]
time for rare (cp) pass through shield		1.13E-07			1.28E-07	1.25E-07	1.21E-07	1.17E-07	1.13E-07	1.10E-07	1.06E-07	1.02E-07	9.55E-08	8.93E-08	8.37E-08	7.86E-08	[illegible]	[illegible]	[illegible]
time for rare(cp) to pass through projectile		6.01E-07			9.01E-07	8.05E-07	7.25E-07	6.58E-07	6.01E-07	5.52E-07	5.09E-07	4.72E-07	4.10E-07	3.62E-07	3.23E-07	2.90E-07	[illegible]	[illegible]	[illegible]
time check on shield thickness		0.0E+00			0.0E+00	2.6E-23	2.6E-23	6.6E-23	0.0E+00	4.0E-23	-1.3E-23	2.6E-23	-7.9E-23	2.6E-23	5.3E-23	-6.6E-23	[illegible]	[illegible]	0.0E+00

ORIGINAL PAGE IS OF POOR QUALITY

Figure A-1 (Cont). Analytical Model Spreadsheet

Bumper Effects following Impact

29-Dec-85

extent of melting x 1000	1000.00	204.96	365.11	571.37	823.81	1000.00	1000.00	1000.00	1000.00	1000.00	1000.00	1000.00	1000.00	1000.00	1000.00	1000.00
target rho/rho o	1.55	1.26	1.33	1.41	1.48	1.55	1.61	1.67	1.73	1.84	1.95	2.04	2.13	2.21	2.29	2.36

Figure A-2. Analytical Model Graphical Results

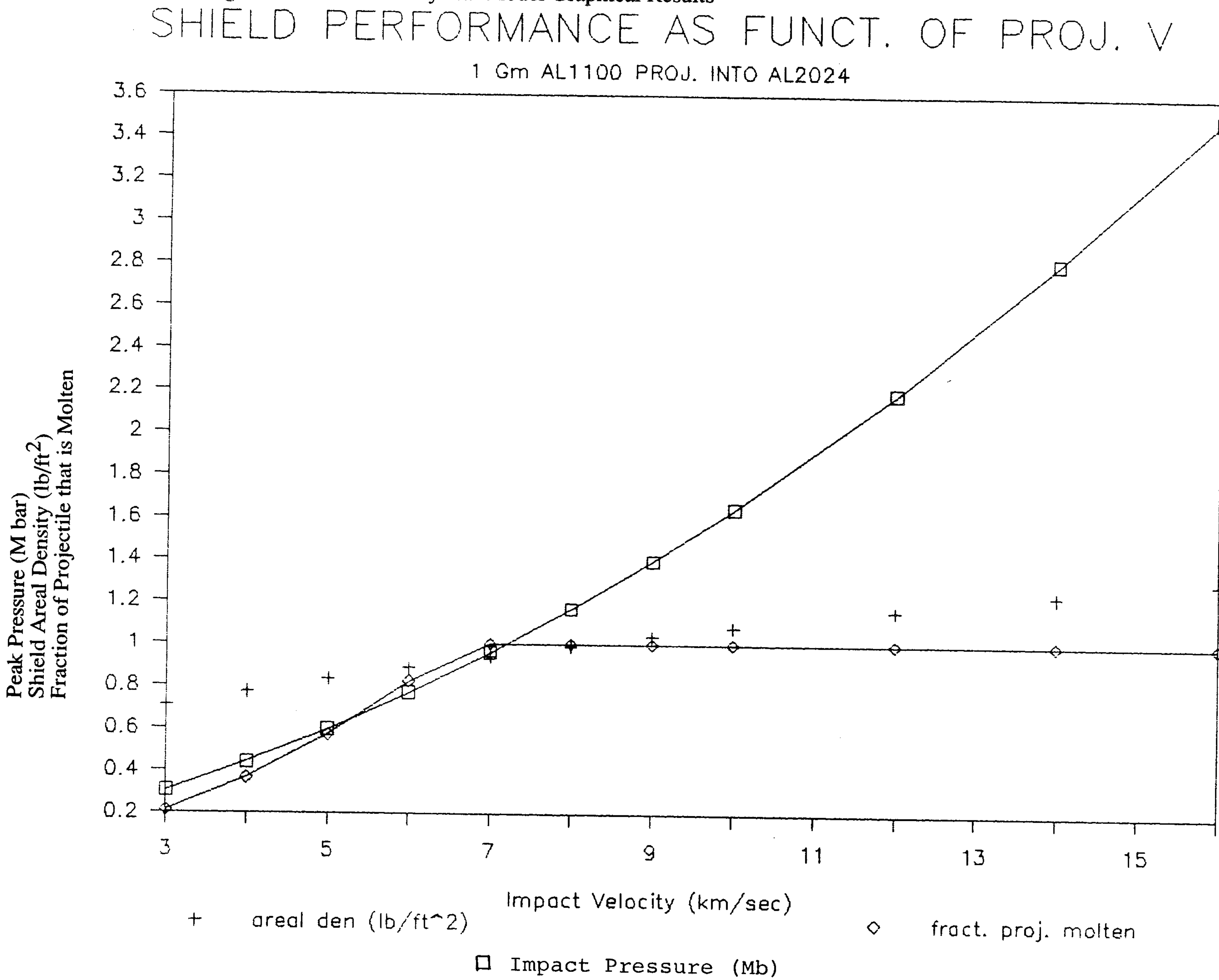

ORIGINAL PAGE IS OF POOR QUALITY

Table A-1. Results of Analytical Model

Material Selection Based on Fraction of Projectile that Melts and Optimal Bumper Areal Density
(Calculations based on one-dimensional impact approximation with a 1 gm, Al 1100, projectile at 7 km/sec)

Rank	Material	Dens (g/cc)	Impact Pressure (Mb)	Opt. Areal Density (lb/ft^2)	State of Al Proj. (Impact P)
LIGHTER THAN BASELINE (IMPACT PRESSURES HIGH ENOUGH TO MELT PROJ.):					
1	Composite C-Phen	1.35	0.72	0.606	Partially Molten
2	Magnesium	1.74	0.71	0.612	Partially Molten
3	Mg AZ31B alloy	1.78	0.72	0.621	Partially Molten
4	Glass Silica	2.20	0.69	0.630	Partially Molten
5	Glass Pyrex	2.23	0.74	0.670	Partially Molten
6	Silica Quartz	2.65	0.81	0.766	Partially Molten
7	Mullite	2.67	0.86	0.812	Molten
8	Anorthosite	2.73	0.86	0.819	Molten
9	Feldspar	2.73	0.87	0.829	Molten
10	Basalt (Ref.10)	2.86	0.89	0.864	Molten
BASELINE:					
11	Aluminum 6061	2.70	0.95	0.929	Molten
HEAVER THAN BASELINE:					
12	Aluminum 1100	2.71	0.96	0.934	Molten
13	Aluminum 2024	2.78	0.96	0.940	Molten
14	Aluminum (Ref.10)	2.75	0.97	0.944	Molten
15	Aluminum 7075	2.80	0.97	0.950	Molten
16	Aluminum 921T	2.83	0.98	0.961	Molten
17	Silicon Carbide	3.12	1.09	1.137	Molten
18	Titanium	4.53	1.10	1.195	Molten
19	Glass High Dens.	5.09	1.10	1.229	Molten
20	Alumina Coors	3.66	1.15	1.247	Molten
21	Alumina Hot press	3.94	1.27	1.468	Molten
22	Cadmium	8.64	1.40	1.871	Molten
23	Iron (Ref.10)	7.86	1.44	1.930	Molten
24	Steel 1018	7.85	1.46	1.985	Molten
25	Lead	11.35	1.47	2.088	Molten
26	Steel-Vasco250	8.13	1.47	2.007	Molten
27	Steel S/S 304	7.90	1.48	2.026	Molten
28	Copper	8.93	1.50	2.102	Molten
29	Uranium 3%Mo	18.45	1.75	3.094	Partially Vaporized
30	Tungsten Carbide	15.02	1.81	3.289	Partially Vaporized
31	Gold	19.24	1.82	3.386	Partially Vaporized
32	Platinum	21.44	1.90	3.832	Partially Vaporized

Table A-1 (Cont). Results of Analytical Model

No	Material	Dens (g/cc)	Impact Pressure (Mb)	Opt. Areal Density (lb/ft^2)	(from impact P consid-eration) State of Al Proj.	(from Thermal Energy Bal.) State of Al Proj.
	MATERIALS LIGHTER THAN BASELINE					
	(with impact pressures lower than 650 kbar indicating shock pressure too low to melt Al projectile by shock compression and release, but from thermal energy balance having enough energy to melt projectile):					
1	Wood Douglas Fir	0.54	0.25	0.194	Solid	Molten
2	H2O Ice	0.91	0.42	0.328	Solid	Molten
3	H2O Water	1.00	0.46	0.362	Solid	Molten
4	Polycarbonate	1.19	0.50	0.405	Solid	Molten
5	Polyamide (Nylon)	1.15	0.52	0.413	Solid	Molten
6	Acrylic	1.19	0.54	0.432	Solid	Molten
7	Epoxy	1.20	0.54	0.437	Solid	Molten
8	Polyimide	1.41	0.56	0.465	Solid	Molten
9	PVC (Boltron)	1.38	0.57	0.470	Solid	Molten
10	Graphite 3D fiber	1.52	0.55	0.473	Solid	Molten
11	Teflon	2.15	0.64	0.597	Solid	Molten

Appendix B

Description of Empirical Model Calculations

INTRODUCTION

NASA is currently planning for tests of several possible materials for meteoroid/debris bumpers to protect spacecraft or space stations from impact by high speed particles (1). Materials currently being considered for these tests include two aluminum alloys, other metallics, Kevlar, graphite/epoxy, other fiber-reinforced composites, alumina, and other ceramic composites. The reference material, to which other materials are to be compared, is aluminum alloy 6061-T6.

This appendix compares properties of possible bumper materials, suggesting possible additional materials to be considered for testing, and considers what criteria ought to be considered for new candidate materials.

MATERIAL SELECTION CRITERIA

The criteria discussed here have been derived from References 2-6, 31-41.

The efficiencies of various shielding materials will be compared for a constant weight launched to orbit. Thus, comparisons between materials will be based on constant <u>weight</u> of shielding per unit area. The <u>thickness</u> of the shielding will be varied to accomplish this for materials of different density.

Although the primary purpose of the bumper is to fragment a projectile through shock processes, it does possess some penetration resistance of its own. Thus, impacts below a certain threshold will not penetrate it. The model calculates a factor, R, that expresses the ability of a fixed areal-density bumper to resist penetration in terms of the bumper's speed of sound (C), hardness (BH), and density (δ_t):

$$R = C^{.67}\, BH^{.25}\, \delta_t^{\,.5}$$

This equation is based on empirical penetration equations into semi-infinite targets (43, 44).

$$P = K\, d_p^{\,1.06}\, BH^{-.25}\, (\delta_p/\delta_t)^{0.5}\, (v_i/C)^{0.67}$$

Combining all the projectile parameters into the proportionality constant results in the penetration equation:

$$P = K' \, C^{-.67} \, BH^{-.25} \, \delta_t^{-.5}$$

Note that the sonic velocity can be determined from:

$$C = [E * (2.54^2 * 32.2 * 12/100^2) / \delta_t]^{.5} * 0.001$$

For a fixed bumper mass per unit area, the areal density for a penetrated bumper becomes:

$$m_t = P \, \delta_t$$

or,

$$m_t = K' \, C^{-.67} \, BH^{-.25} \, \delta_t^{.5}$$

The resistance parameter is proportional to the inverse of penetration distance.

$$R = K'' * 1/P = K'' \, \delta_t/m_t$$

The model assumes that resistance to penetration into thick targets is a useful gauge to differentiate the ability of various thin target materials to resist small particles near the ballistic limit or breakup larger projectiles.

The state of the debris cloud of bumper and projectile fragments projected behind the bumper after impact is the primary factor influencing the performance of dual-wall protection. R. H. Johnston (4) noted that an important means for defeating hypervelocity threats will be to vaporize the particle and a portion of the target. Swift and Hopkins (5) determined that bumpers of a constant areal density (the case we are considering) which exceeded about 2 g/cc provided approximately the same protection. This conclusion was referred to and amplified by J. S. Wilbeck, et. al. (6, ch. 6). Impacts on bumper materials with densities below 2 g/cc do not produce sufficiently intense shock waves to melt the impacting projectiles used in the Reference 5 and 31 studies (3.18 mm diameter aluminum spheres at 6.2-7.4 km/sec). This allows increasingly larger solid fragments of the impacting body to strike the second wall as bumper material density goes down. For all bumper materials above this density, maximum deviations from a constant penetration depth of the second wall due to collision debris were 25 percent. The primary criterion affecting the backwall penetration was the physical state of the debris from the front wall. The thermodynamic properties of the bumper material determine to a great extent the phase of the particles in the debris plume projected behind the bumper. Bumper materials that melted in the collision required less second-wall thickness than materials that only fragmented. Bumper materials that vaporized required less second-wall thickness than materials that melted.

Therefore, to maximize the probability that the bumper material melts or vaporizes from the impact, the shield material should have a low melting temperature (3, 33), T_m, and latent heat of fusion, H_m, as well as low vaporization temperature, T_v, and latent heat of vaporization, H_v (5).

Because aluminum is the current baseline candidate for Space Station module shielding, ratios of the thermodynamic properties of candidate bumper materials and aluminum were determined and a figure-of-merit, FOM, that combines thermodynamic and mechanical properties was developed:

$$FOM = \{Tm\,(al)/Tm * [Hm\,(al)/Hm]^{.5} * [Tv\,(al)/Tv]^{.1} *$$

$$[Hv\,(al)/Hv]^{.1} + 0.25 * R\}\ \delta(al)/\delta$$

The purpose of the figure-of-merit was to suggest possible candidate bumper materials, but it should be regarded as arbitrary until actual impact tests have been done to evaluate its predictive ability. Melting is more likely to occur at typical orbital debris velocities, thus the melting temperature and heat of fusion parameters were thought to be more important and weighted more than the vaporization and latent heat parameters. Because mechanical properties are overshadowed by density effects in hypervelocity impact penetration of thin plates, the mechanical property term, R, was reduced by a 0.25 factor to indicate the penetration resistance of the shield to projectiles below the ballistic limit. A number of materials were evaluated using this expression to determine their effectiveness as bumpers as will be described later in this appendix.

This bumper FOM includes thermodynamic and mechanical properties, but it does not include all properties and factors which could be important in evaluating the best materials for protection such as: fracture toughness, maintainability or repairability, debris cloud dispersion angle, and cost. The qualitative effects of these factors are discussed below.

Other shield material properties may also affect the physical state, direction, speed, and spatial density of the material projected behind the bumper, and therefore the damage potential of debris clouds. Several investigations of bumper materials for recent interplanetary missions such as the European comet Halley probe (32, 35-37) have indicated that low-density, fiber-reinforced plastics or other composites possess certain highly desirable impact characteristics. It was reported that the bumper materials in the projected debris clouds behind kevlar/epoxy plates were much smaller than predicted for aluminum (25, p.79; 36). The individual fragments in the debris cloud consisted of finely divided epoxy powder and short lengths of fine Kevlar fibers. Both materials have less impact damage potential for underlying structures than solid aluminum fragments because; first, the aluminum fragments concentrate more energy and momentum in a smaller area of the back plate; and second, because the density, and thus penetrating ability, of aluminum (2.72 g/cc) is greater than Kevlar fibers (1.44 g/cc) or epoxy fines (1.39 g/cc). Other fiber-reinforced composites seem to have similar breakup characteristics. A recent study provided experimental evidence that the fragment size of particles in debris clouds from graphite/epoxy plates were smaller than from aluminum plates at similar impact energies (with aluminum and nylon projectile velocities typically 5.5-6.5 km/sec) (42). Thus, another material property, perhaps associated with fracture energy or fracture toughness, seems to be important in determining the condition of the debris striking the second plate.

The Kevlar/epoxy material evaluation for Giotto also indicated that Kevlar has a somewhat "self-healing" mechanism (25, p. 53; 36) in that it "fluffs" after impact, leading to partial closure of perforations in the shield. The investigators noted that the total bumper area disrupted by the impact was greater than for aluminum bumpers, but that the majority of this disruption involved debonding between the Kevlar and epoxy substrate. The fibers adjacent to the impact site tend to expand laterally into the hole and effectively decrease hole diameter by twice the plate thickness. This reduction in size of the open holes produced in bumpers having fiber reinforcement would result in reductions of the number and size of undisturbed orbital debris and meteoroids which may be expected to impact the underlying surfaces. Or, it implies that shield maintenance and repairs would be reduced over the ten to thirty year lifetime of the Space Station.

The angle of dispersion of the debris cloud projected behind the bumper depends primarily on the bumper thickness (12, p.118). For a given size impacting particle, the dispersion angle decreases as the bumper thickness becomes thinner. Similarly, the dispersion angle also decreases, for a very thick bumper with the limit being a zero dispersion angle for a bumper at the ballistic limit. Maximum dispersion angles are attained for intermediate thickness bumpers. At constant areal density, bumper thickness depends on the density of the bumper material. Thus, different materials are expected to exhibit different debris cloud dispersion characteristics. Information is lacking on the dispersion angle to be expected for the test materials being considered; therefore, dispersion angle will be determined experimentally. The dispersion angle is important because it defines the momentum loading on the backwall and the necessary spacing between the bumper and backwall to avoid failure. Narrower dispersion angles require larger standoff distances, increased number and size of bumper structural supports, and reduced internal volumes for modules sized to fixed payload envelopes. Or, if the standoff distance is held constant, smaller dispersion angles will increase the thickness and weight of the back plate.

The cost differences between the various metallic and composite bumper candidates has not been included in the FOM but probably will be important in the Space Station design-to-cost program.

MATERIAL COMPARISONS

Table B-1 is a compilation of the physical properties needed for the FOM for several materials. Not all of these are on the list of bumper materials to be tested (1). Values for heat of fusion and vaporization, and melting and vaporization temperatures, are taken from the Engineering Manual (7). Following the values for the four thermodynamic parameters in Table B-1 are ratios of the values for the reference material, aluminum, to the values for the other materials.

The calculated FOM is indicated in the extreme right column of Table B-1, and is in general agreement with the relative efficiencies of bumper materials determined experimentally by Swift (31) as given in Figure B-1. Larger numbers for this figure of merit indicate materials more efficient than aluminum. The use of this figure should be regarded as somewhat preliminary until actual impact tests have been done to evaluate its predictive ability. It can, within its limitations, be used as a means for suggesting possible meteor bumper materials to test in addition to those already scheduled.

Of the materials listed in Table B-1, the highest value in the figure of merit column is magnesium and magnesium alloys, because of their low density and low heats of fusion and vaporization per unit mass, and their low melting and vaporization temperatures. Therefore, consideration could be given for adding these materials to the test schedule. Magnesium alloys have not been used in spacecraft interior applications due to corrosion problems within the cabin environment (65). They could be used in exterior applications as long as a coating is applied to protect from salt-water corrosion during pre-launch storage at the Cape. The thermal protection coating could perhaps satisfy this requirement. A light-weight but stiff support material such as graphite/epoxy should be used to minimize the weight and number of bumper structural support rings needed in an actual Space Station module design.

LIMITATIONS OF THE FIGURE OF MERIT OR EMPIRICAL MODEL

The empirical model is limited in several important ways. The criteria in the FOM are somewhat arbitrary and must be confirmed or revised after more experimental data has been gathered. Several possibly important factors to the evaluation have not been included in the FOM as discussed previously, such as fracture toughness, maintainability or repairability, debris cloud dispersion angle, and cost. The present FOM is limited primarily to evaluating metallic materials. Composites are non-isotropic and it is not possible to specify a single value for many of their material properties because they vary throughout the structure. Therefore, an analytical model was developed from first principles to analyze the potential effectiveness of both metallic and composite bumper materials.

As mentioned above, the FOM uses arbitrary factors to the thermodynamic parameters. It is not clear how the four parameters should be included in the overall figure of merit to give the best prediction for bumper performance. For example, it may turn out that some parameters are much more significant than others and should be weighted more highly in calculating a figure of merit. For instance, the heat of fusion may turn out to be much more (or much less) closely related to overall impact damage than the melting temperature.

It may also turn out that the weighting of these parameters varies with impact speed. The study done by Swift and Hopkins (5, 31) was done with a quite limited range of impact speeds (6.2-7.4 km/sec). Because the average orbital debris speed is above 9 km/sec, lower density bumpers will generate strong enough shock pressures to melt an aluminum projectile and will generate shield debris of far less penetrating potential. The material evaluation should be based on assessing the required total dual-wall areal density to meet the overall module reliability requirement (ie. 0.9955 probability of no impact over ten years) for the integrated orbital debris velocity distribution.

As also mentioned above, the FOM was only applied to simple materials: pure metals or alloys. To apply the evaluation criteria to complex materials such as composites is not clear. Are the appropriate parameter values to use those for the fibers, those for the matrix, a simple average, or some weighted average? Furthermore, the choice may depend on what parameter is being considered. The appropriate value for the heat of vaporization, for example, may be the value for the matrix; once the matrix is vaporized, since the fibers may simply fly apart. But at the same time, the value for the density below which the bumper efficiency no longer approximates a constant may be determine by the value for the fiber. The answers to these questions will require testing.

ACCESS TO SPREADSHEET

The figure-of-merit calculations and physical properties for the materials in Table B-1 are given in the spreadsheet on the diskette at the back of this report. The spreadsheet name is FIGOFMER.WKS.

SYMBOLS

C	=	Acoustic velocity, or velocity of rarefaction (km/sec)
E	=	Elastic modulus in tension (psi)
BH	=	Brinell hardness
d	=	Diameter (cm)
v	=	Velocity (km/sec)
δ	=	Density (gm/cm^3)
m	=	Areal density of bumper penetrated by projectile (g/cm^2)
P	=	Penetration depth (cm)
R	=	Resistance parameter indicating the ability of equal areal density bumpers to resist penetration
H_m	=	Heat of fusion per unit mass (Btu/lb)
H_v	=	Heat of vaporization per unit mass (Btu/lb)
T_m	=	Melting temperature (°C)
T_v	=	Vaporization temperature (°C)
K,K',K"	=	Proportionality constants
(al)	=	Physical property of aluminum baseline (Al 6061-T6)

Subscripts:

i	=	impact
t	=	target
p	=	projectile

Table B-1. Compilation of Physical Property Data and Figure-of-Merit Calculation for Possible Bumper Materials

12/11/86

BUMPER SELECTION BASED ON MATERIAL PROPERTIES

MATERIAL	HEAT OF VAPORIZATION (BTU/lb.)	BOILING TEMP. (deg. C)	HEAT OF FUSION (BTU/lb.)	MELTING TEMP. (deg. C)	RATIOS TO ALUMINUM: E vap (Al)/ E vap [A]	T vap (Al)/ T vap [B]	E m (Al)/ E m [C]	T m (Al)/ T m [D]	Brinell Hardness	Density (lb/in^3)	Elastic Modulus (psi)	Sound Speed (km/sec)	RATIOS TO AL 6061-T6 BASELINE: H/ H(6061) [E]	rho/ rho(6061) [F]	C/ C(6061) [G]	Resistance Factor G^.67*E^.25*F^.5	FIGURE OF MERIT [A^.1*B^.1*C^.5*D+0.25*R]/F
Aluminum Alloys (reference material)	3591	1800	170.2	660	1.000	1.000	1.000	1.000	73 (6061T6)	0.098	9.90E+06	5.02	1.00	1.00	1.00	1.00	1.25
Antimony	671	1380	70.5	631	5.352	1.254	2.414	1.032	42	0.249	1.13E+07	3.36	0.58	2.54	1.14	1.52	0.91
Cadmium	382	767	23.4	321	9.401	1.993	7.274	1.571	38 (?)	0.312	8.00E+06	2.53	0.52	3.18	0.81	1.31	1.89
Copper	2061	2300	88.03	1083	1.742	0.806	1.933	0.688	100 (cold rolled)	0.322	1.70E+07	3.63	1.37	3.29	1.72	2.81	0.52
Iron/Steel	2926	3000	86.4	1535	1.227	0.633	1.970	0.516	385 (301 SS cold rolled)	0.286	2.80E+07	4.94	5.27	2.92	2.83	5.18	0.69
Lead	365	1725	10.5	327	9.838	1.038	16.057	1.555	5 (Chemical Lead)	0.41	2.00E+06	1.10	0.07	4.18	0.20	0.36	1.90
Magnesium Alloys *	2407	1110	160	593	1.492	1.499	1.064	1.077	83 (AZ92A)	0.066	6.50E+06	4.95	1.14	0.67	0.66	0.64	2.03
Nickel	2677	2855	129	1438	1.341	0.654	1.319	0.545	370 (Duranickel)	0.298	3.00E+07	5.01	5.07	3.04	3.03	5.48	0.65
Platinum	986	4299	43.3	1768	3.642	0.453	3.931	0.457	101 (hard)	0.773	2.20E+07	2.66	1.38	7.89	2.22	5.19	0.29
Tantalum	3591 (?)	5425	68	2996	1.000	0.364	2.503	0.285	123 (unannealed sheet)	0.599	2.70E+07	3.35	1.68	6.11	2.73	5.50	0.29
Titanium	3591 (?)	3260	188	1649	1.000	0.587	0.995	0.485	345 (Ti-6Al-4V heat treated)	0.161	1.65E+07	5.05	4.73	1.64	1.67	2.66	0.67
Tungsten	1722	5899	82.2	3367	2.085	0.336	2.071	0.256	290 (hard)	0.697	5.30E+07	4.35	3.97	7.11	5.35	11.52	0.46

Footnote:
* Density is less than 2 grams/cubic centimeter.

Figure B-1. Data Plot for Constant Bumper Areal Density Study Showing States of Bumper and Pellet Materials in the Debris Clouds - Aluminum Sphere Projectiles at Vel. = 6.2-7.4 km/sec (31)

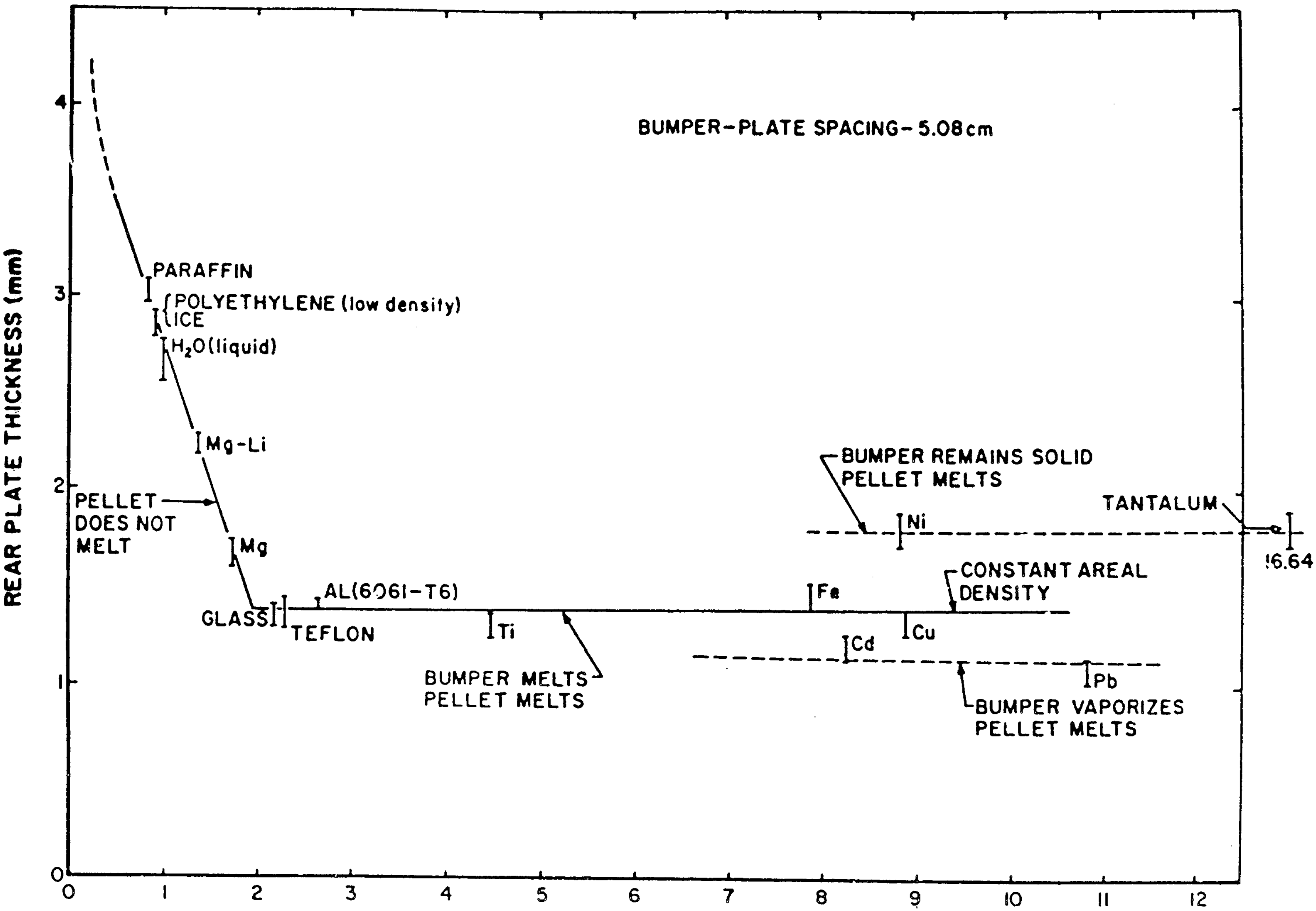

Appendix C

Description of Peak Shock Pressure Calculations

The impact pressures given in Table 4-1 were determined using a spreadsheet that determines the shock pressure in the bumper as a function of particle velocity from

$$P_i = \delta_{0t}\, c_{0t}^{\,2}\, n_t / (1 - s_t n_t)^2 \qquad (1)$$

where the shock compressibility factor, n_t, is

$$n_t = \mu_t / U_t = \mu_t / (c_{0t} + s_t\, \mu_t) \qquad (2)$$

The shock pressure in the projectile as a function of particle velocity is

$$P_i = \delta_{0p}\, c_{0p}^{\,2}\, n_p / (1 - s_p\, n_p)^2 \qquad (3)$$

where the projectile shock compressibility factor, n_p, is a function of impact velocity, v_i:

$$n_p = (v_i - \mu_p) / [c_{0p} + s_p\, (v_i - \mu_p)] \qquad (4)$$

This approach is based on the same one-dimensional approximation, Rankine-Hugoniot relationships, conservation equations, and linear equation-of-state simplifications described in Appendix A. The derivation of the equations is given by McQueen, et. al. (12, p.296).

Based on the assumption that the impact pressure is the same in dumper and projectile, the above equations are solved simultaneously in the spreadsheet and can be represented graphically by the intersection of the two curves resulting from equations 1 and 3 as shown in Figure C-1.

ACCESS TO SPREADSHEET

The peak shock pressure calculations and equation-of-state constants for many metallic, crystalline, polymeric, and composite materials are given in the spreadsheet on the diskette at the back of this report. The spreadsheet name is HUGONIOT.WKS.

SYMBOLS

c	=	First term in the linear shock-velocity/particle-velocity Hugoniot, (in general the term does not equal the acoustic velocity of a material at zero pressure) (km/sec)
s	=	Second term in shock-velocity/particle-velocity Hugoniot (dimensionless)
v	=	Velocity (km/sec)
δ	=	Density (gm/cm^3)
n	=	Shock compressibility factor (dimensionless) equal to the ratio of particle to shock velocities
P	=	Pressure (kilobars)
μ	=	Particle velocity (km/sec)
U	=	Shock Velocity (km/sec)

Subscripts:

blank	=	shocked state
i	=	impact
0	=	rest state
t	=	target
p	=	projectile

Figure C-1. Peak Impact Pressures from One-Dimensional Approximation

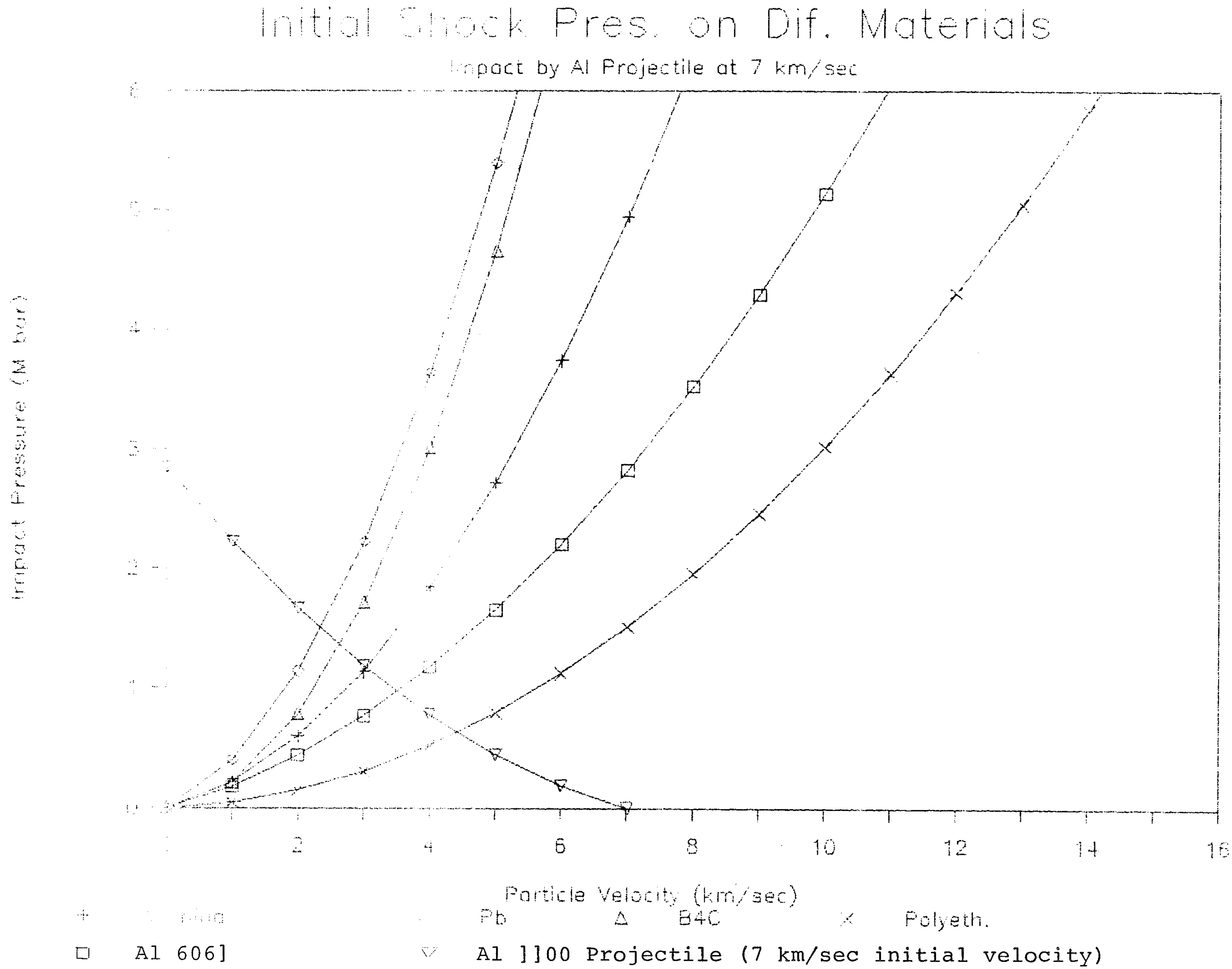

Appendix D

Listing of Shot Data

Table D-1 lists data for all shots of interest in this study. Information is separated on three pages for each shot with the first page listing projectile and bumper data, the second page giving data about the front and back of the second wall (Al 2024-T3), and the third page ejecta catcher and witness plate data.

Table D-2 gives particle size data for the ejecta particles from a metal matrix bumper (shot #A152).

Table D-3 lists the velocity of ejecta and debris plumes expanding from the bumper plate's front and back, respectively, for 6 different shots: Al 6061-T6 (#A150), metal matrix (#A157), Aluminum bonded to graphite/epoxy (#A158), alumina bonded to aluminum (#A159), aluminum mesh (#A161), and Kevlar (#A163). The data was calculated from high speed camera films of each shot.

Table D-1. Listing of Shot Data (chronological order)

JSC Shot	Date	Bumper Mat'l	Bumper Areal Density (g/cm^2)	Bumper Density (g/cc)	Al 2024-T3 Backwall Thickness (in)	Al 1100 Proj. Mass (mg)	Proj. Dia. (mm)	Proj. Vel. (km/s)	Number of Impacts	Cordin Camera Film Y or N?	Comments on Film (Clean impact unless stated)	BUMPER Frnt Crater Dia. (mm)	Hole Dia. (mm)	Back Crater Dia. (mm)	Mass Before Impact (g)	Mass After Impact (g)	Comments on Bumper
A149	10-Mar-87	Al 6061-T6 t = 0.032"	0.22	2.713	0.0627	45.25	3.2		1	N	Impact by Sabot quarter. Nylon sabot, 3.75 mm long, 2 mm d. 1/4 mass = 11.5 mg. The projectile was fragmented in impact with edge of sabot catcher, and impacted bottom corner of bumper.				50.66		Black soot on back of bumper.
A150	11-Mar-87	Al 6061-T6 t = 0.032"	0.22	2.713	0.0623	45.25	3.2	6.45	1	Y		8.1	6.8	7.9	50.43	50.45	Back of bumper covered with small Al droplets that appear to have been vapor or liquid.
A151	11-Mar-87	Al 6061-T6 t = 0.032"	0.22	2.713	0.0493	45.25	3.2	6.60	1	N		8.2	7.0	8.3	50.60	50.63	Back of bumper covered with small Al droplets that appear to have been vapor or liquid.
A152	12-Mar-87	Metal Matrix Al 6061-T6/35v% SiC t = 0.0315"	0.22	2.80	0.0623	45.25	3.2	6.52	1	N		7.6	6.3	7.8	22.70	22.67	More brittle than all Al bumper. Almost no crater lip. Back of bumper covered with small Al droplets that appear to have been vapor or liquid.
A157	18-Mar-87	Metal Matrix Al 6061-T6/35v% SiC t = 0.0315"	0.22	2.80	0.0500	45.17	3.2	6.71	3	Y	Impact by Sabot quarter & proj. Third impact by unknown debris. Proj./Sabot impacts were separated, third followed directly behind proj. Nylon sabot, 3.86 mm long, 2 mm d. 1/4 mass = 11.7 mg.	7.5	6.1	7.6	22.67	22.56	
												5.6	4.8	5.8 From Sabot Impact.			
A158	19-Mar-87	8mil Al 3003-0 bonded to graphite/epoxy t = 0.0628"	0.27	1.68	0.0498	45.24	3.2	6.18	2	Y	Impact by proj. & unknown debris. Debris followed directly behind projectile. Debris probably was half of a sabot quarter. Nylon sabot, 3.84 mm long, 2 mm d. 1/8 mass = 5.8 mg.	26.9	7.1	12.4	62.23	61.40	Al layer (on front) ripped away from impact as indicated by front crater diameter. Some of this damage was caused by second impact.
A159	20-Mar-87	15mil Alumina bonded to 8mil Al 3003-0 t = 0.0302"	0.21	2.77	0.0498	45.33	3.2	6.56	2	Y	Impact by proj. & unknown debris. Debris followed directly behind projectile. Long fiber-like shape.	6.9	6.6	21.6	27.79	27.63	Al layer (on back) ripped away from impact as indicated by back crater diameter.
A160	20-Mar-87	Metal Matrix Al 6061-T6/35v% SiC t = 0.0315"	0.22	2.80	0.0492	45.19	3.2	5.64	5	Y	Impact by proj. & all sabot pieces. Nylon sabot, 3.8 mm l., 4.3 mm d. Mass = 47.17 mg. No separation between impacts.	11.4	10.2	10.7	22.64	22.47	Large irregular hole in bumper due to impact by projectile and all sabot pieces.
A161	23-Mar-87	Al Mesh (5056) 4 sheets	0.20	0.66	0.0499	45.29	3.2	6.50	2	Y	Impact by proj. & unknown debris. Debris followed directly behind	5.6	5.6	21.6	54.65	54.56	

Table D-1 (Cont). Listing of Shot Data (chronological order)

9/15/87

JSC Shot	Mass Before Impact (g)	Mass After Impact (g)	AL 2024-T3 SECOND WALL FRONT: Dia. of Conc. Debris Hits (in)	Max. Dia. of Area for Nearly all Hits (in)	Standoff Dist. (in)	Conc. Debris Spall Dispersion Half-angle (deg)	AL 2024-T3 SECOND WALL BACK: Detached Spall Dia. (in)	Raised Area Dia. (in)	Number of Holes	Dia./Len. of Holes (mm)	Width of Holes (mm)	Number of Cracks	Length of Cracks (mm)	Comments on Second Plate
A149	101.77													
A150	102.00	101.71	1.44	3.88	2	20	0.50	1.38	0			1	11	Obvious through crack. See light through in 2 places along crack.
A151	80.21	79.93	1.5	3.8	2	21	0.55	1.4	1	2.7	1.2	3	8.5 7 6	All through cracks.
A152	102.66	102.39	1.6	3.8	2	22	0.43	1.3	0			1	3.8	Does not appear to be through crack. Smaller craters in periphery on front side of 2nd wall than with Al 6061-T6 bumper.
A157	81.43	81.20	1.7	3.9	2	23	0.5	1.6	1	1.5	0.8	3	7.6 6.4 3.8	All through cracks.
A158	82.70	82.62	1.5	3.5	2	21	0	0.9	3	1.4 0.3 0.1		0		Low blast loading. Projectile or second impact debris not completely disrupted.
A159	81.76	81.49	1.6	3.7	2	22	0.46	1.5	1	0.9		0		
A160	80.17	79.39	1.7	4.0	2	23	0.6	1.6	1	15.2				Large hole in backwall due to impact from combination of proj. & sabot.
A161	81.39	81.28	1.0	3.8	2	14	0	1.0	12	3.3 2.5	2.3 1.8			Some holes overlap. Holes are mostly aligned in cross pattern.

Table D-1 (Cont). Listing of Shot Data (chronological order)

9/15/87

JSC Shot	8-MIL AL 3003-0 BUMPER EJECTA CATCHER: Standoff Dist. (in)	Dia. where Ejecta hits Start (in)	Dia. where Ejecta hits generally End (in)	Min. Ejecta Cone Half-Angle (deg)	Max. Ejecta Cone Half-Angle (deg)	AL 3003-0 SECOND WALL SPALL CATCHER WITNESS PLATE: Thickness (mil)	Standoff Dist. (in)	Mass Before Impact (g)	Mass After Impact (g)	Number Holes	Max. Hole Dia. (mm)	Avg. Hole Dia. (mm)	Number Craters	Max. Crater Dia. (mm)	Approx. Avg. Crater Dia. (mm)
A149															
A150	4	4.3	5.5	28	35										
A151	4	3.8	5.2	25	33										
A152	4	4.05	5.85	27	36										
A157	4	3.5	4.9	24	31	8	4	12.75	12.74	4	4.2	3.4	21	3.3	2
A158	4	0	5	0	32	8	4	12.55	12.56	0			11	0.5	0.3
A159	4	3.5	5.5	24	35	8	4	12.66	12.68	1	3.8	3.8	17	5.3	2.3
A160	4	3.8	5.2	25	33	8	4	12.98	12.77	19					
A161	4	0	0	0	0	8	4			36	2.0	0.5	30	0.8	0.5

Table D-1 (Cont). Listing of Shot Data (chronological order)

JSC Shot	Date	Bumper Mat'l	Bumper Areal Density (g/cm^2)	Bumper Density (g/cc)	Al 2024-T3 Backwall Thickness (in)	Al 1100 Proj. Mass (mg)	Proj. Dia. (mm)	Proj. Vel. (km/s)	Number of Impacts	Cordin Camera Film Y or N?	Comments on Film (Clean impact unless stated)	BUMPER Frnt Crater Dia. (mm)	Hole Dia. (mm)	Back Crater Dia. (mm)	Mass Before Impact (g)	Mass After Impact (g)	Comments on Bumper
		t = 0.1204"									projectile. Debris probably was half of a sabot quarter. Nylon sabot, 3.64 mm long, 2 mm d. 1/6 mass = 5.8 mg.						
A163	24-Mar-87	Kevlar Cloth 8 sheets t = .1384"	0.22	0.64	0.0497	45.30	3.2	7.07	1	Y	Impact by proj. and very small amount of "wispy" debris hitting below projectile. Secondary debris negligibly added to total damage.	6.4	2.8	12.7	47.88	47.74	
A219	10-Jun-87	Shuttle Tile t = 0.44"	0.22	0.199	0.05	45.29	3.2	6.52	1	Y	Bumper is approximately 0.44 inches thick.	5.6	5.6	24.9	45.79	45.22	Impacted tile on black borosilicate side first. Small opening of hole on front side expanded to large opening on back.
A220	11-Jun-87	Metal Matrix Al 6061-T6/35v% SiC t = 0.0315"	0.22	2.80	0.05	45.34	3.2	6.46	1	Y		7.4	6.1	7.4	22.46	22.41	Back of bumper covered with fine aluminum that appear to have been formerly liquid droplets or vapor.
A221	12-Jun-87	15mil Alumina bonded to 8mil Al 3003-0 t = 0.0302"	0.21	2.77	0.05	45.22	3.2	6.30	1	Y	A piece of debris trails directly behind ball (3 us after). Slightly larger than size of ball.	9.4	8.9	18.3	27.63	27.39	Ceramic side was facing direction of impact (as in A159). Aluminum layer at back of bumper peeled away from impact point as reflected in large back crater diameter.
A222	12-Jun-87	SiC (Silicon Carbide cloth - 6 sheets t = 0.3486"	0.23	0.26	0.05	45.16	3.2	6.64	1	Y		6.4	5.3	15.2	38.32	38.18	Silvery aluminum splash marks on back side of bumper.
A223	16-Jun-87	Corrugated Al	0.22	2.74	0.05	45.27	3.2	6.32	1	Y		8.2	7.0	8.2	41.69	41.61	A 12" long sheet of 16 mil Al 3003-0

Table D-1 (Cont). Listing of Shot Data (chronological order)

JSC Shot	Mass Before Impact (g)	Mass After Impact (g)	AL 2024-T3 SECOND WALL FRONT: Dia. of Conc. Debris Hits (in)	Max. Dia. of Area for Nearly all Hits (in)	Standoff Dist. (in)	Conc. Debris Spall Dispersion Half-angle (deg)	AL 2024-T3 SECOND WALL BACK: Detached Spall Dia. (in)	Raised Area Dia. (in)	Number of Holes	Dia./Len. of Holes (mm)	Width of Holes (mm)	Number of Cracks	Length of Cracks (mm)	Comments on Second Plate
										2.8				
										1.8				
										3.6	2.0			
										3.0				
										1.5	1.3			
										2.0	1.3			
										1.5				
										1.4				
										0.9				
										0.8				
A163	80.95	80.76	1.5	1.5	2	21	0	1.5	9	5.1		0		Some holes overlap. Holes and most craters aligned in X pattern. Shield material seems to have only made very slight cuts in front surface of second wall.
										2.8				
										2.3				
										4.6	3.3			
										1.4				
										2.0				
										2.5	2.0			
										1.8				
										3.3	1.3			
A219	67.91	67.72	1.2	3	2	17	0	0.8	2	10.3				Several holes overlap to create larger hole. Aluminum "splash" around central hole indicates some of projectile was molten/vapor.
										1.4				
A220	74.16	73.92	1.7	3.6	2	23	0.47	1.3	1	5.1	2.3	3	11.4	
													10.2	
													2.5	
A221	74.49	74.32	1.4	3.3	2	19	0.44	1.3	1	4.1	1.5	1	3.8	
A222	74.74	74.56	0.9	3.2	2	13	0	0.8	9	8.4	3.3	0		Several holes overlap. Very bright aluminum spray surrounding holes indicates projectile partially melted/vaporized.
										1.5				
										2.8				
										1.8				
										0.8				
										1.5				
										2.3	1.8			
										2.5	1.8			
										3.3				
A223	74.72	74.16	1.0	2.5	2	14	0	-	1	16.5	4.6	0		Hole in backwall directly behind

Table D-1 (Cont). Listing of Shot Data (chronological order)

	8-MIL AL 3003-0 BUMPER EJECTA CATCHER					AL 3003-0 SECOND WALL SPALL CATCHER WITNESS PLATE									
JSC Shot	Standoff Dist. (in)	Dia. where Ejecta hits Start (in)	Dia. where Ejecta hits generally End (in)	Min. Ejecta Cone Half-Angle (deg)	Max. Ejecta Cone Half-Angle (deg)	Thickness (mil)	Standoff Dist. (in)	Mass Before Impact (g)	Mass After Impact (g)	Number Holes	Max. Hole Dia. (mm)	Avg. Hole Dia. (mm)	Number Craters	Max. Crater Dia. (mm)	Approx. Avg. Crater Dia. (mm)
A163	4	0	0	0	0	8	4	13.42	13.44	102	3.0	0.6	46	2.3	0.4
A219															
A220						8	4	11.61	11.64	6	4.1	3.0	18	4.1	1.5
A221						8	4	12.23	12.24	5	3.8	3.3	18	3.0	1.5
A222						8	4	12.26	12.27	125	3.0	0.9	120	3.3	0.5
A223						8	4	11.99	11.99	260	3.3	1.1	80	1.3	0.6

Table D-1 (Cont). Listing of Shot Data (chronological order)

JSC Shot	Date	Bumper Mat'l	Bumper Areal Density (g/cm^2)	Bumper Density (g/cc)	Al 2024-T3 Backwall Thickness (in)	Al 1100 Proj. Mass (mg)	Proj. Dia. (mm)	Proj. Vel. (km/s)	Number of Impacts	Cordin Camera Film Y or N?	Comments on Film (Clean impact unless stated)	BUMPER Frnt Crater Dia. (mm)	Hole Dia. (mm)	Back Crater Dia. (mm)	Mass Before Impact (g)	Mass After Impact (g)	Comments on Bumper
		16 mil Al 3003-0 corrugated at 60 deg. angles															was folded at 60 deg angles (every inch) to produce 6" long corrugated bumper with correct areal density. Hole was elliptical: 8.4 x 5.8 mm. Bumper front surface ejecta sprayed out along surface of bumper and put secondary hole in bumper (approx. 20 mm dia., essentially circular).
A224	17-Jun-87	Mesh (Al 5056) single sheet @ 0.5" standoff from 16 mil thick Al 3003-0 plate. t = .046" (w/out spacing)	0.16	1.40	0.05	45.30	3.2	6.39	1	Y	Much light produced in this impact as shown on Cordin infrared film of the event.	6.6	6.6	6.6	10.16	10.14	Data for aluminum mesh.
												24.1	20.3	20.3	22.63	22.53	Data for Al 3003-0 bumper plate. Great deal of black/blue "smokey-like" coating or film covers Al 3003 plate. 1.5 inches separated Al 3003 plate from backwall (2" from Al mesh to backwall).
A225	17-Jun-87	Graphite/Epoxy w/ cloth both sides (Generic) t = 0.0578"	0.23	1.56	0.05	45.23	3.2	6.61	1	Y		8.4	6.4	8.6	53.14	52.98	
A226	18-Jun-87	Tungsten/ Silicone rubber material. 77 wt.% 2-4 micron tungsten microsperes.	0.34	3.35	0.05	45.13	3.2	6.56	1	Y			8.4		31.11	30.95	
A228		Al 6061-T6 t = 0.032"	0.22	2.713	0.05	45.09	3.2	6.39	1	Y		8.4	6.9	8.1	46.53	46.55	Mass of bumper greater after impact due to large amount of fine slivery droplets of aluminum on back surface of bumper. Proj/bumper material in debris cloud behind bumper is in vap or fine liquid form that apparently rebounds from second wall, and subsequently strikes back of bumper.
A230		Tungsten/ Silicone rubber material. 77 wt.% 2-4 micron tungsten microsperes.	0.34	3.35	0.04	45.03	3.2	6.70	1	Y			8.8		35.50	35.33	
A231		Al 6061-T6	0.22	2.713	0.05	45.18	3.2	6.73	1	Y	Very small particle impacted at	7.9	6.9	8.1	46.18	46.17	Back of bumper covered with fine,

Table D-1 (Cont). Listing of Shot Data (chronological order)

9/15/87

JSC Shot	AL 2024-T3 SECOND WALL: Mass Before Impact (g)	Mass After Impact (g)	FRONT: Dia. of Conc. Debris Hits (in)	Max. Dia. of Area for Nearly all Hits (in)	Standoff Dist. (in)	Conc. Debris Spall Dispersion Half-angle (deg)	AL 2024-T3 SECOND WALL BACK: Detached Spall Dia. (in)	Raised Area Dia. (in)	Number of Holes	Dia./Len. of Holes (mm)	Width of Holes (mm)	Number of Cracks	Length of Cracks (mm)	Comments on Second Plate
														proj. hole in bumper. Ejecta spray hole in bumper did not contribute to damage in backwall. Bumper fragments did separate from projectile debris as per the design plan for this type bumper. The projectile hit at and near a "peak" of a corrugation, and because the corrugation was rounded instead of pointed, the projectile was not completely fragmented/-broken-up. The damage was caused by unshocked projectile particles.
A224	73.88	73.91	1.5	3.0	2	21	0	1.0	2	1.0 0.9	0.5 0.4	0		Great deal of bright aluminum splash and few craters on backwall indicating projectile nearly completely melted/vaporized in impact.
A225	72.80	70.76	1.2	3.5	2	17	0	0	2	28.2 1.3		0		Impact punched out large, nearly circular scalloped area in back-plate. Projectile definitely not completely molten/vaporized.
A226	74.25	74.20	2.1	3.5	2	28	0.10	1.9	0			0		Small craters, projectile seems to have been broken-up particularly well. Two craters produced dimples that had broken spall bubbles (0.07" dia. each).
A228	75.38	75.03	1.5	3.5	2	21	0.49	1.4	1	11.2	6.1	0		In other cases with same target/-backwall combinations (A151, A231), smaller hole has resulted, but with more cracks. In this case, cracks apparently grew and connected, causing larger hole to open up.
A230	57.57	57.52	2.0	3.5	2	27	0	1.8	1	1.9		0		
A231	74.90	74.66	1.4	3.5	2	19	0.5	1.6	1	1.9		4	6.5	All four cracks are obvious through

Table D-1 (Cont). Listing of Shot Data (chronological order)

9/15/87

	8-MIL AL 3003-0 BUMPER EJECTA CATCHER					AL 3003-0 SECOND WALL SPALL CATCHER WITNESS PLATE									
JSC Shot	Standoff Dist. (in)	Dia. where Ejecta hits Start (in)	Dia. where Ejecta hits generally End (in)	Min. Ejecta Cone Half-Angle (deg)	Max. Ejecta Cone Half-Angle (deg)	Thickness (mil)	Standoff Dist. (in)	Mass Before Impact (g)	Mass After Impact (g)	Number Holes	Max. Hole Dia. (mm)	Avg. Hole Dia. (mm)	Number Craters	Max. Crater Dia. (mm)	Approx. Avg. Crater Dia. (mm)
A224						8	4	11.71	11.71	0			12	0.3	0.1
A225						16	4	21.52	21.57	1	0.4	0.4	70	3.3	1.1
A226						8	4	12.21	12.21	0			8	0.8	0.4
A228						8	4	11.72	11.72	8	9.3	3.9	35	4.1	1.7
A230						16	4	23.49	23.50	0			12	0.7	0.3
A231						16	4	23.44	23.47	2	6.6	4.8	30	4.1	1.9

ORIGINAL PAGE IS OF POOR QUALITY

Table D-1 (Cont). Listing of Shot Data (chronological order)

JSC Shot	Date	Bumper Mat'l	Bumper Areal Density (g/cm^2)	Bumper Density (g/cc)	Al 2024-T3 Backwall Thickness (in)	Al 1100 Proj. Mass (mg)	Proj. Dia. (mm)	Proj. Vel. (km/s)	Number of Impacts	Cordin Camera Film Y or N?	Comments on Film (Clean impact unless stated)	BUMPER Frnt Crater Dia. (mm)	Hole Dia. (mm)	Back Crater Dia. (mm)	Mass Before Impact (g)	Mass After Impact (g)	Comments on Bumper
		t = 0.032"									edge of hole in bumper - from film particle followed 10 us behind proj						bright aluminum droplets.
A236		Al 6061-T6 t = 0.032"	0.22	2.713	0.063	45.23	3.2	6.48	1	Y		7.9	6.6	7.9	45.19	45.20	Back of bumper covered with fine, bright aluminum droplets.
A237		Alumina 20 mil AD-85	0.19	3.79	0.05	45.25	3.2	6.40	1	Y	Bright impact film as indicated in film.		6.6		24.93		Ceramic bumper broke into 6 large pieces after impact and many small ones. Back of white ceramic turned bronze color.
A238		Mesh (Al 5056) single sheet @ 0.5" standoff from	0.25	1.23	0.05	45.09	3.2	6.31	1	Y	Bright impact flash between two bumper plates.	6.1	6.1	6.1	10.42	10.42	Data for Mesh.
		generic Graphite/Epoxy (w/ cloth) plate. t = .0807" (w/out spacing)										12.7	10.2	12.2	41.77	41.47	Data for G/E plate.
A241		Al 6061-T6 t = 0.032"	0.22	2.713	0.063	45.30	3.2	6.53	1			7.9	7.1	8.4	16.66	16.60	Purpose of this shot was to test a "waffle" backwall. A 8mil thick 1.25" wide Al 3003-0 strip was mounted perpendicular to the backwall as a "waffle" simulating waffling proposed for station module wall. The impact was off centerline of waffle to see if waffle would substantially funnel debris cloud from bumper into backwall (1" offset).
A287		Al 6061-T6 t = 0.032"	0.22	2.713	0.05	45.30	3.2	7.01	1			7.6	6.9	7.9	16.48	16.42	Repeat of waffle shot with 2" standoff, 16 mil thick 1" wide Al 3003-0 waffle, 0.5" offset to impact, and 0.063" backwall.
A315	20-Aug-87	Al 6061-T6 t = 0.032"	0.22	2.713	0.05	45.33	3.2	6.08	1	N	Impact was at an 45 deg. oblique angle. Proj. vel component = 4.3 km/s.		7.7		16.84	16.73	Elliptical hole 8.6 x 6.8 mm.

9/15/87

Table D-1 (Cont). Listing of Shot Data (chronological order)

JSC Shot	AL 2024-T3 SECOND WALL Mass Before Impact (g)	Mass After Impact (g)	FRONT Dia. of Conc. Debris Hits (in)	Max. Dia. of Area for Nearly all Hits (in)	Standoff Dist. (in)	Conc. Debris Spall Dispersion Half-angle (deg)	AL 2024-T3 SECOND WALL BACK Detached Spall Dia. (in)	Raised Area Dia. (in)	Number of Holes	Dia./Len. of Holes (mm)	Width of Holes (mm)	Number of Cracks	Length of Cracks (mm)	Comments on Second Plate
													3.5 5.5 6.5	cracks, with a width max. of 0.4 mm. The extent of the cracks indicate that a much larger hole nearly occured. Much second wall spall debris embedded in witness plate.
A236	93.06	92.83	1.6	3.5	2	22	0.49	1.5	1	0.7		0		
A237	73.83	73.74	1.5	2.5	2	21	0	1	7	3.9 1.8 1.5 1.1 0.9 1.3 2.0		0		Most of surface lightly cratered. Small size of holes indicates the projectile was nearly completely disrupted in impact. Likely that ceramic failed by cracking/breaking before shock wave had completely traversed projectile.
A238	73.68	73.66	1.4	2.6	2	19	0	0.7	0			0		Only slight dimpling on back surf.
A241	96.60	96.43	2.6	5	4.5	16	0	3	0			0		Dimpling occured in 3" dia. area on back of second plate. No substantial channeling of debris plume was noted although some minor concentration of hits along interface of waffle did occur. Waffle was ripped from adhesive holding it to backwall during impact. Numerous perforations of waffle occured.
A287	99.43	99.20	1.4	3.5	2	19	0.6	1.3	0			0		Waffle was bolted down to backwall. Although waffle severly bent, a definate line of impacts concentrated along waffle, but no real change in damage pattern.
A315	74.42	74.27	2	4	2	27	0	0	7	8.1 3.3 1.0 1.3 1.0 1.0 1.1	3.8	0		Projectile was not completely broken up. Besides holes, numerous dimpling (w/ some spall separation) occured over 2.5" dia. area.

Table D-1 (Cont). Listing of Shot Data (chronological order)

9/15/87

	8-MIL AL 3003-0 BUMPER EJECTA CATCHER					AL 3003-0 SECOND WALL SPALL CATCHER WITNESS PLATE									
JSC Shot	Standoff Dist. (in)	Dia. where Ejecta hits Start (in)	Dia. where Ejecta hits generally End (in)	Min. Ejecta Cone Half-Angle (deg)	Max. Ejecta Cone Half-Angle (deg)	Thickness (mil)	Standoff Dist. (in)	Mass Before Impact (g)	Mass After Impact (g)	Number Holes	Max. Hole Dia. (mm)	Avg. Hole Dia. (mm)	Number Craters	Max. Crater Dia. (mm)	Approx. Avg. Crater Dia. (mm)
A236						16	4	23.05	23.09	1	3.2	3.2	20	5.1	1.5
A237						8	4	11.84	11.84	29	1.3	0.6	100	2	0.6
A238						8	4	11.93	11.93	0			0		
A241															
A287						8	4			2	11.4	6.1	48	3.8	0.8
A315	2					16	4	22.51	22.53	48	2.3	0.8	250	2.0	0.3

Table D-1 (Cont). Listing of Shot Data (chronological order)

JSC Shot	Date	Bumper Mat'l	Bumper Areal Density (g/cm^2)	Bumper Density (g/cc)	Al 2024-T3 Backwall Thickness (in)	Al 1100 Proj. Mass (mg)	Proj. Dia. (mm)	Proj. Vel. (km/s)	Number of Impacts	Cordin Camera Film Y or N?	Comments on Film (Clean impact unless stated)	BUMPER Frnt Crater Dia. (mm)	Hole Dia. (mm)	Back Crater Dia. (mm)	Mass Before Impact (g)	Mass After Impact (g)	Comments on Bumper
A316	21-Aug-87	Al 6061-T6 t = 0.032"	0.22	2.713	0.063	45.15	3.2	5.99	1	Y	Impact was at an 45 deg. oblique angle. Proj. vel. component = 4.2 km/s.		7.7		19.94	19.83	Elliptical hole 8.5 x 7.0 mm.

9/15/87

Table D-1 (Cont). Listing of Shot Data (chronological order)

	AL 2024-T3 SECOND WALL FRONT						AL 2024-T3 SECOND WALL BACK							
JSC Shot	Mass Before Impact (g)	Mass After Impact (g)	Dia. of Conc. Debris Hits (in)	Max. Dia. of Area for Nearly all Hits (in)	Standoff Dist. (in)	Conc. Debris Spall Dispersion Half-angle (deg)	Detached Spall Dia. (in)	Raised Area Dia. (in)	Number of Holes	Dia./Len. of Holes (mm)	Width of Holes (mm)	Number of Cracks	Length of Cracks (mm)	Comments on Second Plate
A316	92.94	92.68	2	3.5	2	27	0	0	4	10.7	2.3	0		Holes overlapped to form long scalloped rectangular holes.Dimpling occured over 1.9" area.
										2.3				
										3.3	2.5			
										3.3	2.0			

Table D-1 (Cont). Listing of Shot Data (chronological order)

9/15/87

	8-MIL AL 3003-O BUMPER EJECTA CATCHER					AL 3003-O SECOND WALL SPALL CATCHER WITNESS PLATE									
JSC Shot	Standoff Dist. (in)	Dia. where Ejecta hits Start (in)	Dia. where Ejecta hits generally End (in)	Min. Ejecta Cone Half-Angle (deg)	Max. Ejecta Cone Half-Angle (deg)	Thickness (mil)	Standoff Dist. (in)	Mass Before Impact (g)	Mass After Impact (g)	Number Holes	Max. Hole Dia. (mm)	Avg. Hole Dia. (mm)	Number Craters	Max. Crater Dia. (mm)	Approx. Avg. Crater Dia. (mm)
A316	2					16	4	22.11	22.19	11	2.3	1.3	60	5.1	1.8

Table D-2. Metal Matrix Ejecta Particle Count

4/16/87

BUMPER EJECTA CATCHER CRATER AND HOLE COUNT
Shot No. 152

Diameter (in) free of impacts: 4.05
Width of strip containing most impacts (in): 0.8 2.0 (cm)
Area of ring (in^2) 12.2 (cm^2) 78.6

Al 3003-0 ejecta catcher thickness (in) 0.008 0.2032 (mm)
Max. Ejecta Velocity (km/s) 5.2

Dens. Al 3003-0 (g/cc) 2.740
Dens. Bumper (g/cc) 2.8
Elastic Modulus Al 3003-0 (psi) 1.00E+07 6.89E+11 (dyne/cm^2)
Speed of Sound Al 3003-0 (km/s) 5.02
Hardness Al 3003-0 (Brinell) 28

Intialization val. 0.000102
calc. min. value 0.081180

												IMPACTS PER SQUARE CM								Min. Max. No.
Quadrant	Hole No.	Crater Dia. (mm)	Hole Dia. (in)	Hole Dia. (mm)	Calc. Part. Dia. (mm)	Newton Rapson Part. Dia. Estimates 1st	2nd	3rd	4th	5th	Part. Dia. based on Suit2 (mm)	No.	Hole Dia. (in)	Crater Dia. (in)	Hole Dia. (mm)	Crater Dia. (mm)	PROJECTILE DIAMETER (mm) Based on Various Sources Suit	RI	JSC	Suit-2
I	1	0.305	0.008	0.20	0.0132	0.001431	0.006436	0.011839	0.013187	0.013231	0.105024	1	0.008	0.012	0.20	0.30	0.059	0.095	0.074	0.105
(20)	2	0.406	0.002	0.05	0.0002	0.000205	0.000242	0.000244	0.000244	0.000244	0.137912	2	0.002	0.016	0.05	0.41	0.078	0.123	0.098	0.138
	3	0.457	0.012	0.30	0.0376	0.002247	0.014097	0.031622	0.037345	0.037601	0.154185	3		0.015		0.38	0.073	0.116	0.092	0.130
	4	0.508	0.015	0.38	0.0640	0.002860	0.021321	0.052537	0.063452	0.063955	0.170362	4		0.003		0.08	0.016	0.027	0.020	0.028
	5	0.457	0.013	0.33	0.0457	0.002451	0.016373	0.038040	0.045336	0.045669	0.154185	5		0.008		0.20	0.040	0.066	0.051	0.072
	6	0.381	0.002	0.06	0.0005	0.000307	0.000451	0.000473	0.000474	0.000474	0.129736	6		0.006		0.15	0.031	0.051	0.039	0.054
	7	0.508	0.005	0.13	0.0036	0.000818	0.002414	0.003442	0.003582	0.003584	0.170362	7		0.003		0.08	0.016	0.027	0.020	0.028
	8	0.381	0.01	0.25	0.0238	0.001839	0.009965	0.020526	0.023657	0.023784	0.129736	8		0.003		0.08	0.016	0.027	0.020	0.028
	9	0.584	0.019	0.48	0.1081	0.003677	0.032692	0.087703	0.107268	0.108114	0.194470	9		0.002		0.05	0.011	0.019	0.014	0.019
	10	0.508	0.012	0.30	0.0376	0.002247	0.014097	0.031622	0.037345	0.037601	0.170362	10		0.01		0.25	0.050	0.080	0.063	0.088
	11	0.406	0.015	0.38	0.0640	0.002860	0.021321	0.052537	0.063452	0.063955	0.137912	11		0.009		0.23	0.045	0.073	0.057	0.080
	12	0.305	0.011	0.28	0.0303	0.002043	0.011959	0.025779	0.030110	0.030296	0.105024	12		0.011		0.28	0.055	0.088	0.068	0.097
	13	0.356	0.002	0.05	0.0002	0.000205	0.000242	0.000244	0.000244	0.000244	0.121530	13		0.008		0.20	0.040	0.066	0.051	0.072
	14	0.457	0.002	0.05	0.0002	0.000205	0.000242	0.000244	0.000244	0.000244	0.154185	14		0.003		0.08	0.016	0.027	0.020	0.028
	15	0.483	0.016	0.41	0.0741	0.003064	0.023985	0.060582	0.073509	0.074100	0.162285	15		0.007		0.18	0.036	0.058	0.045	0.063
	16	0.305	0.011	0.28	0.0303	0.002043	0.011959	0.025779	0.030110	0.030296	0.105024	16		0.005		0.13	0.026	0.043	0.032	0.046
	17	0.254	0.002	0.05	0.0002	0.000205	0.000242	0.000244	0.000244	0.000244	0.088370	17		0.006		0.15	0.031	0.051	0.039	0.054
	18	0.381	0.009	0.23	0.0181	0.001635	0.008122	0.015876	0.018012	0.018091	0.129736	18		0.003		0.08	0.016	0.027	0.020	0.028
	19	0.381	0.001	0.03	0.0000	0.000001	0.000009	0.000023	0.000030	0.000030	0.129736	19		0.017		0.43	0.082	0.130	0.103	0.146
	20	0.254	0.002	0.05	0.0002	0.000205	0.000242	0.000244	0.000244	0.000244	0.088370	20		0.008 *		0.20	0.040	0.066	0.051	0.072
II	21	0.279	0.01	0.25	0.0238	0.001839	0.009965	0.020526	0.023657	0.023784	0.096717	21		0.01		0.25	0.050	0.080	0.063	0.088
(38)	22	0.305	0.009	0.23	0.0181	0.001635	0.008122	0.015876	0.018012	0.018091	0.105024	22		0.009		0.23	0.045	0.073	0.057	0.080
	23	0.279	0.005	0.13	0.0036	0.000818	0.002414	0.003442	0.003582	0.003584	0.096717	23		0.008		0.20	0.040	0.066	0.051	0.072
	24	0.330	0.007	0.18	0.0092	0.001226	0.004916	0.008422	0.009186	0.009207	0.113294	24		0.003		0.08	0.016	0.027	0.020	0.028
	25	0.533	0.018	0.46	0.0962	0.003472	0.029674	0.078182	0.095450	0.096213	0.178418	25		0.006		0.15	0.031	0.051	0.039	0.054
	26	0.432	0.012	0.30	0.0376	0.002247	0.014097	0.031622	0.037345	0.037601	0.146061	26		0.001		0.03	0.006	0.010	0.007	0.010
	27	0.559	0.018	0.46	0.0962	0.003472	0.029674	0.078182	0.095450	0.096213	0.186454	27		0.002		0.05	0.011	0.019	0.014	0.019
	28	0.254	0.009	0.23	0.0181	0.001635	0.008122	0.015876	0.018012	0.018091	0.088370	28		0.002		0.05	0.011	0.019	0.014	0.019
	29	0.381	0.011	0.28	0.0303	0.002043	0.011959	0.025779	0.030110	0.030296	0.129736	29		0.002		0.05	0.011	0.019	0.014	0.019
	30	0.457	0.011	0.28	0.0303	0.002043	0.011959	0.025779	0.030110	0.030296	0.154185	30		0.001		0.03	0.006	0.010	0.007	0.010
	31	0.483	0.012	0.30	0.0376	0.002247	0.014097	0.031622	0.037345	0.037601	0.162285	31		0.006		0.15	0.031	0.051	0.039	0.054
	32	0.330	0.009	0.23	0.0181	0.001635	0.008122	0.015876	0.018012	0.018091	0.113294	32		0.01		0.25	0.050	0.080	0.063	0.088

Table D-2 (Cont). Metal Matrix Ejecta Particle Count

33	0.432	0.014	0.36	0.0545	0.002656	0.018783	0.045017	0.054049	0.054466	0.146061	33	0.002	0.05	0.011	0.019	0.014	0.019
34	0.457	0.012	0.30	0.0376	0.002247	0.014097	0.031622	0.037345	0.037601	0.154185	34	0.008	0.20	0.040	0.066	0.051	0.072
35	0.432	0.011	0.28	0.0303	0.002043	0.011959	0.025779	0.030110	0.030296	0.146061	35	0.002	0.05	0.011	0.019	0.014	0.019
36	0.406	0.01	0.25	0.0238	0.001839	0.009965	0.020526	0.023657	0.023784	0.137912	36	0.002	0.05	0.011	0.019	0.014	0.019
37	0.356	0.009	0.23	0.0181	0.001635	0.008122	0.015876	0.018012	0.018091	0.121530	37	0.002	0.05	0.011	0.019	0.014	0.019
38	0.406	0.013	0.33	0.0457	0.002451	0.016373	0.038040	0.045336	0.045669	0.137912	38	0.001	0.03	0.006	0.010	0.007	0.010
39	0.305	0.01	0.25	0.0238	0.001839	0.009965	0.020526	0.023657	0.023784	0.105024	39	0.002	0.05	0.011	0.019	0.014	0.019
40	0.254	0.008	0.20	0.0132	0.001431	0.006436	0.011839	0.013187	0.013231	0.088370	40	0.006	0.15	0.031	0.051	0.039	0.054
41	0.406	0.012	0.30	0.0376	0.002247	0.014097	0.031622	0.037345	0.037601	0.137912	41	0.003 *	0.08	0.016	0.027	0.020	0.028
42	0.508	0.018	0.46	0.0962	0.003472	0.029674	0.078182	0.095450	0.096213	0.170362	42	0.008	0.20	0.040	0.066	0.051	0.072
43	0.229	0.007	0.18	0.0092	0.001226	0.004916	0.008422	0.009186	0.009207	0.079979	43	0.001	0.03	0.006	0.010	0.007	0.010
44	0.381	0.01	0.25	0.0238	0.001839	0.009965	0.020526	0.023657	0.023784	0.129736	44	0.009	0.23	0.045	0.073	0.057	0.080
45	0.381	0.01	0.25	0.0238	0.001839	0.009965	0.020526	0.023657	0.023784	0.129736	45	0.012	0.30	0.059	0.095	0.074	0.105
46	0.432	0.012	0.30	0.0376	0.002247	0.014097	0.031622	0.037345	0.037601	0.146061	46	0.003	0.08	0.016	0.027	0.020	0.028
47	0.457	0.015	0.38	0.0640	0.002860	0.021321	0.052537	0.063452	0.063955	0.154185	47	0.004	0.10	0.021	0.035	0.026	0.037
48	0.406	0.012	0.30	0.0376	0.002247	0.014097	0.031622	0.037345	0.037601	0.137912	48	0.002	0.05	0.011	0.019	0.014	0.019
49	0.305	0.004	0.10	0.0019	0.000614	0.001459	0.001850	0.001884	0.001884	0.105024	49	0.007	0.18	0.036	0.058	0.045	0.063
50	0.381	0.009	0.23	0.0181	0.001635	0.008122	0.015876	0.018012	0.018091	0.129736	50	0.01	0.25	0.050	0.080	0.063	0.088
51	0.381	0.01	0.25	0.0238	0.001839	0.009965	0.020526	0.023657	0.023784	0.129736	51	0.005	0.13	0.026	0.043	0.032	0.046
52	0.533	0.018	0.46	0.0962	0.003472	0.029674	0.078182	0.095450	0.096213	0.178418	52	0.005	0.13	0.026	0.043	0.032	0.046
53	0.381	0.012	0.30	0.0376	0.002247	0.014097	0.031622	0.037345	0.037601	0.129736	53	0.003	0.08	0.016	0.027	0.020	0.028
54	0.432	0.004	0.10	0.0019	0.000614	0.001459	0.001850	0.001884	0.001884	0.146061	54	0.002	0.05	0.011	0.019	0.014	0.019
55	0.381	0.009	0.23	0.0181	0.001635	0.008122	0.015876	0.018012	0.018091	0.129736	55	0.003	0.08	0.016	0.027	0.020	0.028
56	0.457	0.015	0.38	0.0640	0.002860	0.021321	0.052537	0.063452	0.063955	0.154185	56	0.002	0.05	0.011	0.019	0.014	0.019
57	0.381	0.001	0.03	0.0000	0.000001	0.000009	0.000023	0.000030	0.000030	0.129736	57	0.002	0.05	0.011	0.019	0.014	0.019
58	0.356	0.002	0.05	0.0002	0.000205	0.000242	0.000244	0.000244	0.000244	0.121530	58	0.003	0.08	0.016	0.027	0.020	0.028
59	0.356	0.005	0.13	0.0036	0.000818	0.002414	0.003442	0.003582	0.003584	0.121530	59	0.008	0.20	0.040	0.066	0.051	0.072
60	0.432	0.015	0.38	0.0640	0.002860	0.021321	0.052537	0.063452	0.063955	0.146061	60	0.003	0.08	0.016	0.027	0.020	0.028
61	0.406	0.012	0.30	0.0376	0.002247	0.014097	0.031622	0.037345	0.037601	0.137912	61	0.001	0.03	0.006	0.010	0.007	0.010
62	0.406	0.01	0.25	0.0238	0.001839	0.009965	0.020526	0.023657	0.023784	0.137912	62	0.002	0.05	0.011	0.019	0.014	0.019
63	0.432	0.014	0.36	0.0545	0.002656	0.018783	0.045017	0.054049	0.054466	0.146061	63	0.001	0.03	0.006	0.010	0.007	0.010
64	0.406	0.012	0.30	0.0376	0.002247	0.014097	0.031622	0.037345	0.037601	0.137912	64	0.003 *	0.08	0.016	0.027	0.020	0.028
65	0.305	0.01	0.25	0.0238	0.001839	0.009965	0.020526	0.023657	0.023784	0.105024	65	0.003	0.08	0.016	0.027	0.020	0.028
66	0.381	0.01	0.25	0.0238	0.001839	0.009965	0.020526	0.023657	0.023784	0.129736	66	0.002	0.05	0.011	0.019	0.014	0.019
67	0.254	0.006	0.15	0.0060	0.001022	0.003571	0.005626	0.005996	0.006003	0.088370	67	0.008	0.20	0.040	0.066	0.051	0.072
68	0.432	0.015	0.38	0.0640	0.002860	0.021321	0.052537	0.063452	0.063955	0.146061	68	0.01	0.25	0.050	0.080	0.063	0.088
69	0.457	0.014	0.36	0.0545	0.002656	0.018783	0.045017	0.054049	0.054466	0.154185	69	0.009	0.23	0.045	0.073	0.057	0.080
70	0.406	0.011	0.28	0.0303	0.002043	0.011959	0.025779	0.030110	0.030296	0.137912	70	0.013	0.33	0.064	0.102	0.080	0.113
71	0.279	0.007	0.18	0.0092	0.001226	0.004916	0.008422	0.009186	0.009207	0.096717	71	0.01	0.25	0.050	0.080	0.063	0.088
72	0.279	0.009	0.23	0.0181	0.001635	0.008122	0.015876	0.018012	0.018091	0.096717	72	0.001	0.03	0.006	0.010	0.007	0.010
73	0.356	0.003	0.08	0.0008	0.000410	0.000726	0.000809	0.000812	0.000812	0.121530	73	0.002	0.05	0.011	0.019	0.014	0.019
74	0.381	0.005	0.13	0.0036	0.000818	0.002414	0.003442	0.003582	0.003584	0.129736	74	0.011	0.28	0.055	0.088	0.068	0.097
75	0.406	0.01	0.25	0.0238	0.001839	0.009965	0.020526	0.023657	0.023784	0.137912	75	0.003	0.08	0.016	0.027	0.020	0.028
76	0.229	0.002	0.05	0.0002	0.000205	0.000242	0.000244	0.000244	0.000244	0.079979	76	0.002	0.05	0.011	0.019	0.014	0.019
77	0.305	0.002	0.05	0.0002	0.000205	0.000242	0.000244	0.000244	0.000244	0.105024	77	0.001	0.03	0.006	0.010	0.007	0.010
78	0.203	0.004	0.10	0.0019	0.000614	0.001459	0.001850	0.001884	0.001884	0.071538	78	0.002	0.05	0.011	0.019	0.014	0.019
79	0.432	0.015	0.38	0.0640	0.002860	0.021321	0.052537	0.063452	0.063955	0.146061	79	0.013	0.33	0.064	0.102	0.080	0.113
80	0.381	0.013	0.33	0.0457	0.002451	0.016373	0.038040	0.045336	0.045669	0.129736	80	0.002	0.05	0.011	0.019	0.014	0.019
81	0.330	0.012	0.30	0.0376	0.002247	0.014097	0.031622	0.037345	0.037601	0.113294							
82	0.229	0.006	0.15	0.0060	0.001022	0.003571	0.005626	0.005996	0.006003	0.079979							
83	0.203	0.005	0.13	0.0036	0.000818	0.002414	0.003442	0.003582	0.003584	0.071538							
84	0.483	0.018	0.46	0.0962	0.003472	0.029674	0.078182	0.095450	0.096213	0.162285							
85	0.533	0.017	0.43	0.0849	0.003268	0.026771	0.069137	0.084186	0.084864	0.178418							
86	0.457	0.015	0.38	0.0640	0.002860	0.021321	0.052537	0.063455	0.063955	0.154185							
87	0.483	0.013	0.33	0.0457	0.002451	0.016373	0.038040	0.045336	0.045669	0.162285							
88	0.584	0.018	0.46	0.0962	0.003472	0.029674	0.078182	0.095450	0.096213	0.194470							

Table D-2 (Cont). Metal Matrix Ejecta Particle Count

	89	0.356	0.007	0.18	0.0092	0.001226	0.004916	0.008422	0.009186	0.009207	0.121530
	90	0.330	0.007	0.18	0.0092	0.001226	0.004916	0.008422	0.009186	0.009207	0.113294
	91	0.254	0.008	0.20	0.0132	0.001431	0.006436	0.011839	0.013187	0.013231	0.088370
	92	0.381	0.01	0.25	0.0238	0.001839	0.009965	0.020526	0.023657	0.023784	0.129736
	93	0.330	0.001	0.03	0.0000	0.000001	0.000009	0.000023	0.000030	0.000030	0.113294
	94	0.178	0.002	0.05	0.0002	0.000205	0.000242	0.000244	0.000244	0.000244	0.063040
	95	0.533	0.013	0.33	0.0457	0.002451	0.016373	0.038040	0.045336	0.045669	0.178418
	96	0.279	0.008	0.20	0.0132	0.001431	0.006436	0.011839	0.013187	0.013231	0.096717
	97	0.330	0.01	0.25	0.0238	0.001839	0.009965	0.020526	0.023657	0.023784	0.113294
	98	0.432	0.008	0.20	0.0132	0.001431	0.006436	0.011839	0.013187	0.013231	0.146061
	99	0.356	0.007	0.18	0.0092	0.001226	0.004916	0.008422	0.009186	0.009207	0.121530
	100	0.483	0.012	0.30	0.0376	0.002247	0.014097	0.031622	0.037345	0.037601	0.162285
IV	101	0.254	0.005	0.13	0.0036	0.000818	0.002414	0.003442	0.003582	0.003584	0.088370
(36)	102	0.305	0.009	0.23	0.0181	0.001635	0.008122	0.015876	0.018012	0.018091	0.105024
	103	0.330	0.01	0.25	0.0238	0.001839	0.009965	0.020526	0.023657	0.023784	0.113294
	104	0.305	0.009	0.23	0.0181	0.001635	0.008122	0.015876	0.018012	0.018091	0.105024
	105	0.457	0.014	0.36	0.0545	0.002656	0.018783	0.045017	0.054049	0.054466	0.154185
	106	0.483	0.017	0.43	0.0849	0.003268	0.026771	0.069137	0.084186	0.084864	0.162285
	107	0.305	0.002	0.05	0.0002	0.000205	0.000242	0.000244	0.000244	0.000244	0.105024
	108	0.203	0.001	0.03	0.0000	0.000001	0.000009	0.000023	0.000030	0.000030	0.071538
	109	0.457	0.012	0.30	0.0376	0.002247	0.014097	0.031622	0.037345	0.037601	0.154185
	110	0.432	0.008	0.20	0.0132	0.001431	0.006436	0.011839	0.013187	0.013231	0.146061
	111	0.356	0.005	0.13	0.0036	0.000818	0.002414	0.003442	0.003582	0.003584	0.121530
	112	0.254	0.002	0.05	0.0002	0.000205	0.000242	0.000244	0.000244	0.000244	0.088370
	113	0.381	0.011	0.28	0.0303	0.002043	0.011959	0.025779	0.030110	0.030296	0.129736
	114	0.229	0.005	0.13	0.0036	0.000818	0.002414	0.003442	0.003582	0.003584	0.079979
	115	0.356	0.011	0.28	0.0303	0.002043	0.011959	0.025779	0.030110	0.030296	0.121530
	116	0.432	0.005	0.13	0.0036	0.000818	0.002414	0.003442	0.003582	0.003584	0.146061
	117	0.279	0.009	0.23	0.0181	0.001635	0.008122	0.015876	0.018012	0.018091	0.096717
	118	0.381	0.011	0.28	0.0303	0.002043	0.011959	0.025779	0.030110	0.030296	0.129736
	119	0.356	0.001	0.03	0.0000	0.000001	0.000009	0.000023	0.000030	0.000030	0.121530
	120	0.381	0.002	0.05	0.0002	0.000205	0.000242	0.000244	0.000244	0.000244	0.129736
	121	0.279	0.002	0.05	0.0002	0.000205	0.000242	0.000244	0.000244	0.000244	0.096717
	122	0.457	0.012	0.30	0.0376	0.002247	0.014097	0.031622	0.037345	0.037601	0.154185
	123	0.406	0.005	0.13	0.0036	0.000818	0.002414	0.003442	0.003582	0.003584	0.137912
	124	0.406	0.014	0.36	0.0545	0.002656	0.018783	0.045017	0.054049	0.054466	0.137912
	125	0.356	0.012	0.30	0.0376	0.002247	0.014097	0.031622	0.037345	0.037601	0.121530
	126	0.305	0.007	0.18	0.0092	0.001226	0.004916	0.008422	0.009186	0.009207	0.105024
	127	0.330	0.003	0.08	0.0008	0.000410	0.000726	0.000809	0.000812	0.000812	0.113294
	128	0.305	0.001	0.03	0.0000	0.000001	0.000009	0.000023	0.000030	0.000030	0.105024
	129	0.279	0.001	0.03	0.0000	0.000001	0.000009	0.000023	0.000030	0.000030	0.096717
	130	0.406	0.012	0.30	0.0376	0.002247	0.014097	0.031622	0.037345	0.037601	0.137912
	131	0.432	0.015	0.38	0.0640	0.002860	0.021321	0.052537	0.063452	0.063955	0.146061
	132	0.330	0.001	0.03	0.0000	0.000001	0.000009	0.000023	0.000030	0.000030	0.113294
	133	0.406	0.012	0.30	0.0376	0.002247	0.014097	0.031622	0.037345	0.037601	0.137912
	134	0.279	0.01	0.25	0.0238	0.001839	0.009965	0.020526	0.023657	0.023784	0.096717
	135	0.356	0.005	0.13	0.0036	0.000818	0.002414	0.003442	0.003582	0.003584	0.121530
	136	0.381	0.01	0.25	0.0238	0.001839	0.009965	0.020526	0.023657	0.023784	0.129736

Explanation of Ejecta Particle Size Calculations for Metal Matrix Shot A152 (p.170-172):

The left side of the spreadsheet calculates the particle size that created all 136 holes counted in this plate using a Newton-Rapson iterative technique to solve the following Al on Al impact equation for d (12, p.117):

$$D/d = 0.45 * V * (t_s/d)^{2/3} + 0.9$$

where d is the particle diameter (mm), D is the hole diameter from measurements (mm), t_s is the plate thickness (.2032 mm), and V is the maximum ejecta velocity determined from high speed films (km/s). An alternative approach (Labeled "Suit 2") calculates the particle size based on an Al penetration equation (from Cour-Palais, B: "Revised Hazard Assessment of the 4.3 and 8 psi Space Suits," JSC Memorandum SN3-86-141, June 2, 1986):

$$t = K * p_p^{.167} * m_p^{.352} * V^{.875}$$

where t is the ballistic limit thickness for Al 6061-T6 (cm), m_p is the particle mass (g), V is the particle velocity (km/s), K is 0.57 for Al 6061-T6, and p_p is the particle density (g/cc). The ballistic limit thickness is related to penetration depth into a semi-infinite target, P (cm), and crater diameter, D_{cr} (cm), by t = 1.75 P = 1.75/2 D_{cr}. For purposes of this calculation, D_{cr} = D/10. Since the mass of the particle is the product of density and volume (assumed spherical), the diameter of the particle is then:

$$d = 20 * [0.927167 * D_{cr}/(p_p^{.519} * V^{.875})]^{.94697}$$

The right side of the spreadsheet calculates the particle size that created all significant impacts in a 1 cm^2 area (selected in the inside ring of greatest impacts); a total of 2 holes and 78 craters. The impacting particle diameter was calculated with the following equations (rearranged to solve for d):

("Suit" - Ref.44) $t = 1.8\,P = 1.8\,D_{cr}/2 = 9.2\,d'^{1.06}\,(p_p/p_t)^{.5}\,(V/C)^{.667}\,(BH)^{-.25}$

("RI" - Ref.43) $P = D_{cr}/2 = 1.38\,d'^{1.1}\,p_p^{.5}\,p_t^{-.167}\,V'^{.67}\,BH^{-.25}$

("JSC" - Ref.43) $P = D_{cr}/2 = 5.24\,d'^{1.056}\,p_p^{.5}\,p_t^{-.167}\,V'^{.67}\,BH^{-.25}\,E_t^{-.33}$

("Suit 2" - as before)

where t is the ballistic limit thickness (cm), P is the semi-infinite penetration (cm), D_{cr} is the crater diameter (cm), d' is the particle diameter (cm), d is the particle diameter (mm), p_p is the particle density (g/cc), p_t is the target density (g/cc), V is the particle velocity (km/s), V' is the particle velocity (cm/s), C is the speed of sound in the target (km/s), BH is the target Brinell hardness, and E_t is the target elastic modulus (dyne/cm^2).

Table D-3. Bumper Plate Ejecta and Debris Plume Velocity

JSC SHOT 150 EJECTA AND SPALL VELOCITY

Bumper Type	Al 6061-T6
Projectile Velocity (km/s)	6.45
Ejecta Velocity (km/s)	6.7
Max. Ejecta Cone Half-Angle (deg)	35
Spall Velocity (km/s)	4.7
Conc. Spall Dispersion Half-Angle (deg)	20
Max. Spall Dispersion Half-Angle (deg)	44
Time between frames (microsec)	1.024166
Distance Correction Factor	3.96

	MEASUREMENTS (uncorrected by distance factor)					CALCULATED VALUES (corrected with distance factor)		
Frame	Proj to Plate Dist. (mm)	Ejecta Cone half Angle (deg)	Ejecta Front Dist. (mm)	Spall Front Dist. (mm)	Spall Cone half Angle (deg)	Proj. Velocity (km/s)	Max. Ejecta Velocity (km/s)	Max. Spall Velocity (km/s)
14	3.1							
15	1.6					5.8		
16	0.15					5.7		
17			0.55	0.4				
18		55	2.0	1.5			6.8	4.3
19		52	3.4	2.7			6.7	4.4
20				4.0				4.6
21				5.2				4.6
22				6.5				4.7
23				7.7				4.7
24				9.0				4.75
25				10.2				4.74
26				10.7	57			

Table D-3 (Cont). **Bumper Plate Ejecta and Debris Plume Velocity**

JSC SHOT 157 EJECTA AND SPALL VELOCITY

Bumper Type	Metal Matrix (Al 6061T6/35v% SiC)
Projectile Velocity (km/s)	**6.71**
Ejecta Velocity (km/s)	5.2
Max. Ejecta Cone Half-Angle (deg)	31
Spall Velocity (km/s)	5.4
Conc. Spall Dispersion Half-Angle (deg)	23
Max. Spall Dispersion Half-Angle (deg)	44
Time between frames (microsec)	1.029583
Distance Correction Factor	4.34

MEASUREMENTS (uncorrected by distance factor) | CALCULATED VALUES (corrected with distance factor)

Frame	Proj to Plate Dist.	Ejecta Cone half Angle (deg)	Ejecta Front Dist. (mm)	Spall Front Dist. (mm)	Spall Cone half Angle	Proj. Velocity (km/s)	Max. Ejecta Velocity (km/s)	Max. Spall Velocity (km/s)
24	2.1							
25	0.6					6.3		
26			0.55					
27		47	1.5	1.0			4.7	
28		46	2.5	2.1			4.8	4.6
29			3.7	3.4			5.2	5.1
30				4.9				5.5
31				6.3				5.6
32				7.5				5.5
33				8.7				5.4
34				10.0	28			5.4
35					26			
36					28			

Table D-3 (Cont). Bumper Plate Ejecta and Debris Plume Velocity

JSC SHOT 158 EJECTA AND SPALL VELOCITY

Bumper Type 8 mil Al 3003-0 bonded to graphite/epoxy

Projectile Velocity (km/s)	6.18
Ejecta Velocity (km/s)	3.9
Max. Ejecta Cone Half-Angle (deg)	32
Spall Velocity (km/s)	5.3
Conc. Spall Dispersion Half-Angle (deg)	21
Max. Spall Dispersion Half-Angle (deg)	41
Time between frames (microsec)	1.030416
Distance Correction Factor	4.23

MEASUREMENTS (uncorrected by distance factor) — CALCULATED VALUES (corrected with distance factor)

Frame	Proj to Plate Dist. (mm)	Ejecta Cone half Angle (deg)	Ejecta Front Dist. (mm)	Spall Front Dist. (mm)	Spall Cone half Angle (deg)	Proj. Velocity (km/s)	Max. Ejecta Velocity (km/s)	Max. Spall Velocity (km/s)
32	3.5							
33	2.1					5.7		
34	0.7					5.7		
35	0.2							
36			1.5	1.2				
37			2.5	2.6			4.8	5.7
38		59	3.1	4.0			3.9	5.7
39			3.8	5.3				5.6
40				6.7				5.6
41				7.9				5.5
42				8.9				5.3
43				10.2	38			5.3
44								

Table D-3 (Cont). Bumper Plate Ejecta and Debris Plume Velocity

JSC SHOT 159 EJECTA AND SPALL VELOCITY

Bumper Type 15 mil Alumina bonded to 8 mil Al 3003-0

Projectile Velocity (km/s)	6.56
Ejecta Velocity (km/s)	4.2
Max. Ejecta Cone Half-Angle (deg)	35
Spall Velocity (km/s)	5.0
Conc. Spall Dispersion Half-Angle (deg)	22
Max. Spall Dispersion Half-Angle (deg)	43
Time between frames (microsec)	1.030416
Distance Correction Factor	3.73

	MEASUREMENTS (uncorrected by distance factor)					CALCULATED VALUES (corrected with distance factor)		
Frame	Proj to Plate Dist. (mm)	Ejecta Cone half Angle (deg)	Ejecta Front Dist. (mm)	Spall Front Dist. (mm)	Spall Cone half Angle (deg)	Proj. Velocity (km/s)	Max. Ejecta Velocity [illegible]	Max. Spall Velocity (km/s)
26	5.2							
27	4.4					2.9		
28	2.95					4.1		
29	1.5					4.5		
30								
31								
32			0.7	0.1				
33			1.6	1.8			4.0	6.2
34			2.5	3			4.0	5.3
35			3.4	4.6			4.0	5.4
36		41	4.5	6.0			4.2	5.3
37				7.2				5.1
38				8.4				5.0
39				9.7				5.0
40				10.6	31			4.8

Table D-3 (Cont). **Bumper Plate Ejecta and Debris Plume Velocity**

JSC SHOT 161 EJECTA AND SPALL VELOCITY

Bumper Type	Al 5056 mesh (4 sheets)
Projectile Velocity (km/s)	6.50
Ejecta Velocity (km/s)	2.1
Max. Ejecta Cone Half-Angle (deg)	0
Spall Velocity (km/s)	6.7
Conc. Spall Dispersion Half-Angle (deg)	14
Max. Spall Dispersion Half-Angle (deg)	44
Time between frames (microsec)	1.052916
Distance Correction Factor	4.67

	MEASUREMENTS (uncorrected by distance factor)					CALCULATED VALUES (corrected with distance factor)		
Frame	Proj to Plate Dist. (mm)	Ejecta Cone half Angle (deg)	Ejecta Front Dist. (mm)	Spall Front Dist. [illegible]	Spall Cone half Angle (deg)	Proj. Velocity (km/s)	Max. Ejecta Velocity (km/s)	Max. Spall Velocity (km/s)
26	4.1							
27	2.6					6.7		
28	1.1					6.7		
29	0							
30								
31				0.7				
32			0.3	2.5				8.0
33			0.5	4			0.9	7.3
34			1	5.8			1.6	7.5
35			1.5	7			1.8	7.0
36			2	8.3			1.9	6.7
37			2.5				2.0	
38			3				2.0	
39			3.5				2.0	
40			4		37		2.1	

ORIGINAL PAGE IS OF POOR QUALITY

Table D-3 (Cont). Bumper Plate Ejecta and Debris Plume Velocity

JSC SHOT 163 EJECTA AND SPALL VELOCITY

Bumper Type	Kevlar fabric (8 sheets)
Projectile Velocity (km/s)	**7.07**
Ejecta Velocity (km/s)	2.4
Max. Ejecta Cone Half-Angle (deg)	34
Spall Velocity (km/s)	7.0
Conc. Spall Dispersion Half-Angle (deg)	21
Max. Spall Dispersion Half-Angle (deg)	21
Time between frames (microsec)	1.02125
Distance Correction Factor	4.53

	MEASUREMENTS (uncorrected by distance factor)					CALCULATED VALUES (corrected with distance factor)		
Frame	Proj to Plate Dist. (mm)	Ejecta Cone half Angle (deg)	Ejecta Front Dist. (mm)	Spall Front Dist. (mm)	Spall Cone half Angle (deg)	Proj. Velocity (km/s)	Max. Ejecta Velocity (km/s)	Max. Spall Velocity (km/s)
31	4.3							
32	2.8					6.7		
33	1.5					6.2		
34	0.01					6.3		
35								
36			0.5	0.8				
37			1.1	2.5			3.2	7.5
38			1.5	4.1			2.7	7.3
39			1.9	5.6			2.5	7.1
40			2.3	7.1			2.4	7.0
41		34	2.7	8.5			2.4	
42								
43								

Appendix E

ROM Cost Estimates for Bumper Materials

AMERICAN
MATRIX
INC.™
The Materials Advantage

P.O. Box 23556
Knoxville, TN 37933
USA
118 Sherlake Drive
37922

December 19, 1986

Mr. Eric Christensen
Eagle Engineering Corporation
711 Bay Area
Suite 315
Webster, TX 77598

REF: AMI-JAB-6164

Dear Mr. Christensen:

I apologize for this belated response to your inquiry. I promise you that our future responses will be more timely.

For our mutual convenience, let me restate your requirements as I now understand them:

1. 4 each 0.027 in. thick by 4.00 in. dimension square or circle as SiC hot press plate formed or machined to dimension.

2. 4 each 0.027 in. thick by 4.00 in. dimension square or circle as 20% volume SiC whisker reinforced SiC hot press plate formed or machined to dimension.

3. 4 each 0.034 in. thick by 4.00 in. dimension square or circle as B_4C hot press plate formed or machined to dimension.

4. 4 each 0.034 in. thick by 4.00 in. dimension square or circle as 20% volume B_4C whisker reinforced B_4C hot press plate formed or machined to dimension.

I presume that the dimensional tolerances will not be more restrictive than industry practice.

To be able to provide all four items, American Matrix, Inc. (AMI) will subcontract a portion of the program to Eagle-Picher Industries, Inc. (EPI). EPI and AMI cooperate from time to time on advanced ceramic technology programs because of our complimentary capabilities. The total price to Eagle Engineering is $10,000 FOB Houston, TX.

If you are interested in other tile combinations, we can also provide SiC whisker or B_4C whisker reinforced alumina or SiC platelet reinforced aluminum metal tile. I am enclosing some technical data sheets which describe our SiC whiskers, SiC platelets, and B_4C whisker, platelet, granule mixture. We offer B_4C whiskers as an individual material; however, I an currently out of those data sheets.

I would recommend a technical meeting to discuss your requirements in more depth before any procurement is initiated. We would be pleased to have you visit our facilities in Tennessee or we can meet at Eagle-Picher's facilities in Oklahoma or in yours in Houston as you elect. I am confident that you recognize that your requirements challenge the current state-of-the-art and we need to have a collective understanding of all the performance parameters which may be involved.

Please call me if you have any questions or desire further information.

Sincerely,

James A. Black

James A. Black
Vice President

JAB/jal

AMERICAN MATRIX INC.™
The Materials Advantage
P.O. Box 23556
Knoxville, TN 37933
USA
118 Sherlake Drive
37922

BORON CARBIDE - PFG

American Matrix, Inc. announces a new product, **Boron Carbide - PFG**, which is a mixture of single crystal boron carbide platelets, fibers, and granules. Some of the more important properties of this product are listed below:

Structure: Single Crystals

Shape: Whiskers/Flat Plates

Color: Translucent

Chemistry: 78% Boron (No Free Carbon)

Impurities: Less than 1%

American Matrix can control the median size of the crystals within limits, however all production materials will have a range of sizes around the median size.

The following is a typical size distribution of the product:

Fibers: 10 micron diameter

Platelets: 5 microns thickness

Granules: 3 microns diameter

Boron Carbide - PFG has a theoretical advantage over fiber or whisker materials where it is important to strengthen composite materials and make them more rigid. Because of the high strength of Boron Carbide, the platelets and fibers may be ideal to strengthen most matrices in metal and polymeric matrix materials. Because of the inherent low density and high strength, the product should provide an optimum strength to weight ratio for reinforcement. It should also provide an attractive toughening mechanism in ceramics.

For further information, contact:

American Matrix, Inc.
P. O. Box 23556
Knoxville, Tennessee 37933

(615) 691-8021

BORON CARBIDE FIBERS

SEM Magnification: 100X

SEM Magnification: 200X

ORIGINAL PAGE IS
OF POOR QUALITY

BORON CARBIDE FIBERS

SEM Magnification: 500X

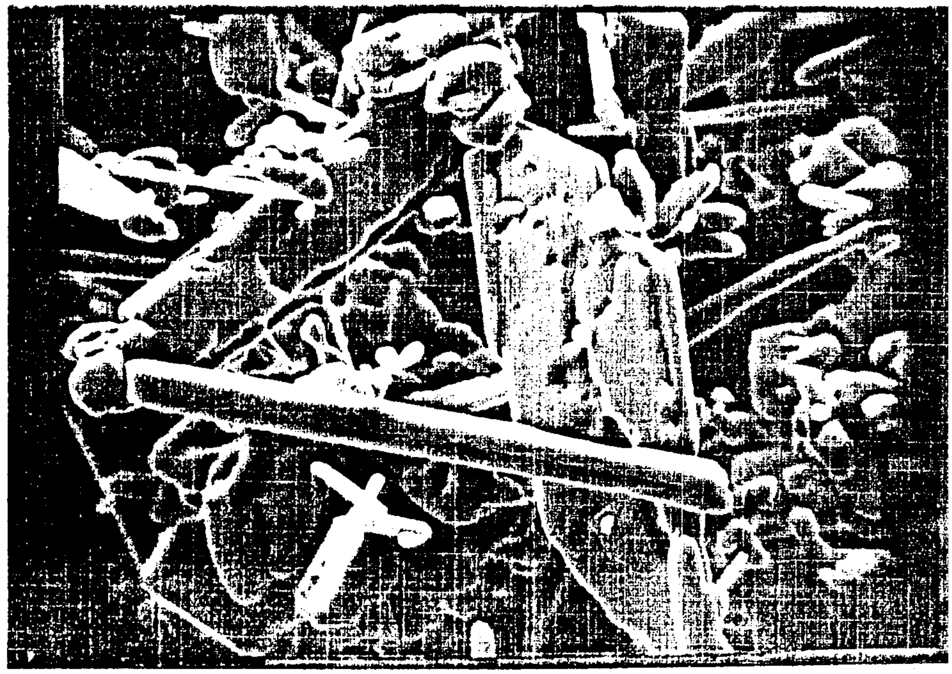

SEM Magnification: 1000X

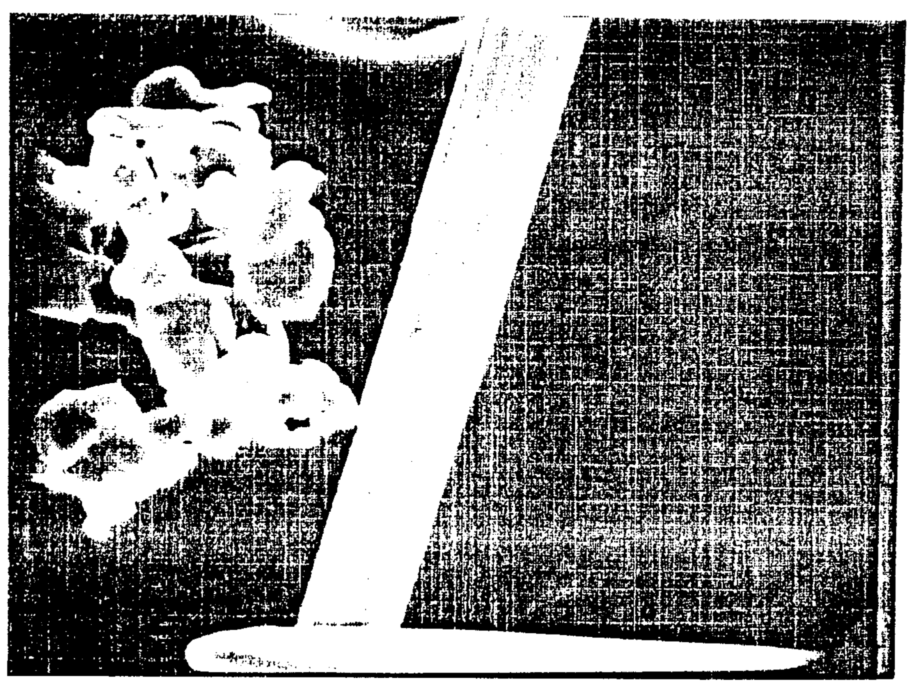

HERCULES

Hercules Aerospace Company
Aerospace Products Group
Bacchus Works
Magna, Utah 84044-0098
(801) 250-5911

28 January 1987

IN REPLY REFER TO:
MISC/M400/21-3/0010

Eagle Engineering, Inc.
P.O. Box 891049
HOuston, TX 77289-1049

Attention: Mr. Eric Christiansen

Dear Eric:

Subject: ROM Estimate Request (TO-86-56) for Hypervelocity Meteoriod and Orbital Debris Shield composite test panels

Hercules is pleased to respond with ROM estimates for the subject composite panels. Based on written correspondence and subsequent telephone conversations, the subject panels have been itemized in Tables I and II.

Table I shows the materials, desired areal density, desired panel thickness (per your correspondence), approximate ply thickness, laminate and estimated panel thickness for the requested 6-inch by 6-inch panels. Table II details some additional materials we spoke of during our phone conversation that may prove to offer additional hypervelocity impact resistance. The graphite/epoxy-balsa core sandwich panel did successfully stop a 6.34 km/sec. projectile in early tests and does provide lightweight protection for the given thickness.

XUHMS is a recently developed high modulus fiber with moderate tensile strength. This fiber shows promise for high stiffness applications such as the space station truss structure. Typical properties are shown in Table III. 8551-7 is Hercules newly developed toughened epoxy. The enclosed brochure will provide you with data on its mechanical properties and superior toughness.

Table II also lists a 3-D, or three-directional material, that is fabricated here at Hercules. This material is automatically woven with fibers to produce reinforcement in the x,y, and z directions. This third plane of reinforcement may demonstrate some encouraging test results.

The ROM estimates for Hercules participation are as follows:

Table I Panels (1 each)	$8,645
Table II Panels (1 each)	$3,340

HERCULES

28 January 1987
MISC/M400/21-3/0010

Assuming all raw materials are available upon contract award, Hercules would anticipate a two-month delivery of all test specimens. Additional panels of each configuration could be provided at a more economic cost under the same purchase order. Although no physical or Non-Destructive Evaluation tests were priced in this ROM quote, they are available to Eagle Engineering once you have determined your needs.

I hope this information has been of help to you. If you have any further questions, please contact me at (801) 251-1739.

Sincerely,

Mark J. Courtney

M. J. Courtney
Space Structures Marketing

MJC:a

Enclosures
5903z

TABLE I

Required 6-Inch x 6-Inch Panels

	Material	Material Designation	Desired Areal Density(lbs/in^2)	Panel Thickness (in)	Ply Thickness (in)	Laminate	Estimated Manuf. Thickness (in)
1)	GR/EP w/Cloth	IM6/3501-6 (Tape) A193P/3501-6 (Cloth)	0.00314	0.056	5.5 mils 7.0 mils	$[\text{cloth},0°,+45,-45,90]_s$	0.058
2)	GR/EP w/Cloth	IM6/3501-6 (Tape) A193P/3501-6 (Cloth)	0.00157	0.028	5.5 mils 7.0 mils	[Cloth,0°,90°,0°,Cloth]	0.031
3)	GR/EP w/o/Cloth	IM6/3501-6 (Tape)	0.00314	0.056	5.5 mils	$[0_2,+45°,-45°,90°]_s$	0.055
4)	GR,Fiberglass/EP	IM6/3501-6 (Tape) S-2/3501-6 (Tape)	0.00314	0.053	5.5 mils 5.0mils	$[0°_{GR},+45°_{GL},90°_{GR}-45°_{GL},0°_{GR}]_s$	0.053
5)	GR/Thermo Plastic	IM6/PEEK (Tape)	0.00314	0.058	5.5 mils	$[0°_2,+45°,-45°,90°]_s$	0.055
6)	Kevlar, GR/EP	Kevlar 49/3501-6 (Tape) IM6/3501-6 (Tape)	0.00314	0.058	8.0 mils 5.5 mils	$[0°_{GR},+45°_{KEV},90°_{GR},-45°_{KEV},0°_{GR},-45°_{KEV},90°_{GR},+45°_{KEV},0°_{GR}]$	0.060
7)	GR Cloth	A193 P (Cloth)	0.00314	0.116	10.5 mils	11 Plies	0.116
8)	GR/EP w/Cloth	AS4/3501-6 (Tape) A193P/3501-6 (Cloth)	-	1.00	5.2 mils 7.0 mils	$\text{Cloth},[(0,+45,-45,90)_s]_{24}$	1.005
9)	GR/EP	IM6/3501-6 (Tape)	-	0.022	5.5 mils	$[0°,90°]_s$	0.022

TABLE II

Optional 6-Inch x 6-Inch Panels

	Material		Material Designation		Desired Areal Density(lbs/in^2)	Panel Thickness (in)	Ply Thickness (in)	Laminate	Estimated Manuf. Thickness (in)
1)	GR/EP	w/Cloth	XUHMS/8551-7 A193P/3501-6	(Tape) (Cloth)	0.00314	0.056	3.5 mils 7.0 mils	Cloth,$[(+30,-30,90)_s]_2$, Cloth	0.056
2)	GR/EP	w/Cloth	IM7/8551-7 A193P/3501-6	(Tape) (Cloth)	0.00314	0.056	5.5 mils 7.0 mils	$[Cloth,0,+45,-45,90]_s$	0.058
3)	GR/EP	w/Cloth	XUHMS/3501-6 A193P/3501-6	(Tape) (Cloth)	0.00314	0.056	3.5 mils 7.0 mils	Cloth,$[(+30,-30,90)_s]_2$, Cloth	0.056
4)	3-D GR/EP		IM7orAS4/3501-6		0.00314	0.060	-	-	0.060
5)	GR/EP	w/Balsa	IM7/8551-7 Balsa	(Tape)	-	0.68	5.5 mils 0.56 mils	$[0,+45,-45,90]_s$, Balsa,$[0,+45,-45,90]_s$	0.68

TABLE III

XUHMS TYPICAL FIBER PROPERTIES *

PROPERTY	TYPICAL VALUE
Unidirectional Laminate Tensile Modulus, $E11_T$ (msi)	39.2
Unidirectional Laminate Tensile Strength, $S11_T$ (ksi)	320
Unidirectional Laminate Tensile Strain, $e11_T$ (%)	0.8
Unidirectional Laminate Compression Modulus, $E11_C$ (msi)	36
Unidirectional Laminate Compression Strength, $S11_C$ (ksi)	150
Short Beam Shear Strength (ksi)	12
Unidirectional Coefficient of Thermal Expansion, CTE (m in/in/°F)	-0.35

* Properties are at 62% Fiber Volume.

Appendix F

Programs on Diskette

The following Lotus 1-2-3 spreadsheets are included on the diskette on the next page. They were converted from Lotus version 2.1 to version 1A, which is more common and can also be read by all subsequent versions. MS-DOS V.3.10 was used to format the diskette. Additional information can be attained by contacting: Eric L. Christiansen, Eagle Engineering, (713)338-2682.

1. IMPACT.WKS Analytical model described in Section 4.2 and Appendix A.

2. HUGONIOT.WKS Calculates peak shock pressure as described in Appendix C.

3. FIGOFMER.WKS Empirical model described in Section 4.1 and Appendix B.

4. DEB_VDIS.WKS Contains orbital debris velocity distribution for typical Space Station orbit. Calculates the fraction of debris below the velocity causing aluminum projectiles to melt as described in Section 3.3.

5. MOD_CRIT.WKS Determines the critical orbital debris and meteoroid size that a Space Station hab or lab module should be designed to protect against based on a 0.9955 probability of no penetration as described in Section 3.3.

6. SSMOD_CE.WKS Determines the number and maximum size of perforations expected in an aluminum bumper of a Space Station common module over its orbital lifetime as discussed in Section 3.3.